

Characterization of three 2-hydroxy-acid dehydrogenases in the context of a biotechnological approach to short-circuit photorespiration

Inaugural-Dissertation

zur

Erlangung des Doktorgrades
der Mathematisch-Naturwissenschaftlichen Fakultät
der Universität zu Köln

vorgelegt von

Martin Engqvist

Aus Dänningelanda, Schweden

Köln, 2010

Die dieser Dissertation zugrunde liegenden experimentellen Arbeiten wurden in der Zeit von September 2007 bis März 2010 am Botanischen Institut der Universität zu Köln angefertigt und in Teilen im Juli 2009 publiziert.

Engqvist, M., Drincovich, MF., Flüge, Ul. and Maurino, VG.

Two D-2-hydroxyacid dehydrogenases in *Arabidopsis thaliana* with catalytic capacities to participate in the last reactions of the methylglyoxal and β -oxidation pathways

Journal of Biological Chemistry (2009) **284**: 25026-25037.

Prüfungsvorsitzender: Prof. Dr. Reinhard Krämer

Berichterstatter: Prof. Dr. Ulf-Ingo Flüge
Prof. Dr. Sabine Waffenschmidt
Prof. Dr. Hermann Bauwe

Tag der mündlichen Prüfung: 02. Juni 2010

“Why spend a day in the library when you can learn the same thing
by working in the laboratory for a month?”

Frank H. Westheimer (1912–2007)

Table of contents

1. Introduction	8
1.1 Photosynthesis.....	8
1.1.1 Light reactions	8
1.1.2 The dark reactions	8
1.2 Photorespiration.....	9
1.2.1 The photorespiratory pathway.....	9
1.2.2 Physiological importance of photorespiration	12
1.2.3 Reasons for decreasing photorespiration	12
1.2.4 C4 photosynthesis	13
1.3 Biotechnological approaches to reducing photorespiration.....	13
1.3.1 Improving RuBisCO	13
1.3.1.1 Heterologous expression of natural RuBisCOs.....	14
1.3.1.2 Rational design of RuBisCO	15
1.3.1.3 Random mutagenesis of RuBisCO	15
1.3.2 Artificial C4-photosynthesis.....	15
1.3.3 Short-circuiting photorespiration.....	16
1.3.3.1 Introducing the bacterial glycerate pathway into chloroplasts	16
1.3.3.2 Introducing a complete glycolate catabolic pathway into chloroplasts.....	17
1.3.3.3 Improving the GMK pathway	18
1.3.3.4 Other 2-hydroxy-acid dehydrogenases.....	19
1.4 Goals of the present study	21
2. Materials and methods	22
2.1 Plant growth conditions	22
2.1.1 Soil composition and stratification.....	22
2.1.2 Greenhouse growth conditions.....	22
2.1.3 Growth chamber conditions.....	22
2.1.4 BASTA selection on soil	22
2.1.5 <i>A. thaliana</i> seed sterilization	22
2.1.6 <i>A. thaliana</i> growth and selection on sterile plates.....	23
2.1.7 Growth of root cultures.....	23
2.2 <i>Escherichia coli</i> strains and growth conditions.....	24
2.3 Molecular biology methods.....	24
2.3.1 PCR.....	24

2.3.2	Extraction of <i>A. thaliana</i> genomic DNA.....	24
2.3.3	Extraction of <i>A. thaliana</i> RNA.....	25
2.3.4	DNase treatment of RNA and first-strand cDNA synthesis.....	25
2.3.5	Isolation of homozygous <i>A. thaliana</i> T-DNA insertion mutants.....	25
2.3.6	Confirmation of knock-out plants by RT- PCR	26
2.3.7	Producing TSS-competent <i>E. coli</i> cells.....	27
2.3.8	Heat-shock transformation of <i>E. coli</i> cells.....	27
2.3.9	Isolation of <i>E. coli</i> plasmid DNA.....	27
2.3.10	Separation of DNA by agarose gel electrophoresis.....	27
2.3.11	DNA elution from agarose gels.....	28
2.3.12	DNA sequencing	28
2.3.13	Cloning of the three candidate enzymes.....	29
2.4	Biochemical methods	29
2.4.1	Expression and purification of recombinant proteins.....	29
2.4.2	SDS-polyacrylamide gel electrophoresis (SDS-PAGE).....	31
2.4.3	Protein determination and Coomassie staining.....	31
2.4.4	Western-Blot	32
2.4.5	Native-PAGE	32
2.4.6	Mitochondrial isolation	33
2.4.6	Size exclusion chromatography.....	33
2.4.7	Analysis of prosthetic groups	33
2.5	Enzyme assays	34
2.5.1	Co-factor analysis	34
2.5.2	pH optimum and substrate screen.....	34
2.5.3	Catalytic constants	35
2.6	<i>In silico</i> protein analysis.....	35
2.6.1	Phylogenetic trees.....	35
2.6.2	Co-expression analysis.....	35
2.6.3	Catalytic site analysis.....	35
2.7	Metabolite and fluorescence measurements	36
2.7.1	Metabolite analysis by GC-MS.....	36
2.7.2	Imaging-PAM measurements.....	36
3.	Results.....	37
3.1	Characterization of the enzyme encoded by At5g06580.....	37

3.1.1 Identification of the candidate enzyme	37
3.1.2 Phylogenetic analysis.....	37
3.1.3 Cloning, heterologous expression and purification of AtD-LDH	40
3.1.4 Quaternary structure of the enzyme.....	40
3.1.5 Analysis of the prosthetic group	41
3.1.6 Co-factor analysis and pH optimum	42
3.1.7 Substrate screening	43
3.1.8 Determination of kinetic constants.....	45
3.1.9 The catalytic site of AtD-LDH.....	46
3.1.10 Isolation of knock-out mutants	46
3.1.11 In-gel assays of knock-out plants	47
3.1.12 Plant feeding experiments	48
3.2 Characterization of the enzyme encoded by At4g36400.....	51
3.2.1 Identification of the candidate enzyme	51
3.2.2 Phylogenetic analysis.....	51
3.2.3 Cloning, heterologous expression and purification of AtD-2HGDH	54
3.2.4 Quaternary structure of AtD-2HGDH	54
3.2.5 Analysis of the prosthetic group	55
3.2.6 Co-factor analysis and pH optimum	56
3.2.7 Substrate screening	57
3.2.8 Determination of kinetic constants.....	57
3.2.9 The catalytic site of AtD-2HGDH	59
3.2.10 Isolation of knock-out mutants	59
3.2.11 In-gel assays of knock-out plants	60
3.2.12 <i>In silico</i> co-expression analysis	62
3.2.13 Dark-induced senescence and metabolite profiling.....	63
3.3 Characterization of the enzyme encoded by At4g18360.....	67
3.3.1 Identification of the candidate.....	68
3.3.2 Isolation of knock-out mutants	70
3.3.3 In-gel assays of knock-out mutants.....	70
3.3.3 Cloning, heterologous expression and purification of AtGOX3.....	71
3.3.4 Co-factor analysis and pH optimum	71
3.3.5 Substrate screening.....	73
3.3.6 Determination of kinetic constants.....	73
3.3.7 Structural considerations	74

3.3.8 Plant feeding experiments	74
4. Discussion	76
4.1 At5g06580 encodes a D-LDH	76
4.1.1 AtD-LDH is conserved in evolution and localizes to mitochondria	76
4.1.2 AtD-LDH is specific for D-lactate and D-2HB	77
4.1.3 AtD-LDH metabolizes D-lactate <i>in vivo</i>	77
4.1.4 Plants may have a second MG detoxification pathway	78
4.1.5 Model	79
4.1.6 Outlook.....	80
4.2 At4g36400 encodes a D-2HGDH.....	80
4.2.1 AtD-2HGDH is conserved in evolution and localizes to mitochondria	80
4.2.2 D-2HG accumulates in <i>d2hgdh</i> mutants.....	81
4.2.3 D-2HG is most likely produced in a condensation reaction	82
4.2.4 Model	82
4.2.5 Outlook.....	83
4.3 At4g18360 encodes an (S)-2-hydroxy-acid oxidase	84
4.3.1 AtGOX3 oxidizes glycolate and L-lactate with high efficiency.....	84
4.3.2 Identifying important amino acids in the catalytic site.....	84
4.3.3 <i>In vivo</i> role of AtGOX3	85
4.3.4 Outlook.....	85
5 Conclusions and future directions	86
6. References	88
7. Abstract.....	99
8. Kurzzusammenfassung.....	100
9. Acknowledgements	101
10. Erklärung	102

1. Introduction

1.1 Photosynthesis

Photosynthesis is a process of crucial importance for life on earth. It is the process by which some photoautotrophic organisms capture light energy from the sun and use it to fix carbon dioxide from the atmosphere. As a by-product of this process oxygen is produced. Almost all hydrocarbons found in nature have once existed as free carbon dioxide and subsequently been fixed by photosynthetic organisms. Consequently, these organisms not only produce the food we eat, but also the oxygen we breathe. Photosynthesis is generally divided up in two parts, the light reactions and the “dark” reactions.

1.1.1 Light reactions

Oxygenic photosynthesis performed by plants, alga and some photosynthetic bacteria uses two photosystems working in sequence. The process takes place in the thylakoid membrane of the chloroplasts where the photosynthetic light reactions absorb light from the sun and capture it in the form of chemical bonds. This feat is performed by photosystem I (PSI) and photosystem II (PSII) in conjunction with their respective light harvesting complexes. Photons captured by the chlorophylls in the light-harvesting complexes are transferred to special protein-chlorophyll reaction centers inside each photosystem through excitation transfer. In the reaction center an electron from one of the chlorophylls is excited and subsequently transferred to a series of acceptors in the electron transport chain. The linear electron transport chain builds up a proton gradient over the membrane, which is used to convert ADP to ATP, and reduces NADP^+ to NADPH. The light reactions thus ultimately serve to produce reduced energy carriers which are further used in the dark reactions to fix atmospheric CO_2 (Taiz and Zeiger, 2006).

1.1.2 The dark reactions

The NADPH and ATP originating from the light reactions are used in the Calvin-Benson cycle to fix atmospheric carbon. In a carboxylation reaction ribulose-1,5-bisphosphate (RuBP) – a 5-carbon unit – is converted into two molecules of 3-phosphoglycerate – a 3-carbon unit. The 3-phosphoglycerate is further reduced to 2,3-bisphosphoglycerate and finally glyceraldehyde-3-phosphate. Glyceraldehyde-3-phosphate exists in equilibrium with dihydroxyacetone phosphate. These photoassimilates can further be exported to the cytosol by the triose phosphate/phosphate translocator (Flügge, 1999), be condensed into fructose-6-phosphate and enter starch synthesis, or re-enter the Calvin-Benson cycle to form RuBP. Typically $1/6^{\text{th}}$ of the generated glyceraldehyde-3-phosphate is exported or used for starch synthesis while $5/6^{\text{th}}$ re-enters the Calvin-Benson cycle. The key enzyme in this cycle, catalyzing the carboxylation reaction, is ribulose-1,5-bisphosphate carboxylase/oxygenase (RuBisCO). This is a hexadecameric enzyme in higher plants, consisting of eight identical large subunits, encoded in the chloroplast, and eight identical small subunits, encoded in the nucleus (Miziorko and Lorimer, 1983; Parry et al., 2003). Despite the supreme importance of

this enzyme for all land plants it is notoriously inefficient, catalyzing only about 4 carboxylation reactions per second (Tcherkez et al., 2006). Plants have adapted to this by producing large amounts of the enzyme and RuBisCO can make up as much as 30-50% of total leaf protein in C3 plants (Parry et al., 2003).

1.2 Photorespiration

In addition to being an extremely slow enzyme, RuBisCO cannot properly discriminate between oxygen and carbon dioxide. Consequently, the enzyme does not only catalyze the carboxylation of RuBP, but also the oxygenation. The latter reaction produces one 3-phosphoglycerate as well as the 2-carbon unit 2-phosphoglycolate (Lorimer, 1981; Ogren, 2003). This 2-phosphoglycolate cannot be readily used by the cell and must first be converted back to the Calvin-Benson cycle intermediate 3-phosphoglycerate through the photorespiratory pathway, stretching over chloroplasts, peroxisomes, mitochondria and the cytosol (Maurino and Peterhänsel, 2010; Tolbert, 1997; Wingler et al., 2000) (Fig. 1). The pathway is ubiquitous in photosynthesizing organisms, being present in plants (Maurino and Peterhänsel, 2010; Tolbert, 1997), unicellular algae (Suzuki et al., 1990; Tian et al., 2006) and cyanobacteria (Bauwe, 2010; Eisenhut et al., 2008).

1.2.1 The photorespiratory pathway

The importance of the photorespiratory pathway is underscored by the fact that most mutants lacking activity in any of the participating enzymes are lethal or display severely compromised growth at ambient CO₂ levels. They can, however, be rescued at high CO₂ levels where no photorespiration occurs. Photorespiration comprises a long series of enzymatic reactions (Fig. 1).

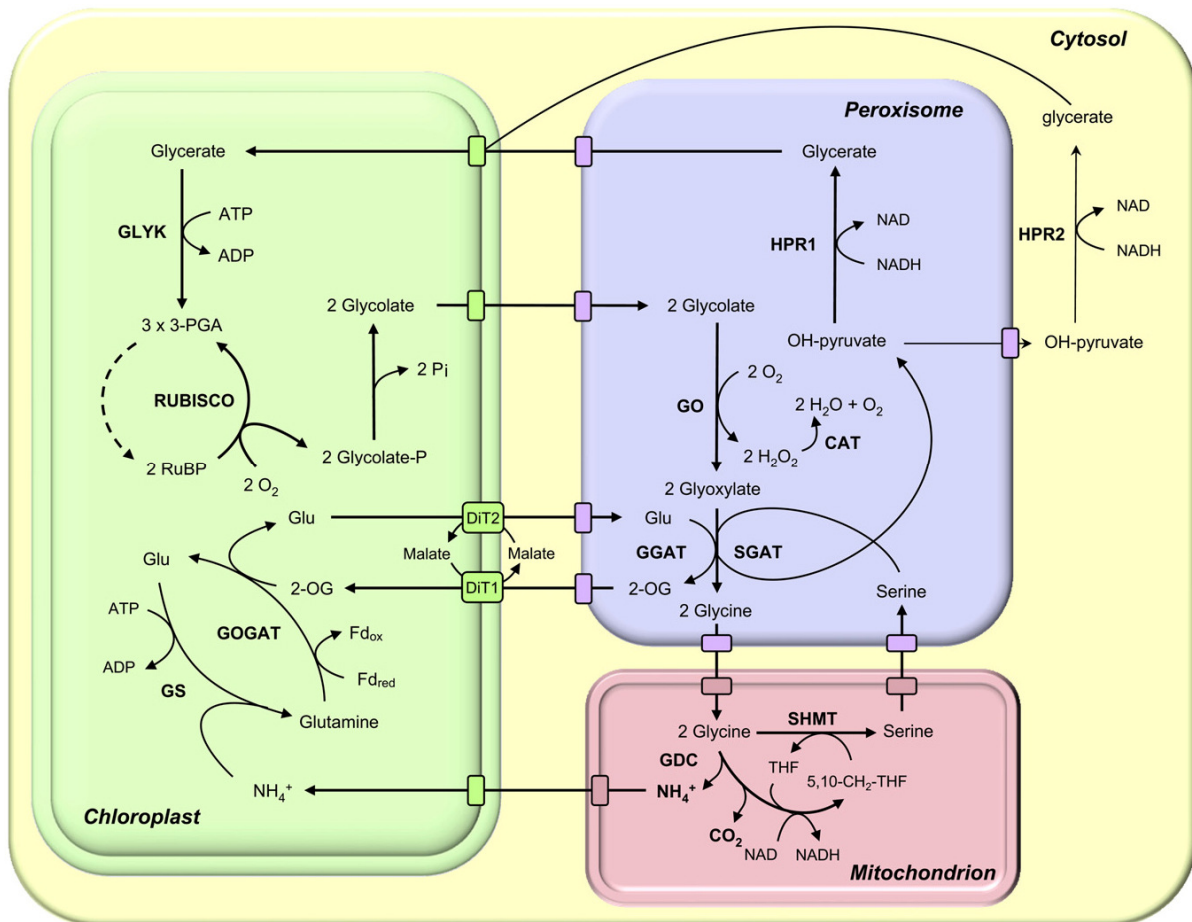


Figure 1. The photorespiratory pathway. The photorespiratory pathway serves to convert 2-phosphoglycolate back to 3-phosphoglycerate. Photorespiration derives its name from the fact that it is a light-dependent uptake of oxygen by RuBisCO with subsequent carbon dioxide release. The figure is re-produced from Maurino and Peterhänsel (2010).

Upon oxygenation of RuBP and subsequent formation of 2-phosphoglycolate this molecule is dephosphorylated into glycolate by 2-phosphoglycolate phosphatase (PGLP) inside the chloroplast (Schwarte and Bauwe, 2007; Somerville and Ogren, 1979). Glycolate is further exported to peroxisomes where it is oxidized to glyoxylate by glycolate oxidase (GO), with the production of H₂O₂ (Xu et al., 2009; Zelitch et al., 2009). *Arabidopsis thaliana* contains three GOs that are closely related to each other (GOX1, GOX2 and GOX3) and two GO-like proteins (HAOX1 and HAOX2) (Reumann et al., 2004) (Fig. 2). There are differences in sequence as well as differences in which tissue these genes are expressed, as determined by microarray experiments (<http://bar.utoronto.ca/efp/cgi-bin/efpWeb.cgi>) (Kamada et al., 2003; Winter et al., 2007). At3g14420 (AtGOX1) and At3g14415 (AtGOX2) are both highly expressed in plant leaves and most likely participate in photorespiration (Xu et al., 2009). In contrast, At4g18360 (AtGOX3) is expressed at much lower levels and almost exclusively in roots. At3g14130 (AtHAOX1) and At3g14150 (AtHAOX2) are expressed at intermediate levels and exclusively in developing seeds. The physiological function of these latter three enzymes is currently unknown.

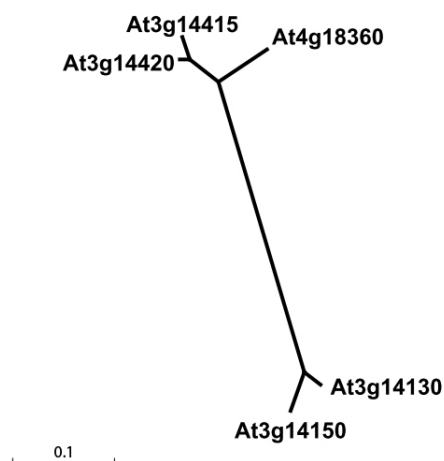


Figure 2. Phylogenetic tree of the three GOs and two GO-like enzymes in *A. thaliana*. At3g14420 (GOX1), At3g14415 (AtGOX2), At4g18360 (AtGOX3), At3g14130 (AtHAOX1) and At3g14150 (AtHAOX2) protein sequences were aligned using ClustalW. The phylogenetic tree was constructed by the neighbor-joining method using BioNJ and visualized using Dendroscope.

The H_2O_2 produced by GOs can severely damage cells and is therefore promptly neutralized to water and oxygen by catalase (CAT) (Kendall et al., 1983; Queval et al., 2007; Vandenabeele et al., 2004). The peroxisomal glyoxylate formed by GO is transaminated by glutamate:glyoxylate aminotransferase (GGAT), with glutamate as an amine donor, resulting in glycine and 2-oxoglutarate (Igarashi et al., 2003; Igarashi et al., 2006). The 2-oxoglutarate is exported from peroxisomes and imported into chloroplasts by the dicarboxylate transporters (DiT1 and DiT2) (Renne et al., 2003; Somerville and Ogren, 1983; Taniguchi et al., 2002; Weber et al., 1995) where it is again converted to glutamate by glutamate:oxoglutarate aminotransferase (GOGAT) (Jamai et al., 2009; Somerville and Ogren, 1980a). Glycine formed by GGAT in the peroxisomes is further transported into mitochondria where, through the combined action of glycine decarboxylase (GDC) (Bauwe and Kolukisaoglu, 2003; Hasse et al., 2010; Somerville and Ogren, 1982) and serine hydroxymethyltransferase (SHMT) (Somerville and Ogren, 1981; Voll et al., 2006), one molecule of glycine is decarboxylated, deaminated and finally the remaining methyl group added to a second molecule of glycine to produce serine. The mitochondrial serine is further exported to peroxisomes where it is converted to hydroxypyruvate through transamination by the action of serine glyoxylate aminotransferase (SGAT) (Liepman and Olsen, 2001; Somerville and Ogren, 1980b). In two final reactions hydroxypyruvate is reduced first to glycerate by hydroxypyruvate reductase (HPR1 and HPR2) (Timm et al., 2008) and finally – after transport to chloroplasts – reduced by D-glycerate kinase (GLYK) (Boldt et al., 2005) into 3-phosphoglycerate, upon which it can re-enter the Calvin-Benson cycle.

Even though all the soluble enzymes of the photorespiratory pathway are known there is a marked lack of knowledge about the transporters involved in photorespiration. Apart from the DiT1 and DiT2 transporters none other has been characterized to date (Reumann and Weber, 2006; Weber et al., 1995).

1.2.2 Physiological importance of photorespiration

The main purpose of photorespiration is thus to return 3/4th of the carbon lost into 2-phosphoglycolate – by oxygenation of RuBP – back into Calvin-Benson cycle intermediates. However, other minor roles have been suggested. Since this process consumes ATP, it has been proposed that the pathway works as a valve to prevent over-reduction of the electron transport chain in chloroplasts (Kozaki and Takeba, 1996), a state where reactive oxygen species are formed. In dry conditions plants close their stomata and intracellular CO₂ concentration dramatically drops. Plants might then use the photorespiratory pathway to free bound CO₂ so that it may get re-fixed by the Calvin-Benson cycle to further consume ATP and NADPH, preventing over-reduction of the electron transport chain (Noctor et al., 2002). The photorespiratory pathway is further needed to produce CH₂-THF from the activity of GDC (Fig. 1), something clearly shown by the fact that GDC is the only photorespiratory mutant that is lethal in both ambient CO₂ as well as high CO₂ conditions (Engel et al., 2007).

1.2.3 Reasons for decreasing photorespiration

Due to loss of fixed carbon, the photorespiratory pathway is a very wasteful process which results in a 20-50% lower carbon fixation rate (Fig. 3) (Long et al., 2006; Mann, 1999). It is therefore widely believed that decreasing it could significantly improve yields for important crops such as potato, wheat and rice (Arp et al., 1998). Since CO₂ and O₂ are competitive substrates for RuBisCO one can artificially decrease photorespiration by increasing the CO₂ concentration, or decreasing the O₂ concentration, and thus evaluate the potential benefits of decreasing photorespiration through biotechnology. Such experiments have shown that plants performing less photorespiration accumulate more total biomass in shorter time as compared to the controls grown in ambient air (Forrester et al., 1966; Long et al., 2006).

The ultimate factor determining the rate of photorespiration is the internal leaf CO₂ to O₂ ratio. When the ratio decreases, the carboxylation to oxygenation ratio of RuBisCO does so too and photorespiration increases. Apart from the ambient CO₂ and O₂ concentration in the atmosphere there are two major factors affecting the CO₂ to O₂ ratio inside plant leaves. Firstly, it depends on whether the plant stomata are open or not. Plants tightly regulate the aperture of their stomata to reduce water loss; this has the effect that in hot and dry conditions, when the stomata are closed, the gas exchange between the leaf and surrounding air is greatly reduced. Since CO₂ is continually consumed by RuBisCO while O₂ is produced by PSII, the internal CO₂ to O₂ ratio then drastically drops. Secondly, the solubility of the two gasses does not increase at the same rate with increasing temperature. The ratio of dissolved CO₂ to O₂ is 0.462 at 15°C while it is 0.0376 at 35°C (Taiz and Zeiger, 2006). Thus, temperature is an extremely important variable affecting photorespiration (Jordan and Ogren, 1984; Ku and Edwards, 1977).

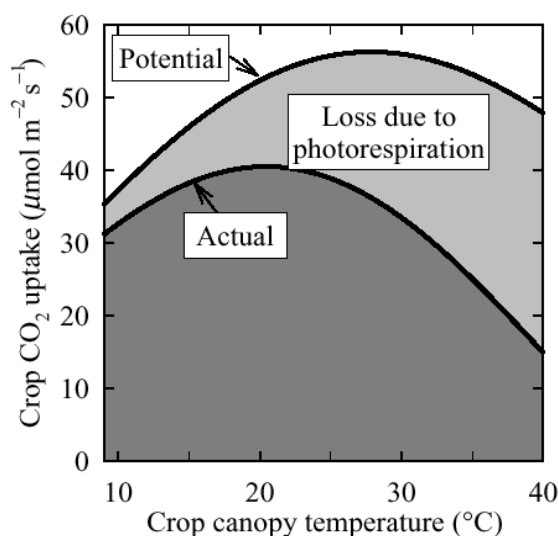


Figure 3. Calculated actual and potential rates of CO₂ uptake. The difference between the actual and potential carbon fixation rates is the loss due to photorespiration. Calculations were done for a photon flux of 1800 $\mu\text{mol m}^{-2} \text{s}^{-1}$, corresponding to full sunlight, and for different temperatures. Figure was reproduced from Long et al., (2006).

1.2.4 C4 photosynthesis

Some plants – corn and sugarcane being the most familiar – have evolved a mechanism to reduce photorespiration, called C4 photosynthesis. In C4 photosynthesis there is an initial carboxylation of phosphoenolpyruvate (PEP) by PEP carboxylase in mesophyll cells, using carbon in the form of HCO_3^- . This reaction produces oxaloacetate, which is further converted to malate or aspartate and transported into the bundle sheath cells where RuBisCO is expressed. In these cells malate and aspartate are decarboxylated to yield CO₂, which can be fixed by RuBisCO. This process results in a much higher CO₂ concentration in bundle sheath cells compared to the rest of the leaf, and consequently RuBisCO can work faster with less oxygenation reactions occurring (Taiz and Zeiger, 2006). In this way, an ATP-dependent CO₂ pump is formed. The spatial separation of these reactions is normally a prerequisite for C4 metabolism, but a few instances of single-cell C4 metabolism have been reported (Edwards et al., 2004; Lara et al., 2002).

1.3 Biotechnological approaches to reducing photorespiration

1.3.1 Improving RuBisCO

Since the ultimate cause for photorespiration lies with the insufficient ability of RuBisCO to distinguish between CO₂ and O₂, improvement of this enzyme has been the focus of much effort. Three distinct approaches can be distinguished: (I) heterologous expression of natural RuBisCOs with more favorable properties in crop plants, (II) rational design of the amino acid sequence of RuBisCO for increased CO₂ specificity and (III) random mutagenesis of RuBisCO with subsequent screening for improved activity.

1.3.1.1 Heterologous expression of natural RuBisCOs

The RuBisCO specificity factor (τ) can be calculated by dividing the catalytic efficiency (K_{cat}/K_m) for CO_2 with that of O_2 (Parry et al., 2003). τ is then a measure of how much better RuBisCO catalyzes the carboxylation of RuBP as opposed to the oxygenation. RuBisCOs found in nature differ significantly in their specificity factor (Table 1), with higher land plants having τ -values between 90 and 96, bacteria and cyanobacteria around 45 (Uemura et al., 1996) and single subunit RuBisCOs from *Rhodobacter sphaeroides* and *Rhodospirillum rubum* having a specificity factor of 9 and 15, respectively (Read and Tabita, 1994). The highest τ -value ever measured is that from the unicellular red algae *Galdieria partita* with a τ -value of 238, which is about 2.5 times greater than that reported for RuBisCO from crop plants (Uemura et al., 1997).

Table 1. The relative specificity of RuBisCO varies in nature. The specificity factor ($K_{cat\text{CO}_2}/K_{m\text{CO}_2})/(K_{cat\text{O}_2}/K_{m\text{O}_2}) = (\tau)$ of RuBisCOs from land plants, algae, and cyanobacteria are shown. References are: a (Uemura et al., 1996), b (Read and Tabita, 1994), c (Uemura et al., 1997).

RuBisCO source	τ	Reference
<i>Galdieria partita</i>	238	c
<i>Porphyra yezoensis</i>	145	a
<i>Spinacea oleaceae</i>	93	a
<i>Nicotiana tabacum</i>	91	a
<i>Pisum sativum</i>	90	a
<i>Zea mays</i>	96	a
<i>Chlamydomonas reinhardtii</i>	71	a
<i>Synechococcus PCC7942</i>	45	a
<i>Chromatium vinosum</i>	44	a
<i>Rhodospirillum rubum</i>	15	b
<i>Rhodobacter sphaeroides</i>	9	b

One approach to improve RuBisCO function would thus be to heterologously express natural RuBisCO variants with superior catalytic properties in crop plants. Several such attempts have been made. For instance, the *rbLS* operon, encoding the large and small subunit of RuBisCO, from *G. partita* and *Phaeodactylum tricornutum* was introduced in chloroplasts of *Nicotiana tabacum*. Transgenes of both constructs had abundant transcript, but most of the small subunit and all of the large subunit protein was insoluble (Whitney et al., 2001). In another approach, models of photosynthesis predicted that the RuBisCO from *Chromatium vinosum* should out-perform the native RuBisCO in higher plants. However, as the *C. vinosum* RuBisCO large subunit was introduced into *Nicotiana tabacum*, abundant transcript could be detected, but no functional protein was formed (Madgwick et al., 2002). A few approaches, expressing the large subunit from *Helianthus annuus* (Kanevski et al., 1999) or *Rhodospirillum rubum* (Whitney and Andrews, 2001), were successful in recovering active enzymes, but these displayed catalytic efficiencies inferior to the wild-type RuBisCO. Thus, while this method may have potential for improving crop yield, problems concerning proper protein folding must first be resolved.

1.3.1.2 Rational design of RuBisCO

The fact that different RuBisCO enzymes found in nature have a large range of specificity factors suggests that there is room for improvement through rational design of the enzyme. Indeed, many attempts at improving the active site of RuBisCO have been performed, but generally the modified enzymes have lower catalytic efficiencies than the wild-type one (Hartman and Harpel, 1994; Spreitzer and Salvucci, 2002; Watson and Tabita, 1997). There is a further complication to improving RuBisCO since the enzyme from higher plants is extremely difficult to heterologously express as a functional enzyme (Gatenby et al., 1981). This is due to improper folding of RuBisCO by the chaperones present in the heterologous host (Gutteridge and Gatenby, 1995). Many researchers have thus resorted to using the cyanobacterial RuBisCO as it can be readily cloned and expressed in heterologous hosts such as *E. coli*. However, these RuBisCOs have much lower τ -values than their counterparts in higher plants (Table 1). Even though much structure-function knowledge about RuBisCO has been gained through these approaches, researchers have yet to improve the cyanobacterial RuBisCOs to be on par with the plant enzymes (Parry et al., 2003).

1.3.1.3 Random mutagenesis of RuBisCO

In parallel to the attempts of rational design there have been attempts at directed evolution of RuBisCO. This method consists in random mutagenesis of the enzyme with subsequent screening to identify beneficial mutations. Early attempts at creating tools for such a method resulted in engineered *Synechocystis PCC6803* strains lacking native RuBisCO as well as carboxysomes and could consequently not grow at ambient CO₂, but only at 5% CO₂ (Amichay et al., 1993; Pierce et al., 1989). However, these tools were never widely adapted. More recently, screens using the unicellular algae *Chlamydomonas reinhardtii* (Du et al., 2000; Hong and Spreitzer, 1997; Spreitzer et al., 2001) and the red algae *Rhodobacter capsulatus* (Smith and Tabita, 2003) have been performed, but with limited success. A recent approach to screen a mutant library of the *Synechococcus PCC6301* RuBisCO large subunit in *E. coli* (Parikh et al., 2006) shows promise, resulting in mutants with improved folding, 12% increased catalytic rate and a 15% increase in affinity for CO₂ (Greene et al., 2007). Other approaches involve screens for suppressor mutants to find mutants that perform worse than wild-type and thus find new amino acid targets for rational design (Mueller-Cajar et al., 2007; Smith and Tabita, 2003).

1.3.2 Artificial C4-photosynthesis

There is a keen interest in introducing C4 photosynthesis in C3 plants. Most of these approaches aim at expressing a few key C4 enzymes to achieve a higher CO₂ concentration in plastids (Matsuoka et al., 2001). In contrast to the failed attempts to express novel RuBisCOs in plants (section 1.3.1.1) these approaches succeeded in expressing active C4 enzymes in C3 plants (Häusler et al., 2002; Leegood, 2002; Miyao, 2003). In this manner, genes for phosphoenolpyruvate carboxylase, pyruvate-phosphate-dikinase or the NADP-malic enzyme were expressed in rice (Fukayama et al., 2003; Jiao et al., 2002; Ku et al., 1999; Takeuchi et al., 2000). However, no beneficial effect on the plant photosynthetic properties could be

obtained, but instead detrimental effects resulted when NADP-malic enzyme was over-expressed in rice plants (Takeuchi et al., 2000). The recent sequencing of specific C3 and C4 plants enables comparative proteomic and transcriptomic analyses which may prove instrumental to designing better approaches for introducing C4 metabolism in C3 plants (Weber and von Caemmerer, 2010).

1.3.3 Short-circuiting photorespiration

Recently, two independent approaches aimed at reducing photorespiration have introduced bacterial glycolate assimilation pathways inside plant chloroplasts. Both pathways have in common the intraplastidic conversion of glycolate – produced from the RuBisCO oxygenation reaction – into metabolites useful to the cell (Fahnenstich, 2008; Kebeish et al., 2007; Maurino and Flügge, 2009). These recent approaches show great promise as they both result in higher photosynthetic rates and increased plant biomass.

1.3.3.1 Introducing the bacterial glycerate pathway into chloroplasts

In the approach pursued by Kebeish et al., (2007), the entire *E. coli* glycerate pathway was modified for posttranslational targeting to chloroplasts and introduced into the *A. thaliana* nuclear genome. The pathway thus comprised three genes coding for the *E. coli* glycolate dehydrogenase (GDH) as well as the two genes coding for glyoxylate carboligase (TSS) and tartronate semialdehyde reductase (TSR) (Fig. 4). Together, the enzymes encoded by these genes convert glycolate to glycerate, with the reaction intermediates being glyoxylate and tartronate semialdehyde. In this pathway CO₂ is released at the same amount as in the photorespiratory pathway, but shifting the CO₂ release from mitochondria to chloroplasts increases the CO₂ concentration around RuBisCO, which reduces its oxygenase activity (Kebeish et al., 2007). The approach was successful and the transgenic plants showed a decreased glycine to serine ratio, indicative of decreased photorespiration, as well as larger rosette diameter and fresh weight (Kebeish et al., 2007). Surprisingly, these beneficial effects were also seen in plants only overexpressing the glycolate dehydrogenase and the physiological cause for this is not known.

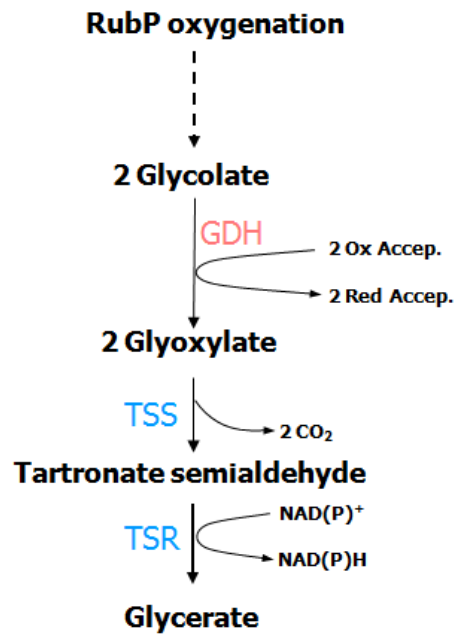


Figure 4. The chloroplastic glycerate pathway. By targeting glycolate dehydrogenase (GDH), glyoxylate carboligase (TSS) and tartronate semialdehyde reductase (TSR) to chloroplasts the phosphoglycolate produced by RuBisCO is converted to glycerate which can be phosphorylated and re-enter the Calvin-Benson cycle.

1.3.3.2 Introducing a complete glycolate catabolic pathway into chloroplasts

The approach pursued by Maurino and Flügge (2009) comprised three enzymes targeted to plastids, glycolate oxidase (GO, EC 1.1.3.15), malate synthase (MS, EC 2.3.3.9) and catalase (Cat, EC 1.11.1.6), forming the so called chloroplastic GMK pathway. Together with malic enzyme and pyruvate dehydrogenase, two enzymes already present in chloroplasts, these enzymes completely oxidize the glycolate resulting from the RuBisCO oxygenase activity to CO₂ inside the chloroplast (Fig. 5). The produced CO₂ is then available for re-fixation and should work to inhibit further oxygenase activity by RuBisCO. Through this pathway plant biomass accumulation as well as the photosynthetic efficiency was enhanced (Fahnenstich, 2008).

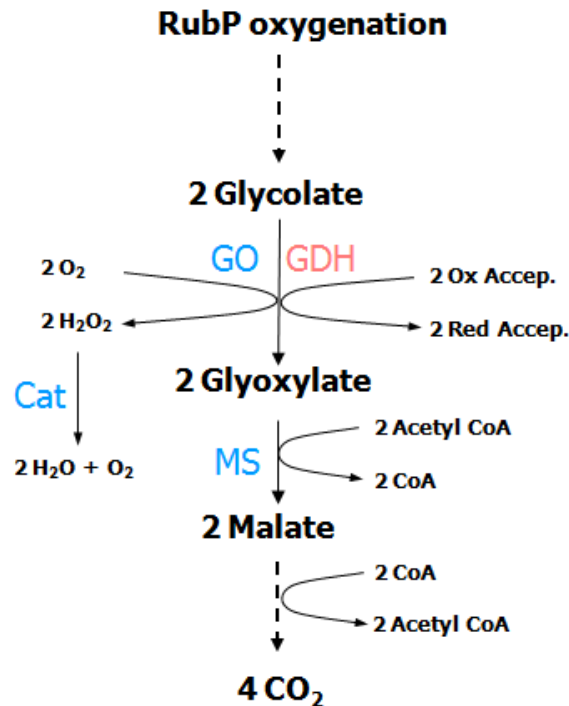


Figure 5. The chloroplastic GMK pathway. The phosphoglycolate produced by RuBisCO is completely oxidized into CO₂ through introduction of either glycolate oxidase (GO) and catalase (Cat) or glycolate dehydrogenase (GDH) together with malate synthase (MS). As the produced CO₂ is close to the site of RuBisCO further photorespiration is inhibited.

1.3.3.3 Improving the GMK pathway

The benefits of these two pathways developed by Kebeish et al. (2007) and by Maurino and Flügge (2009) were achieved despite the fact that the common first step of both pathways, the conversion of glycolate to glyoxylate, was catalyzed by either the *E. coli* glycolate dehydrogenase (Kebeish et al., 2007) or the *A. thaliana* glycolate oxidase (Fahnenstich, 2008; Maurino and Flügge, 2009). The *E. coli* enzyme is a heterotrimer using an unknown acceptor, making its cloning and targeting to chloroplasts cumbersome and the behavior unpredictable. This is underscored by the fact that plants transformed with only this enzyme generate increased amounts of biomass, an effect that still has no physiological explanation (Kebeish et al., 2007). The *A. thaliana* glycolate oxidase produces H₂O₂ which is toxic to the cell and leads to photobleaching unless it is counteracted by the expression of high levels of catalase. These problems could be solved by employing a single gene glycolate dehydrogenase (GDH) in the place of GO and *E. coli* glycolate dehydrogenase. However, very few GDHs have been identified to date.

There are reports of a *Synechocystis sp. PCC 6803* glycolate dehydrogenase with homology to the *E. coli* GlcD subunit of glycolate dehydrogenase (Eisenhut et al., 2006). However, the activity measured with this subunit was very low and it is possible that it consists of several subunits *in vivo* in a way similar to the *E. coli* GDH. Moreover, algae are known to use GDHs instead of GOs for glycolate metabolism. The *C. reinhardtii* GDH has been identified (Nakamura et al., 2005) and might be used for the pathway, but it is a very large protein and

has not been completely characterized. Recently, a mitochondrial single gene GDH in *A. thaliana* was reported (Bari et al., 2004; Niessen et al., 2007). The enzymatic properties of AtGDH were partially characterized in crude extracts from *E. coli* cells overexpressing the corresponding gene, as the enzyme could not be purified. In these extracts AtGDH was shown to oxidize glycolate to glyoxylate, using 2,6-dichlorophenol-indophenol (DCIP) as an acceptor as well as reducing pyruvate to lactate with NADH as an electron donor, but the relative rates of these reactions were not determined (Bari et al., 2004).

1.3.3.4 Other 2-hydroxy-acid dehydrogenases

In addition to GDHs, which are 2-hydroxy-acid dehydrogenases, there are other 2-hydroxy-acid dehydrogenases that have the capacity of glycolate oxidation. For instance, some types of lactate dehydrogenases frequently have activity with glycolate. There are four types of lactate dehydrogenases which are evolutionarily unrelated (Cristescu et al., 2008). Lactate dehydrogenases are specific for either the D- or L- form of lactate and use either NAD(P)⁺ or cytochrome c as an electron acceptor, yielding four distinct types of enzyme: L-lactate NAD oxidoreductase (L-LDHn, EC 1.1.1.27), L-lactate cytochrome c oxidoreductase (L-LDHc, EC 1.1.2.3), D-lactate NAD oxidoreductase (D-LDHn, EC 1.1.1.28) and D-lactate cytochrome c oxidoreductase (D-LDHc, EC 1.1.2.4). Both L-LDHn and L-LDHc are found in eubacteria, archaebacteria, and eukaryotes. The only identified lactate dehydrogenase in plants belongs to the L-LDHn group (Davies and Davies, 1972; Passarella et al., 2008; Paventi et al., 2007) where it is involved in L-lactate production during hypoxic stress (Dolferus et al., 2008). L-LDHn and L-LDHc belong to the most intensely studied enzyme families (Lodi and Guiard, 1991; Passarella et al., 2008), but the knowledge about their structure, kinetics, and biological function is limited.

Even though the L-LDHn and D-LDHn have been shown to catalyze the reduction of glyoxylate to glycolate, the K_m values were in the millimolar range (Betsche, 1981; Davies and Davies, 1972; Kochhar et al., 1992; Mulcahy and Ocarra, 1997; Shinoda et al., 2005), and there is little evidence for the catalysis of glycolate oxidation. Also for the L-LDHc enzymes there is little evidence for glycolate oxidation. In contrast, many D-LDHc enzymes have activity with glycolate (Table 2). These enzymes have mainly been identified in mammals (Flick and Konieczny, 2002), fungi (Gregolin and Singer, 1963; Lodi and Ferrero, 1993; Lodi et al., 1994) and algae (Brockman and Wood, 1975; Horikiri et al., 2004; Nakamura et al., 2005; Nelson and Tolbert, 1970; Paul and Volcani, 1976; Reed and Hartzell, 1999), but in some instances they also occur in bacteria (Lord, 1972; Ogata et al., 1981). Recently, Atlante et al. (2005) showed that externally added D-lactate caused oxygen consumption by mitochondria and that this metabolite was oxidized by a mitochondrial flavoprotein in *Helianthus tuberosus*, indicating that the D-LDHc enzyme may also be present in plants.

Table 2. Heterogeneity in D-lactate dehydrogenases. A summary of the catalytic properties displayed by D-lactate cytochrome c oxidoreductases. The relative V_{max} is given in % compared to the best substrate for each enzyme. K_m is given in mM, - indicates that the value was not determined. References: a (Brockman and Wood, 1975), b (Paul and Volcani, 1976), c (Ogata et al., 1981), d (Reed and Hartzell, 1999), e (Horikiri et al., 2004), f (Lord, 1972), g (Nelson and Tolbert, 1970), h (Gregolin and Singer, 1963).

Organism	Glycolate	D-lactate	L-lactate	2-hydroxybutyrate	Co-factor	Reference
	V_{max} (%) : K_m (mM)					
<i>Chlamydomonas reinhardtii</i>	100 : 0.22	50-70 : 1.5	10-25 :-	50-75 :-	DCIP	g
<i>Chlamydomonas reinhardtii</i>	100 :-	100 :-	25 :-	:-	Cyt c	b
<i>Chlorella pyrenoidosa</i>	100 :-	70 :-	5 :-	:-	DCIP	g
<i>Scenedesmus obliquus</i>	100 :-	88 :-	0 :-	:-	DCIP	g
<i>Escherichia coli</i>	88 : 0.04	100 : 0.7	14 :-	:-	Cyt c	f
<i>Acetabularia mediterranea</i>	81 :-	100 :-	4 :-	:-	DCIP	g
<i>Euglena gracilis</i>	50 :-	100 :-	13 :-	:-	DCIP	g
<i>Peptostreptococcus elsdenii</i>	2 :-	100 : 26	0 :-	57 :-	Cyt c	a
<i>Saccharomyces cerevisiae</i>	:-	100 : 0.285	:-	41 : 1.4	Cyt c	h
<i>Archaeoglobus fulgidus</i>	:-	100 : 0.15	:-	:-	Cyt c	d
<i>Rhodospseudomonas palustris</i>	0 :-	100 : 0.8	0 :-	44 :-	DCIP	e
<i>Desulfovibrio vulgaris</i>	0 :-	89 : 0.8	2 :-	100 :-	Cyt c-553	c

In eukaryotic cells, D-lactate results from the glyoxalase system (Atlante et al., 2005; Thornalley, 1990) (Fig. 6). The system comprises the enzymes glyoxalase I (lactoylglutathione lyase, EC 4.4.1.5) and glyoxalase II (hydroxyacylglutathione hydrolase, EC 3.1.2.6) and metabolizes methylglyoxal (MG), a cytotoxic compound, into D-lactate. MG is formed primarily as a by-product of glycolysis through nonenzymatic phosphate elimination from dihydroxyacetone phosphate and glyceraldehyde 3-phosphate (Kalapos, 1999; Phillips and Thornalley, 1993), as well as enzymatically from several enzymes involved in carbohydrate metabolism (Lyles and Chalmers, 1992; Pompliano et al., 1990; Ray and Ray, 1981). The glyoxylase system is present in plants as shown by the characterization of glyoxylase II from several plants species, such as rice (Yadav et al., 2007), *A. thaliana* (Maiti et al., 1997; Ridderström and Mannervik, 1997), Maize (Norton et al., 1989) and *H. tuberosus* (Atlante et al., 2005).

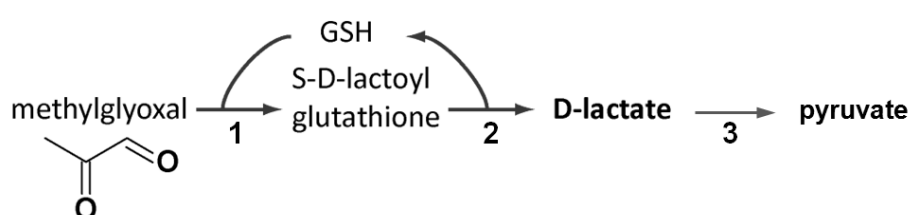


Figure 6. The main glyoxylate detoxification pathway. Methylglyoxal is converted to D-lactate in two steps by the action of glyoxalase I (1) and glyoxalase II (2). The D-lactate is further metabolized to pyruvate by the action of a D-LDH (3).

1.4 Goals of the present study

The main goal of this study is to employ forward and reverse genetics to identify candidate glycolate dehydrogenases in *Arabidopsis thaliana* and to biochemically characterize them. An enzyme is sought with catalytic properties suitable for efficient intraplasmidic conversion of glycolate to glyoxylate. Such an enzyme should: 1) be encoded by a single gene, 2) have high specificity for- and be highly active with glycolate, 3) use a co-factor that is present inside chloroplasts, 4) have a structure that allows for correct folding inside chloroplasts. Upon successful completion of this goal, the characterized enzyme would be used for improving the GMK pathway. Moreover, the physiological role of the candidate enzymes will be explored *in silico* through analysis of co-expressed genes and phylogenetic relationships and *in vivo* through metabolic analysis and substrate feeding experiments using wild-type and candidate gene knock-out plants.

2. Materials and methods

2.1 Plant growth conditions

All plant work in this thesis, including that performed with knock-out mutants, was performed with *Arabidopsis thaliana* accession Columbia-0.

2.1.1 Soil composition and stratification

A. thaliana seeds were sown on moist soil containing a mixture of 3 parts soil (Gebr. Patzer KG, Sinntal-Jossa) and one part of vermiculite (Basalt Feuerfest, Linz). The sown seeds were then covered with a plastic hood to trap the soil moisture, stratified in the dark for 2 days at 4°C and subsequently transferred to either the greenhouse or a growth chamber. Approximately 14 days after sowing, single plants were transferred to large pots to allow enough space for normal growth.

2.1.2 Greenhouse growth conditions

The greenhouse was run at long-day conditions with a 16:8 light:dark period. The humidity was approximately 40% and the temperatures were approximately 22°C during the day and 18°C during the night. The incoming sunlight was either shaded off if it was too strong or supplemented with fluorescent light if it was too weak, as to keep a photon flux density of approximately 150-200 $\mu\text{mol m}^{-2} \text{s}^{-1}$. Plants were only grown in the greenhouse when performing BASTA selection or to generate seeds.

2.1.3 Growth chamber conditions

The growth chambers were set to either long-day conditions with a 16:8 light:dark cycle or to short-day conditions with a 8:16 light:dark cycle. The humidity was kept constant at 60% and the temperature at 22°C during the day and 18°C at night. The photon flux density in the growth chambers was 75 $\mu\text{mol m}^{-2} \text{s}^{-1}$.

2.1.4 BASTA selection on soil

BASTA selection of plants was performed on 2-week old soil-grown seedlings. These were sprayed with a solution containing 0.001% (w/v) glufosinat and 0.1% (v/v) Tween 20. This treatment was repeated on 3 consecutive days. Approximately 7 days after the first treatment resistant plants were transferred to new pots.

2.1.5 *A. thaliana* seed sterilization

To generate *A. thaliana* seeds without microbial or fungal contamination they were either sterilized using chlorine gas or with ethanol. The chlorine gas protocol is well suited when dealing with small amounts of seeds, whereas the ethanol protocol is well suited for large amounts of seeds. In the chlorine gas sterilization protocol a small amount of seeds were placed at the bottom of a 2 ml eppendorf tube with the lid open. This tube was further placed inside a sealed exsiccator together with a beaker containing 100 ml 12% NaClO with 3 ml 37% HCl recently added. The sterilization was allowed to proceed for 16 h. The tubes

were then put under a sterile bench with the lids open for 10-20 minutes before closing to allow any residual chlorine gas to dissipate.

In the ethanol sterilization protocol seeds were placed in an eppendorf tube and washed, with occasional vortexing, for 10 minutes in a solution containing 70% ethanol and 0.05% Triton X-100 in water. When left standing the seeds settled at the bottom of the tube and the supernatant could be removed. The seeds were further washed, with vortexing, for 5 minutes in 100% ethanol. The supernatant was again removed and new 100% EtOH was added. In a sterile hood the seeds were then poured out on a filter paper soaked in 100% ethanol. The filter paper was allowed to dry the seeds were directly sown on sterile plates or stored in sterile eppendorf tubes.

2.1.6 A. *thaliana* growth and selection on sterile plates

Growth of plants in sterile conditions was achieved on ½ MS agar plates. Sterile *A. thaliana* seeds were sprinkled over the plate or put in rows with a sterile toothpick. The plates were incubated at 4°C for two days to allow for stratification before being put in growth chambers. For antibiotic selection the ½ MS plates were supplemented with either 50 µg/ml kanamycin, or 5 µg/ml sulfodiazin. For plant feeding analysis of plants, ½ MS plates without saccharose were supplemented with substrates as indicated. All substances used to supplement the ½ MS plates were sterile-filtered before being added.

½ MS Agar plates

1% (w/v) Saccharose
0.22% (w/v) Murashige & Skoog (MS)
0.8% (w/v) Agar
Millipore water to target volume
Adjust to pH 5.6
Autoclave

2.1.7 Growth of root cultures

To generate large amounts of root tissue, 15-20 sterile *A. thaliana* seeds were put in a 100 ml sterile culture flask containing 50 ml of root growth medium. These were incubated at 4°C for two days to allow for stratification. Germination was further enhanced by putting the cultures in a growth chamber to give a 3-6 h light pulse. The cultures were subsequently put in an orbital shaker moving at 210 rpm at 28°C in the dark. After 2 weeks, a large amount of root tissue had been formed. This was taken out from the culture flask and gently washed with tap water. The pale cotyledons attached to the roots were removed, the roots dabbed of with a piece of paper, and immediately frozen in liquid N₂.

Root growth medium

3% (w/v) Saccharose
0.46% (w/v) Murashige and Skoog (MS)
Millipore water to target volume
Adjust to pH 5.6
Autoclave

2.2 *Escherichia coli* strains and growth conditions

The *Escherichia coli* strains used in this work are DH5 α and BLR. The DH5 α strain was used for all cloning procedures. It has the following genotype: supE44 Δ lacU169 (Φ 80, lacZ Δ M15) hsdR17 recA1 endA1 gyrA96 thi-1 *relA1*. The BLR strain was used for expression of recombinant protein. BLR has the genotype: F⁻ *ompT hsdS_B(r_B⁻ m_B⁻) gal dcm* (DE3) Δ (srl-recA)306::Tn10 pLysS (Cam^R, Tet^R)

E. coli cells were grown either in sterile LB liquid cultures at 37°C in an orbital shaker at 220 rpm or on LB solid plates at 37°C. Antibiotics were used in the following concentrations: 50 μ g/ml kanamycin, 50 μ g/ml carbenicillin, 50 μ g/ml chloramphenicol, and 5 μ g/ml tetracycline. Permanent stock cultures were made by combining *E. coli* culture in the logarithmic growth phase with an equal volume of sterile 60% glycerol. The stocks were stored at -80°C.

LB- solid and liquid medium

1 % (w/v) Trypton

0.5 % (w/v) Yeast extract

1 % (w/v) NaCl

1.5 % (w/v) Bacto-Agar (only for plates)

Autoclave

2.3 Molecular biology methods

2.3.1 PCR

PCR reactions performed for genotyping of bacteria or plants were performed using the DreamTaq DNA polymerase (Fermentas) according to the manufacturers' instructions. PCR reactions for cloning of DNA fragments were performed using the proof-reading *Pfu* turbo DNA polymerase (Stratagene) according to the manufacturers' instructions.

2.3.2 Extraction of *A. thaliana* genomic DNA

Two to three *A. thaliana* leaves were homogenized in an eppendorf tube using a drill with a blunt drill head and 400 μ l extraction buffer was added. The samples were vortexed 3-4 s and subsequently centrifuged for 2 min at 20,000 x g to remove cell debris. Supernatant was transferred to a fresh tube, 300 μ l isopropanol added and the tube contents mixed. Following a 5 min incubation at room temperature the precipitated DNA was pelleted by a 5 min centrifugation at 20,000 x g. The supernatant was discarded and the pellet was air dried. The dry DNA pellet was subsequently dissolved in 50 μ l H₂O and was either directly used for PCR or stored at -20°C.

Extraction buffer

200 mM Tris-HCl pH 7.5

250 mM NaCl

25 mM EDTA

0.5% (w/v) SDS

Autoclave

2.3.3 Extraction of *A. thaliana* RNA

A. thaliana RNA was extracted using the Trizol reagent (Invitrogen). For this, 50–100 mg plant material was collected in an eppendorf tube and frozen in liquid N₂. The plant material was homogenized using a drill with a blunt drill head and 1 ml Trizol reagent was added. Following 5 min incubation at room temperature, 200 µl chloroform was added and the samples were vortexed for 15 seconds. After 2 min incubation at room temperature the samples were centrifuged at 12,000 x g for 10 min. The supernatant was transferred to a fresh eppendorf tube containing 0.5 ml isopropanol to precipitate the RNA. The samples were incubated for 10 min at room temperature and subsequently centrifuged for 5 min at 12,000 x g. The resulting RNA pellet was washed with ethanol, dried and was re-suspended in 30 µl RNase-free water. The RNA samples were stored at -80°C.

2.3.4 DNase treatment of RNA and first-strand cDNA synthesis

Before making cDNA, isolated RNA was DNase-treated. 2 µg of RNA was combined with 1.5 µl 10x Ambion DNase free buffer, 1 µl DNase I and water to 15 µl in an eppendorf tube. The reaction was incubated for 30 min at 37°C. 2 µl of DNase Inactivation reagent was then added and the sample incubated for 2 min at room temperature. The tube was centrifuged at 11,000 x g for 1 min and the supernatant was transferred to a fresh tube and stored at -80°C.

This DNase-treated RNA was then used for first-strand cDNA synthesis. 2 µg of DNase-treated RNA, 1 µl Oligo-dT Primer (100 nmol) and H₂O to 12 µl was pipetted in a PCR tube. The tube was incubated for 5 min at 70°C and then transferred directly to ice. 1 µl 10 mM dNTPs, 4 µl Biorline Buffer, 2.75 µl H₂O and 0.25 µl Bioscript reverse transcriptase was further added. This reaction mixture was shortly vortexed and subsequently incubated for 1 h at 37°C. The reaction was then stopped by heating to 70°C for 10 min. The cDNA was either stored at -20°C or directly used for PCR.

2.3.5 Isolation of homozygous *A. thaliana* T-DNA insertion mutants

Seeds of T-DNA insertion lines *dldh1-1*, *dldh1-2*, *d2hgdh1-1*, *d2hgdh1-2*, *d2hghd1-3* and *gox3-1* were obtained from the Nottingham Arabidopsis Stock Center. Genomic DNA was extracted and used to test for homozygosity of the T-DNA insertions by PCR. Two sets of PCR primers were used for each line, one that amplified the wild-type gene (WT primers) and one that amplified the gene with a T-DNA insertion (KO primers). Only plants that show a band with the KO primers, but no band with the WT primers are homozygous.

Materials and methods

<u>Name</u>	<u>Gene</u>	<u>Line</u>	<u>WT primers</u>	<u>KO primers</u>
<i>dldh1-1</i>	At5g06580	SALK_026859	D-LDH1-1-F D-LDH1-1-R	SALK-LB D-LDH1-1-R
<i>dldh1-2</i>	At5g06580	SALK_001490	D-LDH1-2-F D-LDH1-2-R	SALK-LB D-LDH1-2-F
<i>d2hgdh1-1</i>	At4g36400	SALK_061383	D-2HGDH1-1-F D-2HGDH1-1-R	SALK-LB D-2HGDH1-1-R
<i>d2hgdh1-2</i>	At4g36400	SAIL_844_G06	D-2HGDH1-2-F D-2HGDH1-2-R	SAIL-LB D-2HGDH1-2-R
<i>d2hgdh1-3</i>	At4g36400	GABI_127F12	D-2HGDH1-3-F D-2HGDH1-3-R	GABI-LB D-2HGDH1-3-R
<i>gox3-1</i>	At4g18360	GABI_523D09	GOX3-1-F GOX3-1-R	GABI-LB GOX3-1-F

<u>Primer</u>	<u>Sequence (5'-3')</u>
D-LDH1-1-F	ATGGCTTTCGCTTCAAATTC
D-LDH1-1-R	GTAGCACACATGCCTCCTATGG
D-LDH1-2-F	ATAAGAAAAGAGGGCGCTGTGG
D-LDH1-2-R	TTAGAAACATACATGAGGAGGAATTAACCTTCCC
D-2HGDH1-1-F	CGAGACAACAGGGAGTGATG
D-2HGDH1-1-R	GTTGGAGAAGAGAGAGTGAGGAAG
D-2HGDH1-2-F	CTTTGTTTGGATTGCGATGA
D-2HGDH1-2-R	CATTGTACAAGCACAAGCCAAT
D-2HGDH1-3-F	ATGATGATGCAGAAATTGAGAAG
D-2HGDH1-3-R	TAATATGCATCCTGCTTCACACAC
GOX3-1-F	TGTGAAACGAGCTGAAGAAGC
GOX3-1-R	CAGCTTGGCCGAGAGGTA
SALK-LB	TGGTTCACGTAGTGGGCCATCG
SAIL-LB	TAGCATCTGAATTCATAACCAATCTCGATACAC
GABI-LB	ATAATAACGCTGCGGACATCTACATTTT
Actin2-F	TAACTCTCCCGCTATGTATGTCGC
Actin2-R	CCACTGAGCACAATGTTACCGTAC

2.3.6 Confirmation of knock-out plants by RT- PCR

It is possible for a plant gene containing a T-DNA insertion line to still have native transcript, especially if the T-DNA is inside an intron where it might be spliced out during RNA processing. The lack of native transcript in knock-out lines must therefore be confirmed by performing RT-PCR. For the *dldh* and *d2ghd* lines this was done using leaf cDNA for the *gox3* line using root cDNA. The primers used are those listed in section 2.3.5 under WT primers. As a positive control, the *actin2* gene was amplified using the Actin2-F and Actin2-R primers

2.3.7 Producing TSS-competent *E. coli* cells

The production of TSS-competent *E. coli* cells was performed according Chung and Miller (Chung et al., 1989). An over-night culture of DH5 α was grown at 37°C in LB-medium without antibiotics. On the following day, 1 ml of the over-night culture was used to inoculate 100 ml LB medium. This culture was grown at 37°C until it reached an OD₆₀₀ of 0.4 and the cells were harvested by a 10 min centrifugation at 4°C and 4,000 x g. The pellet was re-suspended in 20 ml ice cold TSS medium, stored 15 min on ice, aliquated in 50 μ l portions in 1.5 ml eppendorf tubes and frozen in liquid N₂. The cells were stored at -80°C for up to two months.

TSS-Medium

10 % (w/v) PEG- 8000

5 % (v/v) DMSO

20-50 mM MgCl₂

20-50 mM MgSO₄

pH 6.5 with NaOH

Autoclave

2.3.8 Heat-shock transformation of *E. coli* cells

A tube with 50 μ l TSS-competent *E. coli* was thawed on ice. The plasmid DNA to be transformed was added and the tube was incubated on ice for 10 min. The actual transformation event took place during a subsequent heat-shock for exactly 90 s in a water-bath pre-heated to 42°C. After the heat-shock the tube was directly cooled on ice for 5 min. 1 ml LB medium was added and the cells were allowed to recover for 1 h at 37°C. 100 μ l of the transformed cells were then plated on a solid LB plate containing appropriate antibiotics. The rest of the cells were pelleted at 20,000 x g for 30 s. The pellet was re-suspended in 100 μ l LB medium and evenly spread on an LB plate containing appropriate antibiotics and incubated over night at 37°C.

2.3.9 Isolation of *E. coli* plasmid DNA

Plasmid DNA was isolated from 5 ml over-night cultures using the Quantum Prep Plasmid Miniprep Kit (BioRad), according to the manufacturers' instructions. In a slight modification of the protocol, the binding of the DNA was done on home-made binding matrix in re-usable columns.

Binding matrix

5.2 M Guanidin-HCl

20 mM Tris-HCl

0.15 g/ml Diatomaceous earth

2.3.10 Separation of DNA by agarose gel electrophoresis

All agarose gel electrophoreses for DNA separation was performed as previously published (Sambrook and Russel, 2002). Briefly, 0.8-2% (w/v) agarose was dissolved in 1 x TAE buffer by heating in a microwave. Ethidium bromide was added to the melted agarose solution at a

relationship of 1:20,000. The solution was then poured in a plastic mold with a comb placed inside as to create pockets inside the gel. When the gel had been solidified the comb was removed and DNA, mixed in a loading buffer, was loaded in the pockets. To enable subsequent size determination of the fragments 5 µl of the 1 kb DNA ladder (Invitrogen) was also loaded on the gel. The use of the 1 kb ladder also enables the optical quantification of DNA bands by comparing the intensity of the 1.6 Kb band, containing 10 ng DNA per µl, with a sample of unknown concentration. The loaded DNA was run at 1.5 mA/cm² in 1 x TAE buffer. Through the intercalation of ethidium bromide with DNA it could be visualized on a UV table.

50 x Tris-Acetate-Buffer (TAE)

2 M Tris/ HAc, pH 7.5

50 mM EDTA

2.3.11 DNA elution from agarose gels

When cloning, it was frequently needed to elute DNA from an agarose gel. This was achieved by quickly cutting out an agarose gel piece containing the DNA on top of a UV-table. The DNA inside the agarose gel was isolated using the QIAquick Gel Extraction Kit (Qiagen) according to the manufacturers' instructions.

2.3.12 DNA sequencing

Sequencing reactions were performed on a thermocycler using the Big Dye Terminator V 3.1 cycle sequencing kit (Applied Biosystems). After the sequencing reaction each sample was diluted with 10 µl HPLC-grade H₂O. The readout of the sequence was performed by the Institute of Genetics at University of Cologne using an ABI 3730 Genetic Analyser (PE Applied Biosystems GmbH). The resulting sequences were analyzed using the Chromas LITE version 2.0.

Sequencing mix

10-100 ng DNA

0.5 µl Primer (10 µmol/µl)

1 µl Buffer

2 µl BigDye 3.1

To 10 µl with HPLC-grade H₂O

Sequencing reaction

96°C for 20 sec

96°C for 10 sec

55°C for 10 sec

60°C for 4 min

4°C ∞

Step 2-4 was repeated a total of 35 times.

2.3.13 Cloning of the three candidate enzymes

The pET16b expression vector (Novagen) was used to clone the entire *AtGOX3* coding sequence and the part of *AtD-LDH* and *AtD-2HGDH* coding sequence that encode the mature enzymes. This was done through PCR amplification with *Pfu* Turbo DNA polymerase (Stratagene) with plant cDNA as a template and either *AtGOX3*-CDS-F and *AtGOX3*-CDS-R or *AtD-LDH*-CDS-F and *AtD-LDH*-CDS-R or *AtD-2HGDH*-CDS-F and *AtD-2HGDH*-CDS-R primers, for *AtGOX3*, *AtD-LDH* and *AtD-2HGDH*, respectively. For *AtD-LDH* and *AtD-2HGDH* leaf cDNA was used and for *AtGOX3* root cDNA. The PCR fragments were cloned into the pCR-Blunt II-Topo vector (Invitrogen) according to the manufacturers' instructions, transformed into DH5 α cells and selected on kanamycin. The resulting colonies were tested for presence of the correct constructs by colony PCR and the correct clones were used to start 5 ml overnight cultures in LB with antibiotics.

The plasmids were isolated from these cultures and the inserts were sequenced to confirm that no mutations had occurred. The inserts were further cut out of the vector with BamHI, using BamHI restriction sites had been introduced through the PCR primers. The inserts were ligated into a BamHI linearized, dephosphorylated, pET16b vector. Restriction enzyme digestion, DNA dephosphorylation and ligation were all performed according to the manufacturers' instructions (Fermentas). The resulting plasmids, pET16b-*AtD-LDH*, pET16b-*AtD-2HGDH* and pET16b-*AtGOX3* were sequenced – to assure that no mutation had been introduced in the inserts – and were then transformed in the BLR *E. coli* strain (Novagen) and selected on tetracycline, chloramphenicol and carbenicillin.

<i>AtD-LDH</i> -CDS-F	GGATCCGGCGATAGCTGCCTCCG
<i>AtD-LDH</i> -CDS-R	GGATCCTTAGAAACATACATGAGGAGGAATTAAC
<i>AtD-2HGDH</i> -CDS-F	GGATCCGGTGTCAGGCTTTGTG
<i>AtD-2HGDH</i> -CDS-R	GGATCCTTAGTTGGAGAAGAGAGAGTGAGG
<i>AtGOX3</i> -CDS-F	GGATCCGATGGAGATAACAAACGTGATGGA
<i>AtGOX3</i> -CDS-R	GGATCCCTACAGCTTGGCCGAGAGG

2.4 Biochemical methods

2.4.1 Expression and purification of recombinant proteins

The vectors pET16b-*AtD-LDH*, pET16b-*AtD-2HGDH* and pET16b-*AtGOX3* generate fusion proteins with an N-terminal His tag, facilitating the purification of the recombinant proteins. Pre-cultures with the BLR cells transformed with these vectors were started in LB containing carbenicillin, chloramphenicol, and tetracycline and grown overnight. These pre-cultures were used to inoculate 1 l of fresh LB medium in a relationship of 1:50. The cultures were grown at 37 °C in an orbital shaker at 220 rpm until the culture reached an OD₆₀₀ of 0.6. Expression of recombinant *AtD-LDH*, *AtD-2HGDH* and *AtGOX3* was induced by adding 1 mM isopropyl β -D-thiogalactopyranoside to the culture. The *AtD-LDH* and *AtD-2HGDH* cultures were then allowed to grow for 1 h before being harvested by centrifugation at 4,000 x g for 10 min. The *AtGOX3* culture was allowed to grow for 4 h before being harvested. The cell

Materials and methods

pellets were then resuspended in 35 ml of extraction buffer and incubated at 4°C for 15 minutes to allow the lysozyme to take effect. To further disrupt the cells the solutions were sonicated 6 times for 30 s, with cooling in between, using a sonicator set at max output, 95% duty cycle and using a blunt tip. The disrupted cells were centrifuged at 10,000 x *g* for 15 min at 4°C to remove cell debris. The supernatant was used for protein purification using immobilized metal ion chromatography on Ni²⁺-nitrilotriacetic acid-agarose (Ni²⁺-NTA, Qiagen).

For AtD-LDH and AtD-2HGDH purification, 2 ml Ni²⁺-NTA slurry was equilibrated with wash buffer and the *E. coli* supernatant passed over the column through gravitational flow to allow for protein binding. The column was subsequently washed with 10 ml wash buffer. Bound protein was eluted using 2 ml of elution buffer. The first 900 µl emanating from the column were discarded as they contained no protein. To remove damaging imidazole and to concentrate the protein samples they were spun on Centricon YM-30 spin columns (Amicon) and re-suspended in 20 mM Tris-HCl pH 8.0. The purified protein samples were kept on ice, in the dark and directly used for enzyme measurements.

Extraction buffer

20 mM Tris-HCl pH 8.0
0.5 mg/ml PMSF
~2 mg DNase
~2 mg RNase
~2 mg Lysozyme
Water to 35 ml

Wash buffer

100 mM Na₂PO₄ pH 8.0
300 mM NaCl
10 mM Imidazole

Elution buffer

100 mM Na₂PO₄ pH 7.2
250 mM Imidazole

For purification of recombinant AtGOX3, 2 ml Ni²⁺-NTA slurry was equilibrated with wash buffer 1. The *E. coli* supernatant was passed over the column through gravitational flow to allow for protein binding and was subsequently washed with 4 ml wash buffer 1 and 4 ml wash buffer 2. The protein was eluted using 2 ml elution buffer 1. The first 900 µl emanating from the column were discarded as they contained no protein. To remove damaging salt and imidazole the purified protein was passed over a PD-10-column (GE Healthcare) pre-equilibrated with elution buffer 2. The protein was eluted by adding one volume of elution buffer 2. The purified enzyme was kept on ice, in the dark and used directly for enzyme measurements.

Extraction buffer

20 mM Tris-HCl pH 8.0
500 mM NaCl
0.5 mg/mL PMSF
~2 mg DNase
~2 mg RNase
~2 mg Lysozyme
1 mM DTT
Water to 35 ml

Wash buffer 1

20 mM Tris-HCl pH 8.0
500 mM NaCl
1 mM DTT
40 mM Imidazole

Wash buffer 2

20 mM Tris-HCl pH 8.0
500 mM NaCl
1 mM DTT
80 mM Imidazole

Elution buffer 1

20 mM Tris-HCl pH 8.0
 500 mM NaCl
 1 mM DTT
 300 mM Imidazole

Elution buffer 2

20 mM Tris-HCl pH 8.0
 1 mM DTT

2.4.2 SDS-polyacrylamide gel electrophoresis (SDS-PAGE)

The size-dependent separation of denatured protein was performed according to Laemmli (Laemmli, 1970). The polyacrylamide gels required for this purpose were cast in a minigel system (System 2050 Midget, Pharmacia). In the finished gels up to 20 µl of sample was loaded in each well. To be able to estimate the protein size, prestained molecular weight markers were used (Fermentas). The gels were run at 10 mA until all protein had entered the separation gel and were subsequently run at 25 mA.

4 x Stacking gel buffer

0.5 M Tris-HCl pH 6.8
 0.4 % (w/v) SDS

Acrylamide stacking gel

25 % (v/v) 4 x Stacking gel buffer
 15 % (v/v) Acrylamid-Bisacrylamid-Solution (37.5 : 1)
 0.3 % (w/v) TEMED
 0.06 % (w/v) APS

4 x Seperation gel buffer

1.5 M Tris-HCl pH 8.8
 0.4 % (w/v) SDS

12.5% Acrylamide separation gel

25 % (v/v) 4 x Seperation gel buffer
 42 % (v/v) Acrylamid-Bisacrylamid-Solution (37.5 : 1)
 0.05 % (w/v) TEMED
 0.05 % (w/v) APS

10 x Running buffer

250 mM Tris
 192 mM Glycin
 0.5 % (w/v) SDS

5 x Sample buffer

312.5 mM Tris-HCl pH 6.8
 50 % (v/v) Glycerin
 12.5 % (w/v) SDS
 12.5 % (v/v) β-Mercaptoethanol
 0.00625 % (w/v) Bromphenolblue

2.4.3 Protein determination and Coomassie staining

Protein concentration was determined according to the method of Bradford (Bradford, 1976). 200 µl Roti-Quant solution (Roth) was mixed with 800 µl H₂O and 2 µl sample. After a 10 min incubation at room temperature the Abs₅₉₅ was measured. The absorption at this wavelength is proportional to the protein amount in the sample. A standard curve was made using samples with known protein concentration. This was then used to calculate the protein content of the unknown samples.

Proteins on polyacrylamide gels were visualized through over-night incubation with a staining solution containing 0.5% (w/v) Coomassie-Brilliant-Blue (Serva-Blue G250, Fa. Serva) in 80% (v/v) methanol and 20% (v/v) acetic acid. The gel was further de-stained for a few hours using a solution of 40% (v/v) methanol, 10% (v/v) acetic acid and 50% (v/v) water.

2.4.4 Western-Blot

Transfer of proteins from polyacrylamide gels onto a PVDF-membrane (BioRad) was achieved using a semi-dry-blot transfer chamber (Carboglass, Schleicher & Schuell). Anode and cathode buffers were purchased from Roth (RotiBlot-System, Roth) and the manufacturers' instructions were used for the setup and protein transfer. The protein transfer was achieved by applying 1 mA/cm² of gel area for 2 h. Following transfer, the membrane was incubated in blocking solution for at least one hour. The blocking solution was then exchanged for the primary rabbit anti-His antibody (Qiagen), which was diluted 1:2,500 in blocking buffer. Following an incubation of 1-3 h the membrane was washed twice for 10 min with TBST-T and once for 10 min with 1x TBS. The membrane was then incubated 1-2 h with an alkaline phosphatase- conjugated goat anti-rabbit antibody (Sigma) diluted 1:3,000 in blocking buffer. After repeating the TBST-T and 1x TBS wash steps the positions of the His-tagged proteins were visualized by incubating the membrane 30-120 s in the staining solution.

Buffer A

100 mM Tris- HCl pH 9.5
100 mM NaCl
5 mM MgCl₂

10x TBS

100 mM Tris-HCl pH 7.4
1.5 M NaCl

TBST-T

10% (v/v) 10x TBS
0,2% (v/v) Triton X-100
0.05% (v/v) Tween 20

Staining solution

10 ml Buffer A
33 µl 5% (w/v) BCIP in DMF
66 µl 5% (w/v) NBT in 70% DMF

Blocking solution

4% (w/v) Milk powder in 1x TBS

2.4.5 Native-PAGE

In-gel analysis of enzyme activity was performed using native-PAGE. The buffers and methods for making the gels were prepared according to Laemmli (1970) (section 2.4.2), with the exception that SDS and β-mercaptoethanol was excluded from all buffers. Plant tissue was ground in liquid N₂ in the presence of an equal amount (v/w) of 20 mM Tris-HCl (pH 8.0) containing 0.05% Triton X-100 and 1 mg/ml PMSF. The homogenate was clarified by centrifugation at 4°C and 20,000 x g for 5 min and the protein concentration in the extract was determined according to Bradford (section 2.4.3). Up to 50 µg protein was loaded in each well on an 8% native-gel and run for 2.5 h at 100 V and 4°C. The gels were subsequently cut in slices, when needed, and stained in 5 ml of medium containing 50 mM K₂PO₄ at pH 8.5, 5 mM substrate, 0.05% nitro blue tetrazolium (NBT) and either 150 µM PMS or 1 mM NAD⁺ or NADP⁺. The reactions were allowed to continue at 30°C in the dark for a time period between 2 h and 20 h, depending on which enzyme was assayed.

2.4.6 Mitochondrial isolation

Mitochondrial isolation and purity testing of the preparations was performed as previously described (Keech et al., 2005). In brief, 5 g of *A. thaliana* root material was ground in a mortar together with 0.5 g of acid-washed seesand and 20 ml grinding buffer. The pulp was filtered through 2 layers of Miracloth and subsequently centrifuged at 2,500 x g for 5 min to remove cell walls and plastids. The supernatant was transferred to a new tube and centrifuged for 15,000 x g for 15 min to pellet the mitochondria. The resulting pellet was gently re-suspended in 20 ml wash buffer and subsequently centrifuged at 15,000 x g for 15 min. Supernatant was removed and the mitochondrial pellet was re-suspended in 200 µl wash buffer. All steps in this purification process were performed on ice or at 4°C. The enriched mitochondrial preparation was analyzed by Western blot using antibodies raised against the cytosolic malate dehydrogenase from *Ananas comosus*, which react with the cytosolic and chloroplastic isoforms but not with the mitochondrial one (donated by Florencio Podestá, University of Rosario).

Grinding buffer

0.3 M Sucrose
60 mM TES
10 mM EDTA
10 mM K₂PO₄ pH 8.0
25 mM Tetra sodium pyrophosphate
1 mM Glycine
1 % (w/v) PVP-40
1 % (w/v) Defatted BSA

Wash buffer

0.3 M Sucrose
10 mM TES
1 mM EDTA
10 mM K₂PO₄ pH 7.5

Added just before grinding

50 mM Na-ascorbate
20 mM Cysteine

2.4.6 Size exclusion chromatography

The native molecular masses of recombinant proteins were estimated by gel filtration chromatography on an ÄKTA purifier system (GE Healthcare), using a Superdex 200 10/300 GL column (GE Healthcare). The column was equilibrated with 20 mM Tris-HCl (pH 8.0) and calibrated using molecular mass standards. The samples and the standards were applied separately in a final volume of 10 µl at a constant flow rate of 0.5 ml/min.

2.4.7 Analysis of prosthetic groups

The prosthetic group of AtD-LDH and AtD-2HGDH were released from the purified recombinant proteins (0.7 mg) by heating at 95°C for 15 min, and the denatured protein was removed by centrifugation. The resulting supernatants, containing the prosthetic group, were analyzed using a Hach DR 5000 UV-visible spectrophotometer in 2 nm steps. Furthermore, the resulting supernatants (20 µl), riboflavin (2 µl, 2 mM), FMN (2 µl, 2 mM), and FAD (2 µl, 2 mM) were spotted on cellulose 300 thin layer chromatography plates and run in the dark with buffer A consisting of 5% Na₂HPO₄ in aqueous solution or, alternatively, with buffer B consisting of 1-butanol:HAc:water (4:1:5). Sample positions were subsequently

detected under UV light. The same samples were analyzed on a native polyacrylamide gel (0.75 M Tris, pH 8.45) consisting of an 8% T, 3% C stacking gel and an 18% T, 6.1% C separation gel. In this context T designates the total amount of acrylamide and bis-acrylamide in a gel whereas C designates how many percent of the total that is made up by bis-acrylamide. The gel was run at 100 V in darkness using as anode buffer 0.2 M Tris (pH 8.9) and as cathode buffer 0.1 M Tris and 0.1 M Tricine (pH 8.25). The samples were subsequently identified under UV-light.

2.5 Enzyme assays

All enzyme assays were conducted at 25°C using a Tecan Infinite 200 plate reader. A base line was determined by monitoring the reaction mixes for 4 min before the reactions were started through the addition of purified enzyme. The standard reaction mixture for each enzyme is indicated below.

AtD-LDH and AtD-2HGDH standard reaction

50 mM K₂PO₄ pH 8.75

10 mM substrate

Co-factor

0.2-20 µg enzyme

Water to 200 µl

AtGOX3 standard reaction

100 mM TRIS-HCl pH 7.5

10 mM substrate

Co-factor

1-2 µg enzyme

0.5 mM EDTA

5 mM MgCl₂

0.01 mM FMN

Water to 200 µl

2.5.1 Co-factor analysis

The best co-factor for the enzymes was evaluated in the standard reaction mixes with varying the type of co-factor and detection wavelength. The different co-factors used in these experiments were as follows: Cytochrome c (200 µM used, detected at 550 nm, extinction coefficient $\epsilon = 18.6 \text{ cm}^{-1} \text{ mM}^{-1}$), 2,6 dichlorophenol-indophenol (DCIP) (200 µM used, detected at 600 nm, extinction coefficient $\epsilon = -22 \text{ cm}^{-1} \text{ mM}^{-1}$, always used together with 3 mM phenazine methosulfate (PMS)), NAD(P)H (1 mM used, detected at 340 nm, extinction coefficient $\epsilon = 6.22 \text{ cm}^{-1} \text{ mM}^{-1}$). When assaying with cytochrome c, the resulting absorption was divided by 2 because 2 moles of cytochrome c are reduced for each mole of substrate oxidized. Moreover, to measure enzyme activity with O₂ the 2-keto-acid product was detected through addition of 4 mM phenylhydrazine. The resulting phenylhydrazones were detected at 324 nm and their extinction coefficients are: Glyoxylate-phenylhydrazone $\epsilon = 17 \text{ cm}^{-1} \text{ mM}^{-1}$, Pyruvate-phenylhydrazone $\epsilon = 10.4 \text{ cm}^{-1} \text{ mM}^{-1}$, 2-hydroxybutyrate-phenylhydrazone $\epsilon = 13 \text{ cm}^{-1} \text{ mM}^{-1}$.

2.5.2 pH optimum and substrate screen

The pH optimum of the enzymes was further determined by varying the pH of the buffer between 6.0 and 9.5 while using the best co-factor and substrate for each of the enzymes. For AtD-LDH this was D-lactate and either cyt c or DCIP, for AtD-2HGDH it was

D-2-hydroxyglutarate with DCIP and for AtGOX3 it was glycolate and either O₂ or DCIP. The substrate range of the enzymes was assayed using 10 mM substrate at the pH optimum using the preferred co-factor for each enzyme. When needed, substrates were neutralized with NaOH before use in the assays.

2.5.3 Catalytic constants

The K_m and k_{cat} values for the substrates were determined using the best co-factor at the pH optimum (8.75 for AtD-LDH and AtD-2HGDH and 7.5 for AtGOX3). All parameters were kept constant except for the substrate concentration which was varied between 5 μ M and 50 mM. Data was collected from at least two different enzyme batches, with each containing at least triplicate determinations of each data point. All constants were calculated by fitting the data to a nonlinear regression plot (SigmaPlot).

2.6 *In silico* protein analysis

2.6.1 Phylogenetic trees

Protein sequences were downloaded either from UniProt (<http://www.uniprot.org/>) or NCBI (<http://www.ncbi.nlm.nih.gov/>). For phylogenetic analysis the sequences were aligned using ClustalW (Thompson et al., 1994), the alignment was curated using Gblocks (Castresana, 2000) and the phylogenetic trees were constructed by the neighbor-joining method using BioNJ (Gascuel, 1997) and visualized using Dendroscope (Huson et al., 2007).

2.6.2 Co-expression analysis

Genes that are co-expressed with At4g36400 were identified using the ATTED-II data base (Obayashi et al., 2009). The Mutual Rank, which is based on weighted Pearson correlation coefficients, is used to assess the extent of gene co-expression. The Mutual Rank is calculated as the geometric mean of the correlation rank of gene A to gene B and of gene B to gene A. The Gene Ontology annotations were manually actualized and corrected.

2.6.3 Catalytic site analysis

Protein crystal structures and homology models for analysis of the catalytic site were downloaded from the SWISS-MODEL repository (<http://swissmodel.expasy.org/repository/>) and visualized using the SWISS-PdbViewer (Guex and Peitsch, 1997). The SWISS-MODEL repository is an initiative to provide annotated 3D models for all sequences in Swiss-Prot (Kiefer et al., 2009). In this initiative, proteins of unknown structure are modeled based on a known crystal structure of a homologous protein that is automatically sought out based on its suitability for the modeling process.

2.7 Metabolite and fluorescence measurements

2.7.1 Metabolite analysis by GC-MS

Metabolite analysis was performed as previously published (Fiehn, 2007). Control samples were taken in the middle of the light period of 5-week old short-day grown wild-type and *d2hghdh* plants. At the end of the light period the plants were transferred to complete darkness for 4 days. During this dark incubation further samples were taken after 16 hours of darkness, which is the normal length of the night, and subsequently after 24, 48, 72 and 96 hours of extended darkness. For each time point and genotype 12 entire rosettes were collected and divide up on 4 samples with 3 whole rosettes each. Samples were directly frozen in liquid N₂ and stored at -80°C until extracted. The extraction proceeded by grinding the plant sample in liquid N₂. 50 mg of the sample powder was transferred to a new tube and the rest was stored at -80°C for future analysis. The metabolites were extracted from the 50 mg sample powder using 1.5 ml of extraction buffer pre-cooled at -20°C (H₂O:methanol:CHCl₃ in the proportions 1:2.5:1 and containing 15 µl of 60 mM ribitol per 45 ml of buffer as a standard). The samples were quickly vortexed for 10-20 seconds and then placed immediately on crushed ice at 0°C with NaCl and stored there for a maximum of 10 min while preparing the rest of the samples. All tubes were then shook for 6 min at 4°C and centrifuged for 2 min at 20,000 x g at room temperature. One ml of the supernatant was placed in a new eppendorf tube which was stored at -80°C until analyzed.

The tubes were vortexed for 10 sec and 200 µl of the solution was transferred into a glass insert. 5 µl of the Phenylalanine-d5 + Valine-d8 mixture (500 µM) was added to all samples which were subsequently dried in a speedvac concentrator to complete dryness. Samples were stored at -20°C in a dessiccator prior to analysis. The following steps are done automatically by the autosampler. 10 µl of methoxyamine hydrochloride (20 mg/ml) was added to the dried fraction. Samples were incubated for 90 min at 30°C with continuous shaking, 90 µl MSTFA added followed by a 30 min incubation at 37°C with continuous shaking. 100 µl of the mixture was transferred in a glass insert. After 120 min at room temperature the samples were analyzed using a GC/MS instrument. The data was evaluated using the ChemStation program. To be able to analyze the samples in scan mode and so simultaneously screen for large numbers of metabolites a databank with the retention times and different ions was set up with all metabolites of interest. Using this databank it was possible to automatically evaluate the runs.

2.7.2 Imaging-PAM measurements

Changes in the plant photosynthetic efficiency were measured using an IMAGING-PAM Maxi (Heinz-Walz Instruments). Plants were incubated in the dark for at least 20 minutes immediately before measurement. Basic variables, such as variable fluorescence (Fv), current fluorescence yield (Ft), maximal fluorescence yield (Fm'), basic fluorescence in dark-adapted leaves (F₀) and maximal fluorescence in dark-adapted leaves (Fm) were determined and used to calculate the nonphotochemical quenching (qN), photochemical quenching (qP) and the Fv/Fm ratio (Schreiber et al., 1986).

3. Results

3.1 Characterization of the enzyme encoded by At5g06580

3.1.1 Identification of the candidate enzyme

Recently, a mitochondrial GDH encoded by At5g06580 in *A. thaliana* was reported (Bari et al., 2004; Niessen et al., 2007). However, the enzymatic properties of this enzyme were only partially characterized. Thus, to investigate whether the At5g06580 gene product is a true glycolate dehydrogenase and to determine whether it can be used for the chloroplastic GMK pathway (Fig. 5), a full characterization of the enzyme was undertaken.

3.1.2 Phylogenetic analysis

A phylogenetic analysis was conducted for the enzyme encoded by At5g06580 to get a better idea of the distribution of orthologous sequences. The At5g06580 protein sequence was used for a basic local alignment search tool (BLAST) search in the NCBI databank (<http://www.ncbi.nlm.nih.gov/>). Representative sequences from plants, animals and fungi were selected and used to construct a phylogenetic tree through the neighbor joining method (Fig. 7). A few homologous proteins were found in bacteria, such as the *E. coli* glycolate oxidase subunit GlcD, and *Synechocystis sp. PCC 6803* GlcD, but these shared so few conserved residues that a meaningful alignment with the other sequences could not be done and they were thus left out. The protein is well-conserved in eukaryotes, being found in plants, animals, unicellular and multicellular fungi. Interestingly, each organism contains only one sequence of high similarity. Moreover, the closest ortholog to At5g06580 in both mammals (Flick and Konieczny, 2002) and unicellular fungi (Gregolin and Singer, 1963; Lodi and Ferrero, 1993; Lodi et al., 1994) are cytochrome c- dependent D-lactate dehydrogenases (EC 1.1.2.4). Due to the close homology of At5g06580 to D-lactate dehydrogenases it will be referred to as AtD-LDH for Arabidopsis thaliana D-lactate dehydrogenase in the remainder of this work.

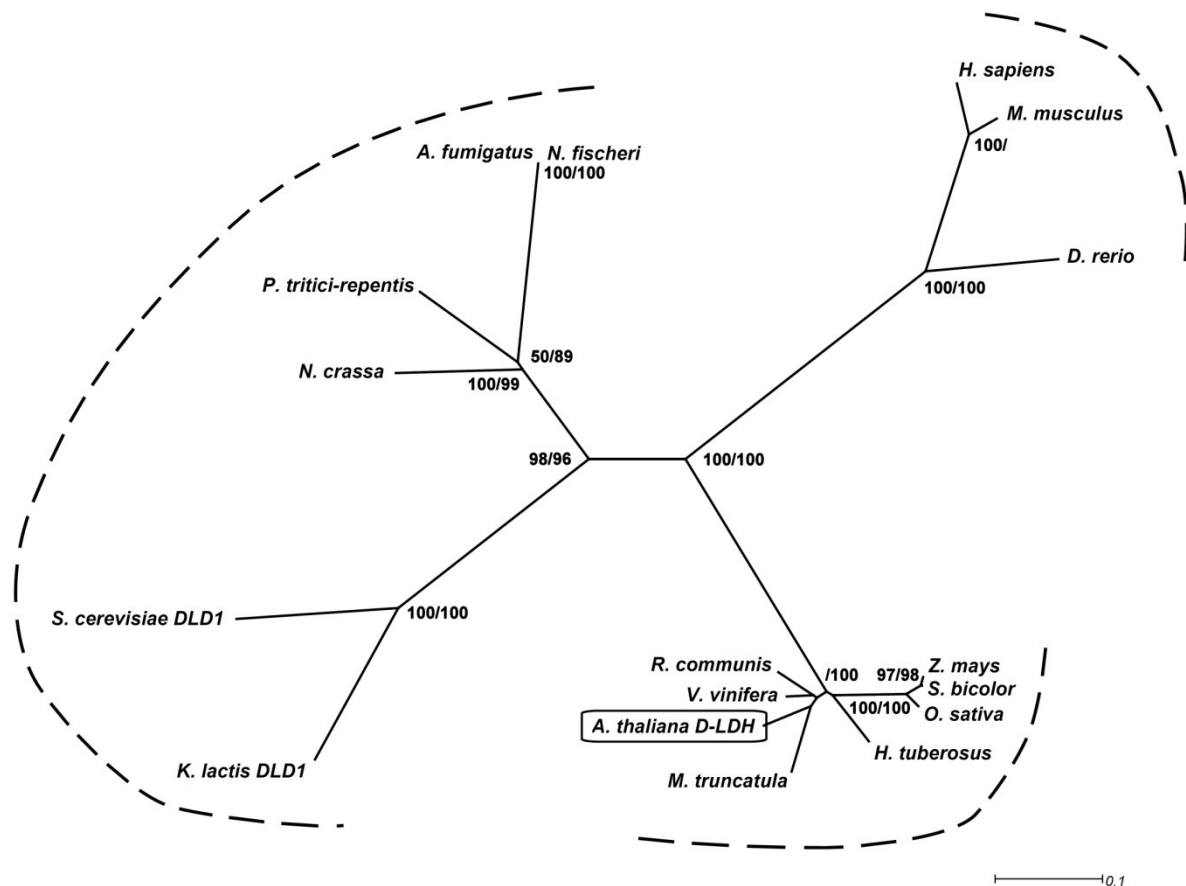


Figure 7. Phylogenetic relationships of the At5g06580 (AtD-LDH) protein sequence. Protein sequences were aligned using ClustalW2. The phylogenetic tree was constructed by the neighbor-joining method using BioNJ and visualized using Dendroscope (Huson et al., 2007). Bootstrap values at the nodes represent the percentage support from 500 replicates with neighbor-joining and maximum likelihood, respectively. Only bootstrap values over 50% are shown. The following sequences are included: *Arabidopsis thaliana* D-LDH (Q94AX4); *Helianthus tuberosus* (EL444323, EL437620, and EL440912); *Zea mays* (B4G146); *Sorghum bicolor* (Sb02g003640); *Oryza sativa* (B9FVM4); *Ricinus communis* (B9SDP2); *Vitis vinifera* (A7Q036); *Medicago truncatula* (BF636550, BF636365, BF636697, BQ123259, CA858805, CA858793, and DY617162); *Homo sapiens* (Q86WU2); *Danio rerio* (Q803V9); *Mus musculus* (Q7TNG8); *Saccharomyces cerevisiae* DLD1 (P32891); *Kluyveromyces lactis* (Q12627); *Neurospora crassa* (Q7SE05); *Pyrenophora tritici-repentis* (B2WBK4); *Aspergillus fumigatus* (Q4WE96); and *Neosartorya fischeri* (A1D828).

To gain further insights into the conserved regions in these enzymes, an alignment between AtD-LDH and the human and yeast orthologs was produced using ClustalW2 (Fig. 8). While the N-terminal domains of the three enzymes are rather heterogeneous there are patches of very high homology throughout the sequence. Moreover, all three enzymes retain a predicted FAD binding domain, indicated in yellow, and a C-terminal FAD-linked oxidase domain, indicated by red in Fig. 8.

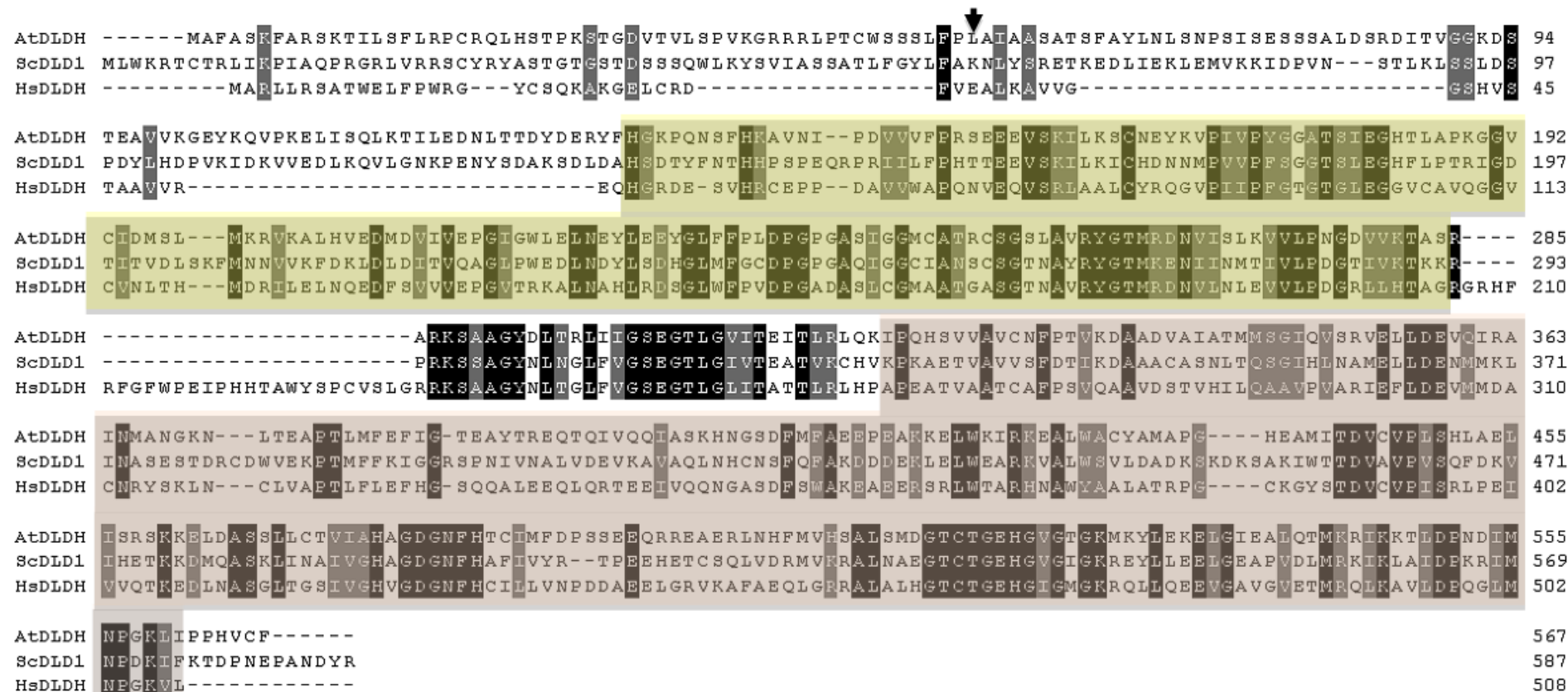


Figure 8. Multiple sequence alignment of AtD-LDH and homologs. Protein sequences from *Arabidopsis thaliana* D-LDH (Q94AX4), *Saccharomyces cerevisiae* DLD1 (P32891) and *Homo sapiens* DLD (Q86WU2) were aligned using the ClustalW2 algorithm (<http://www.ebi.ac.uk/Tools/clustalw2/index.html>). Identical amino acids are indicated in black while similar amino acids are indicated in grey. The FAD binding domain and FAD-linked oxidase domain predicted by Pfam (<http://pfam.sanger.ac.uk/>) are indicated in yellow and red, respectively.

3.1.3 Cloning, heterologous expression and purification of AtD-LDH

By using the MitoProt II v1.101 software (Claros and Vincens, 1996), the At5g06580 gene product was predicted to have a mitochondrial targeting sequence ending before amino acid residue 53. To express the mature protein the cDNA of At5g06580 was cloned starting at the codon following downstream of the predicted processing site (indicated by an arrowhead in Fig. 8). The sequence was cloned in frame with the N-terminal His-tag of the pET-16b expression vector, and subsequently expressed in the *E. coli* BLR strain by IPTG induction. *E. coli* extracts from the induced and uninduced cells were analyzed by SDS-polyacrylamide gel electrophoresis (SDS-PAGE). A band of approximately 61 kDa, closely corresponding to the predicted 59 kDa, was clearly detected in the extract from the induced cells (Fig. 9, lane 2), but not in extracts from the uninduced ones (Fig. 9, lane 1). The protein corresponding to this band was purified to apparent homogeneity (Fig. 9, lane 4) by Ni²⁺-NTA affinity chromatography with yields of approximately 2 mg protein per liter of *E. coli* culture.

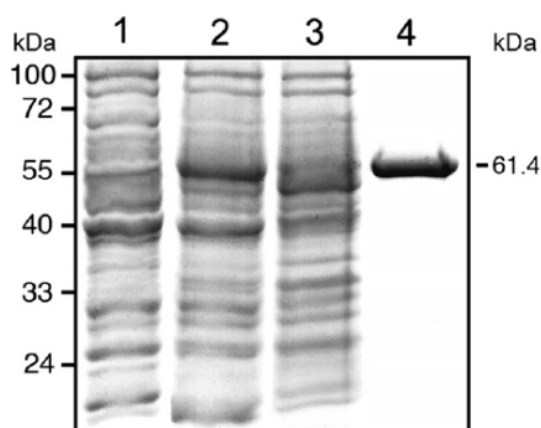


Figure 9. Purification and analysis by gel electrophoresis of recombinant enzyme. Lane 1, 20 μg of uninduced cell culture lysate. Lane 2, 20 μg of cell culture lysate after 2 h of induction with isopropyl β -D-thiogalactopyranoside. Lane 3, 20 μg of Ni²⁺-NTA column flow through. Lane 4, 5 μg of purified recombinant D-LDH. The molecular mass of the purified protein is indicated on the right. Molecular weight markers run in parallel are indicated on the left.

3.1.4 Quaternary structure of the enzyme

Purified AtD-LDH was analyzed by native-PAGE and displayed an apparent size of approximately 140 kDa (Fig. 10). Gel-filtration electrophoresis indicated a molecular weight of 135 kDa. These results show that AtD-LDH forms homodimers. Additionally, when performing in-gel enzymatic assays with glycolate and D-lactate as substrates, a band of activity occurs at 140 kDa showing that the homodimer comprises the catalytically active form of the enzyme (Fig. 10). It is also worth noting that the rate of enzymatic conversion of D-lactate in the gels was much greater than that for glycolate since only 1/10th of the enzyme was needed with D-lactate to achieve the same staining as with glycolate (Fig. 10).

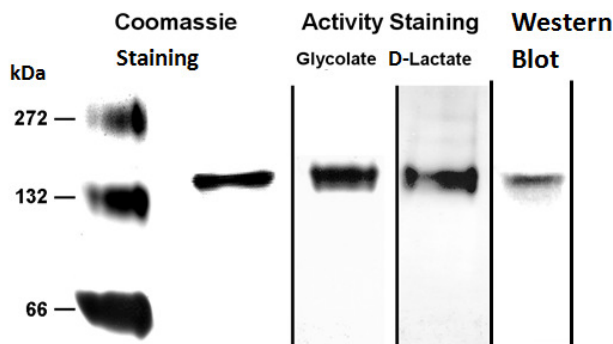


Figure 10. Native-PAGE stained for AtD-LDH activity. Approximately 10 μg of purified enzyme was loaded for Coomassie staining and the glycolate dehydrogenase activity staining, whereas 1 μg protein was loaded for the D-LDH activity staining assay and Western blot. Molecular weight markers were run in parallel and stained with Coomassie blue.

3.1.5 Analysis of the prosthetic group

The purified AtD-LDH was brightly yellow, which is indicative of a flavin prosthetic group. This group was isolated from the enzyme through boiling with subsequent removal of denatured protein by centrifugation. The visible absorption spectrum for the unknown sample and FMN and FAD standards was then recorded (Fig. 11). Both the enzyme and standards displayed absorption maxima at 375 and 450 nm, confirming the presence of a flavin prosthetic group in the enzyme.

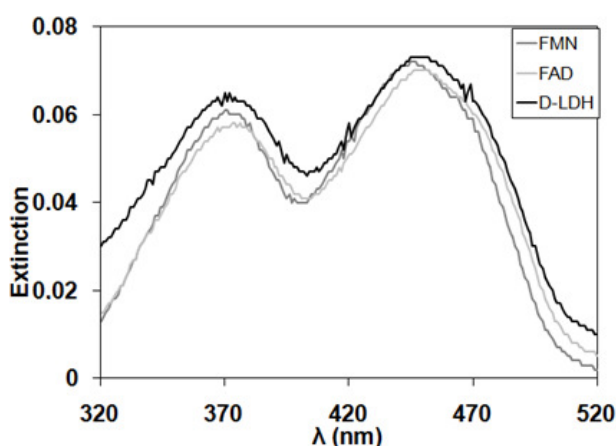


Figure 11. Absorption spectra of prosthetic group and standards. The visible spectrum of FMN, FAD and the isolated enzyme prosthetic group was recorded in 2 nm steps between 320 and 520 nm.

To determine the identity of the molecule bound to the enzyme, the prosthetic group was analyzed by thin-layer chromatography and by a self-developed polyacrylamide gel electrophoresis protocol, using FAD, FMN and riboflavin as standards. For both methods, the R_f value of the enzyme prosthetic group was highly similar to that of FAD and not to that of FMN or riboflavin (Table 3).

Table 3. Chromatographic separation of the prosthetic group. The enzyme prosthetic group was released by boiling and was spotted together with standards on a cellulose thin layer chromatography plate. The plates were run in the dark with the buffer systems (A) 5% Na₂HPO₄ in aqueous solution and (B) 1-butanol:HAc:water in a 4:1:5 relationship. Sample positions were subsequently detected under UV. Samples were also analyzed on an 18% polyacrylamide gel and run in the dark with subsequent determination of sample position under UV light. The values presented represent the determined R_F-values.

	Flavin standard			AtD-LDH
	FMN	Riboflavin	FAD	Group
TLC A	0.72	0.38	0.61	0.58
TLC B	0.22	0.45	0.07	0.07
PAGE	0.94	0.09	0.82	0.80

Additionally, using FAD isolated from 120 µg of boiled enzyme in a final volume of 500 µl the absorption at 450 nm was 0.05. Taking into account that the extinction coefficient of FAD is 11.3 mM⁻¹ cm⁻¹ and the calculated molecular mass of the recombinant enzyme is 59 kDa, it was calculated that each mole of enzyme binds one mole of FAD.

3.1.6 Co-factor analysis and pH optimum

To characterize the enzymatic activity of purified AtD-LDH, the pH optimum as well as the best electron acceptor was determined. The AtD-LDH oxidative activity was assayed using D-lactate and glycolate as substrates and the reductase activity was assayed using pyruvate and glyoxylate as substrates. The acceptor molecules used were NAD⁺, NADP⁺, cytochrome c or DCIP for the oxidation of the substrates and NADH or NADPH for the reduction of substrates. The enzymatic activity with the acceptors NAD(P)⁺ and NAD(P)H was very low with all substrates (Table 4). Major enzymatic activity could only be detected using either DCIP or cytochrome c as electron acceptors and D-lactate as substrate.

Table 4. Co-factor analysis of AtD-LDH. The preferred co-factor of AtD-LDH was tested with purified enzyme, 10 mM substrate and either of 200 µM cytochrome c, 200 µM DCIP and 3 mM PMS, 1 mM NAD(P)⁺ or 1 mM NAD(P)H. The activity given is the activity relative to the best acceptor. The values presented are the average of two independent experiments.

Substrate + Acceptor	Activity (%)
D-lactate + Cytochrome c	89
D-lactate + DCIP	100
D-lactate + NAD(P) ⁺	-
Pyruvate + NAD(P)H	4.1
Glycolate + Cytochrome c	0.2
Glycolate + DCIP	0.5
Glycolate + NAD(P) ⁺	-
Glyoxylate + NAD(P)H	4.0

The AtD-LDH pH optimum was determined using D-lactate in assays with 50 mM potassium phosphate buffer adjusted to pH values ranging from 6.0 to 9.5. With cytochrome c as an

electron acceptor, AtD-LDH has a pH optimum between pH 8.5 and 9.25, whereas the activity decreases linearly from pH 8.5 down to pH 6.0 where the enzyme retains only 20% activity (Fig. 12, left panel). At low pH values the profile with DCIP was similar, and also displaying an optimum at 8.75, but in contrast to the pH profile measured with cytochrome c the activity sharply decreased at pH values over 8.75. Since the pH optimum with both acceptors is 8.75, this pH was used for the remaining measurements.

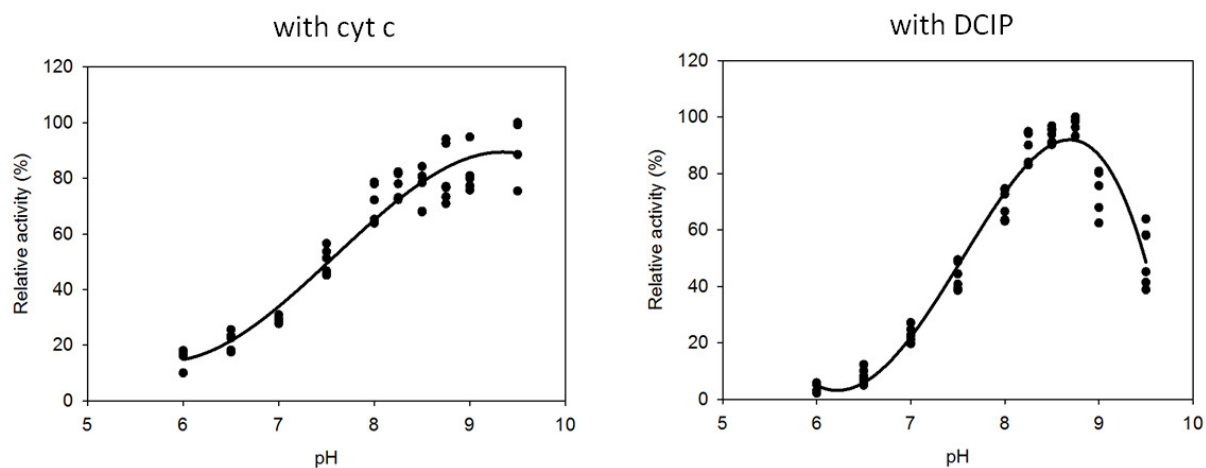


Figure 12. pH optimum of AtD-LDH. The pH optimum was determined using D-lactate with cytochrome c or DCIP and PMS in 50 mM potassium phosphate buffer adjusted at different pH values.

3.1.7 Substrate screening

Thus far, AtD-LDH displayed high activity with D-lactate, and poor activity with glycolate (Fig. 10 and Table 4). To determine whether the enzyme could use other substrates a substrate screening was initiated. The screening was performed using a range of carboxylic acids with similar structure to lactate. Both cytochrome c and DCIP were used in the screen and both acceptors yielded similar results. Only the results obtained using cytochrome c are presented (Fig. 13).

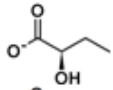
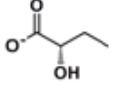
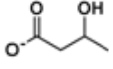
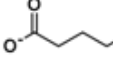
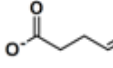
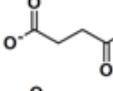
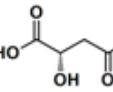
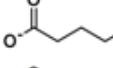
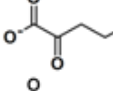
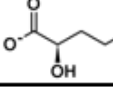
Structure	Name	Activity (%)	Structure	Name	Activity (%)
	Acetate	0.0		D-2-Hydroxybutyrate	100.0
	Ethanol	0.0		L-2-Hydroxybutyrate	0.0
	Glycolate	0.2		DL-3-Hydroxybutyrate	0.0
	Propionate	0.0		4-Hydroxybutyrate	0.0
	D-Lactate	76.9		Succinate Semialdehyde	0.0
	L-Lactate	5.6		Succinate	0.0
	D-Glycerate	4.3		L-Malate	0.0
	DL-Glycerate	2.9		Glutarate	0.0
				2-Oxoglutarate	0.0
				D-2-Hydroxyglutarate	0.2

Figure 13. Substrate screening with AtD-LDH. Purified AtD-LDH was used to assay a range of substrates at a concentration of 10 mM using cytochrome c as an electron acceptor at pH 8.75. The change in absorption was monitored at 550 nm. The values presented are activity relative to the best substrate and are the averages of two separate experiments.

The data in Fig. 13 is arranged according to how many carbons the substrate contains and the values represent relative activity compared to the best substrate. From the two-carbon substrates only glycolate was used by the enzyme, but at a low rate. The reaction with substrates containing three carbon atoms – such as D-lactate, L-lactate and D-glycerate – proceeded much faster than with their two-carbon counterparts, reaching activities of 77, 6 and 4 percent, respectively (Fig. 13, bottom left panel). The highest activity, however, was detected when using D-2-hydroxybutyrate (D-2HB) in the assay (Fig. 13, top right panel). Interestingly, the enzyme was entirely specific for the D- enantiomer of this substrate. Moreover, hydroxybutyrate molecules lacking the 2-hydroxyl group but instead having one at either the 3- or 4- position did not function as substrates (Fig. 13, top right panel). Finally, a very low activity (0.2%), comparable to that with glycolate, could be detected using D-2-hydroxyglutarate (D-2HG) as a substrate (Fig. 13, bottom right panel).

3.1.8 Determination of kinetic constants

As the pH optimum, co-factor and preferred substrates have now been determined; the biochemical characterization of AtD-LDH can proceed by determining the enzyme kinetic constants. First, using saturating levels of D-lactate, the enzyme affinity (K_m) for cytochrome c was determined to be 51 μM . Thus, 200 μM cytochrome c was further used in the assays for determining the enzyme kinetic constants as this is well over saturating levels of the acceptor. The substrates tested were the four best ones from the substrate screen, D-2HB, D-lactate, L-lactate, D-glycerate and additionally glycolate (Fig. 13). In order to compare the catalytic constants for one substrate with different acceptors they were additionally determined for D-lactate, L-lactate and glycolate using the acceptor DCIP (Table 5). In general, the K_m - values were lower when using cytochrome c, than with DCIP.

Table 5. **AtD-LDH kinetic constants.** Assays were performed with 1 μg purified enzyme, in 50 mM potassium phosphate buffer pH 8,75 with either 200 μM cytochrome c or 3 mM PMS and 200 μM DCIP as acceptors in a reaction volume of 200 μl . Substrate concentrations between 50 mM and 5 μM were assayed and the catalytic constants were determined using non-linear regression. The values presented are the averages of three separate experiments and the standard error is indicated.

AtD-LDH	with cytochrome c		
	K_m (μM)	k_{cat} (min^{-1})	k_{cat}/K_m ($\text{min}^{-1} \text{mM}^{-1}$)
D-2HB	61 \pm 2	88 \pm 1.2	1450
D-lactate	164 \pm 11	65 \pm 1.8	395
L-lactate	4486 \pm 374	7.0 \pm 0.3	2.0
D-glycerate	8871 \pm 1379	6.0 \pm 0.8	1.0
Glycolate	432 \pm 31	0.1 \pm 0.0	0.2
	with DCIP		
	K_m (μM)	K_{cat} (min^{-1})	K_{cat}/K_m ($\text{min}^{-1} \text{mM}^{-1}$)
D-lactate	317 \pm 31	73 \pm 1.7	231
L-lactate	7134 \pm 456	5 \pm 0.1	0.7
Glycolate	596 \pm 44	0.4 \pm 0.0	0.7

The best substrate affinity was 61 μM , for D-2HB, using cytochrome c as an acceptor. However, the affinity for D-lactate and glycolate with cytochrome c was also high, with the K_m value for D-lactate being 164 μM , and 432 μM for glycolate (Table 5). The highest K_m - values – being in the mM range – were determined for L-lactate and D-glycerate. The catalytic rate, k_{cat} , also differed significantly between the different substrates with the highest ones being 88 min^{-1} and 65 min^{-1} for D-2HB and D-lactate, respectively. By far the slowest catalytic rate was measured with glycolate, whereas L-lactate and D-glycerate were converted at an intermediate rate.

3.1.9 The catalytic site of AtD-LDH

Very little is known about the catalytically important residues in cytochrome c- dependent D-LDH enzymes. In an attempt to identify conserved, potentially catalytic residues, all the homologous sequences used to create the phylogenetic tree (Fig. 7), and in addition, the AtD-2HGDH sequence was included in a new alignment. This procedure resulted in a small amount of conserved residues (Fig. 14). The AtD-2HGDH sequence was included since it is not so closely related to AtD-LDH, but still retains catalytic activity with 2-hydroxyacids (section 3.2.7), the substrate binding pocket may be changed, but the catalytic residues should be conserved. Finding out which of these conserved residues are catalytic is a challenge, because there are no crystal structure for cytochrome c dependent D-LDH enzymes.

However, the SWISS-MODEL repository (<http://swissmodel.expasy.org/repository/>) is an initiative to provide annotated 3D models for all sequences in Swiss-Prot (Kiefer et al., 2009). In this initiative, proteins of unknown structure are modeled based on a known crystal structure of a homologous protein that is automatically sought out based on its suitability for the modeling process. From this repository, a homology model of AtD-LDH, based on the crystal structure of the Alkyldihydroxyacetonephosphate synthase (PDB ID: 2uuu) from the slime mold *Dictyostelium discoideum* was downloaded for analysis. This particular model is, however, based on a sequence which is not very homologous to AtD-LDH. Due to this, conclusions about the exact position and function of each amino acid are not possible, but residues close to the active site can still be identified. The conserved residues that are close to the active site are indicated in black.

```

MAFASKFARSKTILSFLRPCRQLHSTPKSTGDVTVLSPVKGRRRLPTCWSSSLFPLAIAASATSFAYLNLSNP
SISESSALDSRDITVGGKDSTEAVVKGEYKQVPKELISQLKTILEDNLTDDYDERYFHGKPKNSFHKAVNIP
DVVVFPRSEEEVSKILKSCNEYKVPIVPYGGATSIEGHTLAPKGGVCIDMSLMKRVKALHVEDMDVIVEPG
IGWLELNEYLEEYGLFFPLDPGPGASIGGMCATRCSGSLAVRYGTMRDENVISLKVVLNPGDVVKTASRAR
KSAAGYDLTRLIIGSEGLGVITEITLRLQKIPQHSVAVCNFPTVKDAADVAIATMMSGIQVSRVLELLDEV
QIRAINMANGKNLTEAPLTMFEFIGTEAYTREQTQIVQQIASKHNGSDFMFAEEPEAKKELWIKIRKEALW
ACYAMAPGHEAMITDVCVPLSHLAELISRSKELDASSLLCTVIAHAGDGNFHTCIMFDPSSEEQRREAER
LNHFMVHSALSMDGTCTGEGHGVGTGKMKYLEKELGIEALQTMKRIKKTLDPNDIMNPGKLIIPPHVCF

```

Figure 14. Conserved residues in AtD-LDH. An alignment was made with AtD-LDH and 16 homologous sequences, including that of AtD-2HGDH. Based on a homology model of AtD-LDH residues close to the catalytic site were identified. Conserved residues that are not close to the active site are indicated in grey. Conserved residues that are close to the active site are indicated in black.

3.1.10 Isolation of knock-out mutants

Now that the *in vitro* biochemical constants of AtD-LDH have been determined, the question is which substrate the enzyme uses *in vivo* and what the physiological function of the enzyme is. As all tested substrates except D-2HB and D-lactate were poorly used by the

enzyme due to either a very high K_m or a very low K_{cat} , it is highly likely that either D-2HB or D-lactate is indeed the physiological substrate. To investigate the physiological role of AtD-LDH, plant knock-out mutants were isolated.

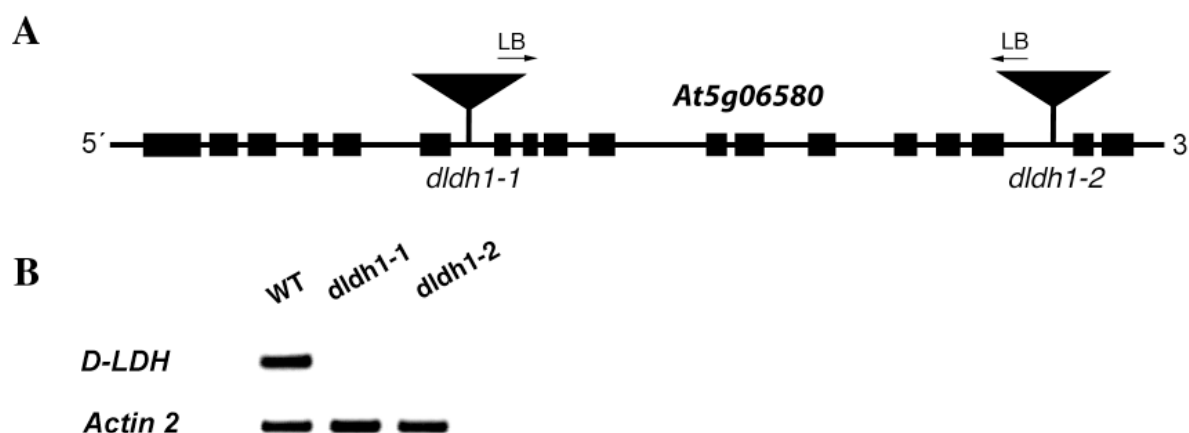


Figure 15. Confirmation of At5g06580 T-DNA insertion mutants. (A) A schematic representation of At5g06580, exons are represented by blocks and introns by lines. Sites of T-DNA insertions are indicated. T-DNA insertions are not drawn to scale. (B) To confirm gene disruption, RNA was extracted from knock-out- and wild-type plants and first-strand cDNA synthesis was performed. Primers spanning the T-DNA insertion sites were used for PCR-amplification and were separated through agarose gel electrophoresis.

Two independent T-DNA insertion lines SALK_026859 and SALK_001490, here named *dldh 1-1* and *dldh 1-2*, respectively, were ordered from the Nottingham Arabidopsis stock centre (NASC) (Fig. 15 A) and grown until homozygous for the T-DNA insertion. cDNA was prepared from these homozygous mutants and RT-PCR primers spanning the T-DNA insertions were used to determine whether native transcript was present. Both knock-out lines had a complete lack of such transcript (Fig. 15 B).

3.1.11 In-gel assays of knock-out plants

Wild-type and *dldh 1-1* root protein extracts were used to test for activity with D-lactate and related substrates in a native-PAGE activity assay. One band with high mobility was observed when testing for D-LDH activity using D-lactate (Fig. 16). However, the banding pattern of wild-type and *dldh 1-1* protein extracts were identical (Fig. 16). Similar results were obtained when assaying leaf protein extracts (data not shown). Thus, none of the activities seen on these native gels – including that with D-lactate – can originate from AtD-LDH. Despite extensive testing of different extraction methods and assay conditions no band corresponding to the activity of AtD-LDH could be detected on gels assayed with D-lactate. It is possible that the enzyme lost its activity during either extraction or electrophoresis.

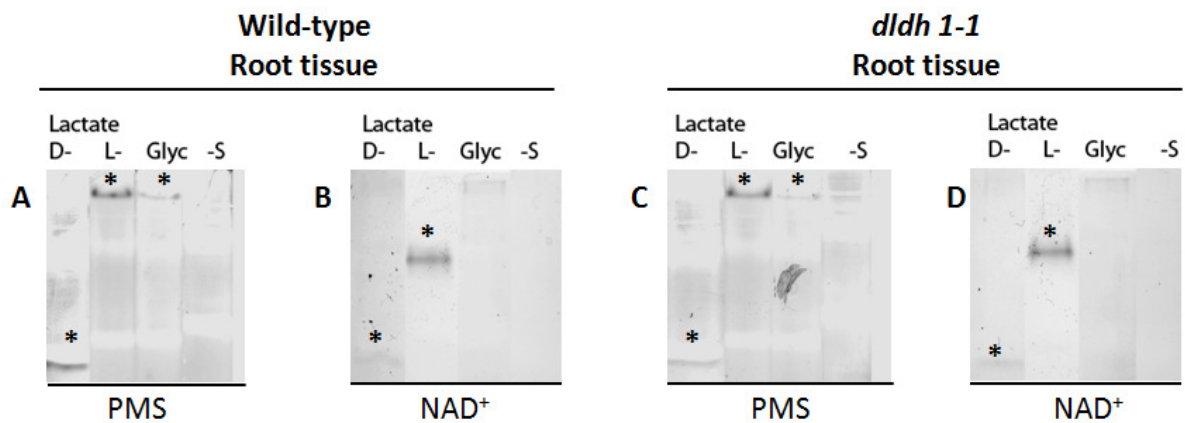


Figure 16. In-gel activity assays of plant protein extracts. Total root protein was extracted from *A. thaliana* wild-type and *dldh* knock-out plants and was run on native-PAGE (50 μ g protein in each lane). The gels were subsequently cut in pieces and assayed for activity with different substrates and acceptors during 16 h in the dark at 30°C.

3.1.12 Plant feeding experiments

The two AtD-LDH knock-out lines had no visible phenotype compared to wild-type plants when grown on soil in short- or long-day conditions (data not shown). To investigate the physiological function of AtD-LDH, plants were grown on sterile medium supplemented with various substrates. The underlying assumption being that plants impaired in a certain pathway, due to the loss of AtD-LDH, would perform poorly when fed with high concentrations of a substrate involved in that pathway. When *A. thaliana* wild-type, *dldh 1-1* and *dldh 1-2* plants were fed with either glycolate or L-lactate, wild-type and knock-out plants were equally inhibited (Fig. 17). In contrast, when fed with D-lactate or D-2HB, the knock-out plants performed much more poorly than wild-type plants (Fig. 17), indicating that AtD-LDH can metabolize these substrates *in vivo*. It is also worth noting that while wild-type plants exhibit stunted growth with 10 mM D-lactate, as much as 50 mM of L-lactate is needed to achieve the same effect.

In vivo, D-lactate is derived from the detoxification of MG. To test whether AtD-LDH might participate in the MG detoxification pathway (Fig. 6), wild-type and knock-out plants were further grown on different levels of D-lactate and methylglyoxal (MG). As previously shown (Fig. 17), the *dldh* knock-out plants performed worse than wild-type plants on medium containing D-lactate (Fig. 18). Moreover, when plants were fed MG, the knock-out plants also performed worse than wild-type (Fig. 18). Furthermore, the toxic effect was concentration-dependent for both substrates but MG was toxic at lower concentrations than D-lactate. This data enforces the notion that AtD-LDH participates in the MG detoxification pathway. However, when grown on 200 mM NaCl or 100 mM mannitol, conditions where the MG pathway should be of increased importance, knock-out plants did not show increased sensitivity (data not shown).

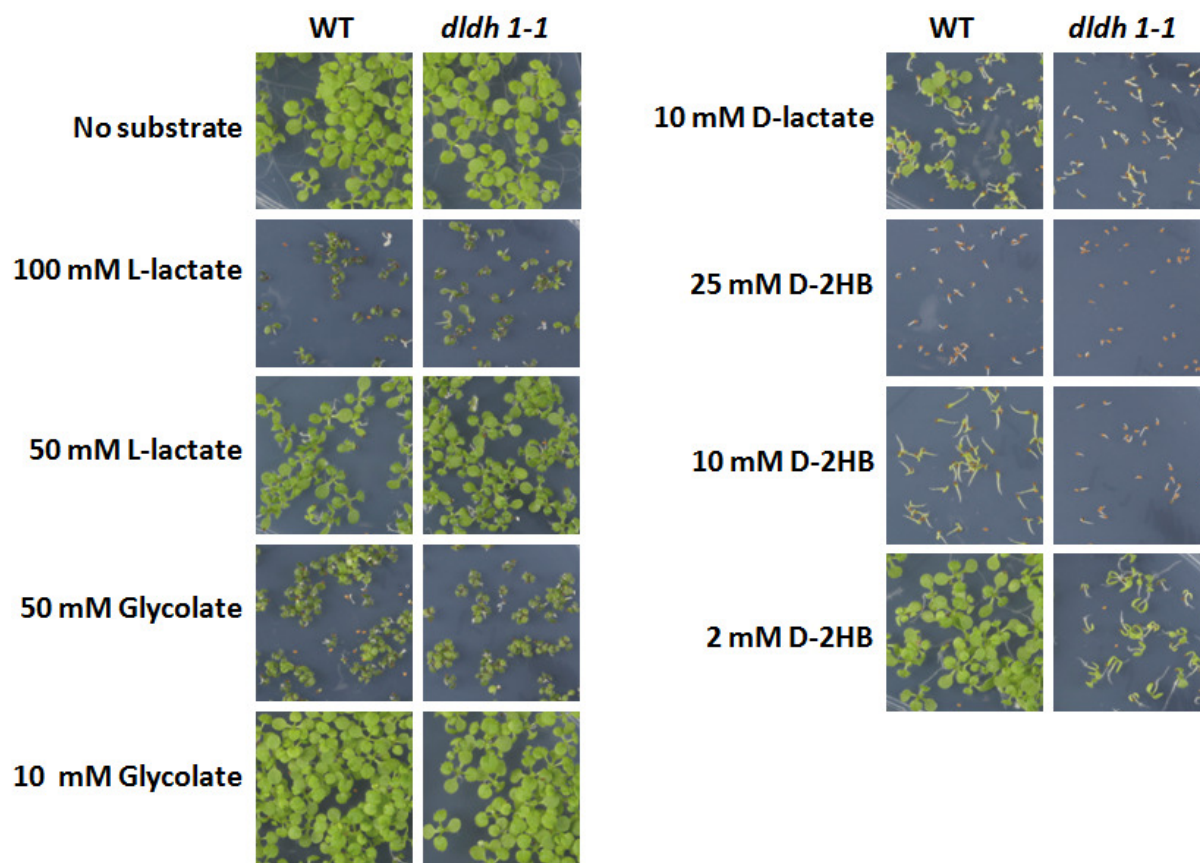


Figure 17. Substrate screening of wild-type and *dldh* mutant plants. $\frac{1}{2}$ MS plates without sugar were supplemented with substrates as indicated. Plants were grown at $100 \mu\text{mol m}^{-2} \text{s}^{-1}$ photons in LD conditions for two weeks.

In mammals and bacteria there are alternative pathways for MG breakdown, but it is not known if they exist in plants. These pathways commonly depend on aldehyde dehydrogenases converting the aldehyde of MG to a carboxylic acid group, forming pyruvate in the process. To test whether such an enzyme is present in wild-type plants, leaf and root protein extracts were used in an in-gel activity assay using 5 mM MG and either PMS, NAD^+ or NADP^+ as electron carriers. Assaying leaf protein extracts with PMS as an electron carrier yielded an unspecific band with low mobility (Fig. 19, A). This band is always present when leaf extracts are stained with PMS, it is of a different color than “true” activity bands, and is present also in no substrate controls. It thus represents unspecific staining and can be disregarded. In root extracts a putative aldehyde dehydrogenase activity could be detected (indicated by a star in Fig. 19, B), thus indicating that a second possible pathway for the catabolism of MG may exist in *A. thaliana*.

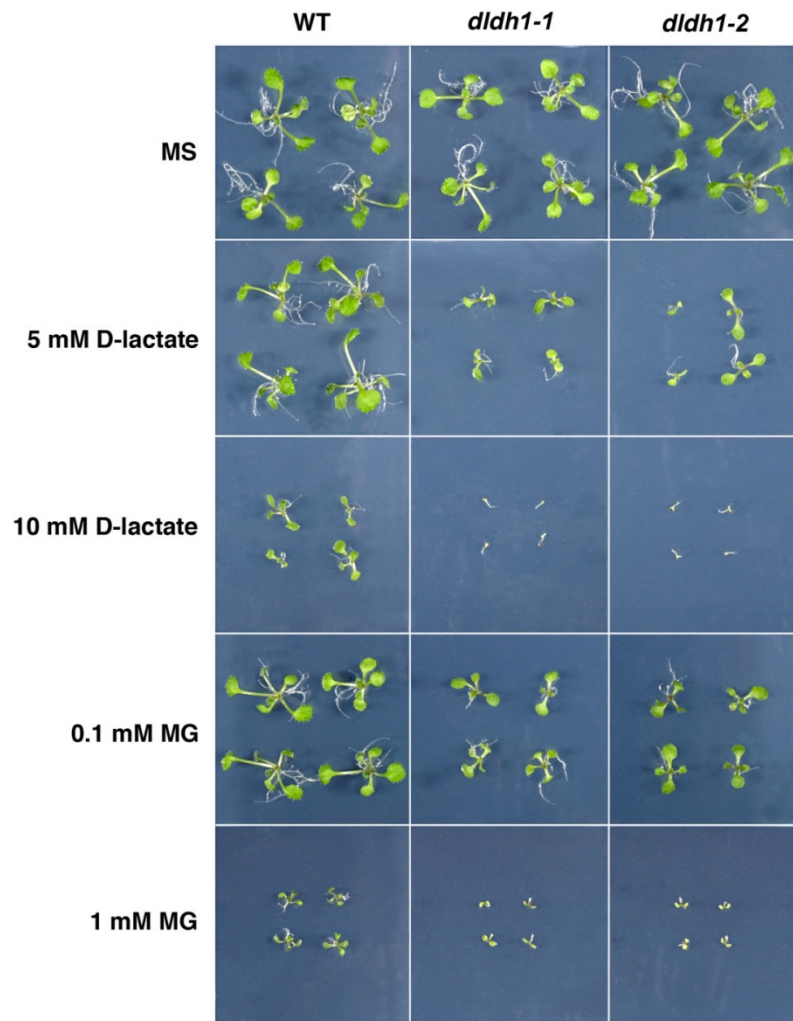


Figure 18. Plant feeding experiments of wild-type and *dldh* mutant plants. $\frac{1}{2}$ MS plates without sugar were supplemented with substrates as indicated. Plants were grown at $100 \mu\text{mol m}^{-2} \text{s}^{-1}$ photons in LD conditions for two weeks.

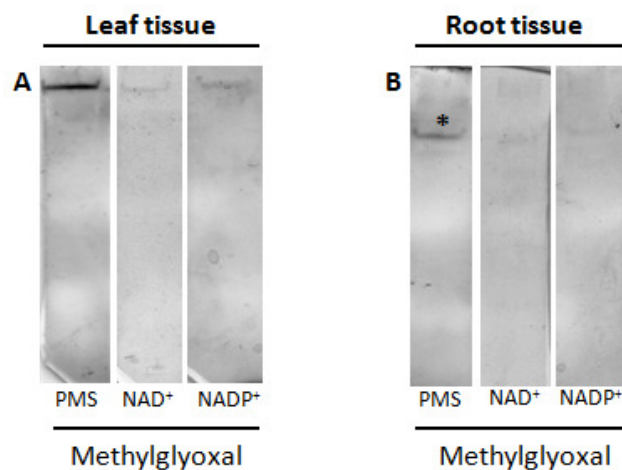


Figure 19. Activity staining for aldehyde dehydrogenases acting on MG. Wild-type leaf (A) and root (B) protein extracts were run on a native-PAGE and stained 16 h at 30°C in the dark with 5 mM MG and either PMS, NAD^+ or NADP^+ as electron carriers. 50 mg protein was added in each lane. The band in (A) represent the unspecific bands that always appear in leaf extracts, regardless of substrates added. Putative aldehyde dehydrogenase activity with MG is indicated by a star in (B).

3.2 Characterization of the enzyme encoded by At4g36400

3.2.1 Identification of the candidate enzyme

As AtD-LDH does not use glycolate efficiently, but rather D-lactate and D-2HB, it cannot be used in the chloroplastidic GMK pathway (Fig. 5) and a new candidate enzyme must be sought. Lactate dehydrogenases perform similar reactions as glycolate dehydrogenases – the oxidation of a 2-hydroxyl group to a keto group – only with a slightly larger substrate. A paralog of the newly characterized AtD-LDH is thus likely to also perform this type of reaction, but might have an active site that allows for better binding of glycolate. At4g36400, the closest paralog of AtD-LDH with 24% identity, was chosen for further study.

3.2.2 Phylogenetic analysis

To get a picture of the distribution of orthologs of At4g36400, the amino acid sequence was used for a BLAST search against the NCBI databank. Representative sequences from animals, fungi and plants were selected and used to construct a phylogenetic tree (Fig. 20). Each organism only contains one sequence of high similarity, except for *S. cerevisiae*, which contains two. The enzymatic activities of four orthologous enzymes, *Homo sapiens* D-2HGDH, *Rattus norvegicus* D-2HGDH, *S. cerevisiae* DLD2 and *S. cerevisiae* DLD3 are already known; the first two being D-2-hydroxyglutarate dehydrogenases (D-2HGDH), and the latter two D-LDHs. However, as the *S. cerevisiae* enzymes have not been tested with D-2-hydroxyglutarate (D-2HG) as a substrate it cannot be excluded that these too are in fact D-2HGDHs. The enzyme encoded by At4g36400 will thus be referred to as AtD-2HGDH for *Arabidopsis thaliana* **D-2-hydroxyglutarate dehydrogenase** in the remainder of this work.

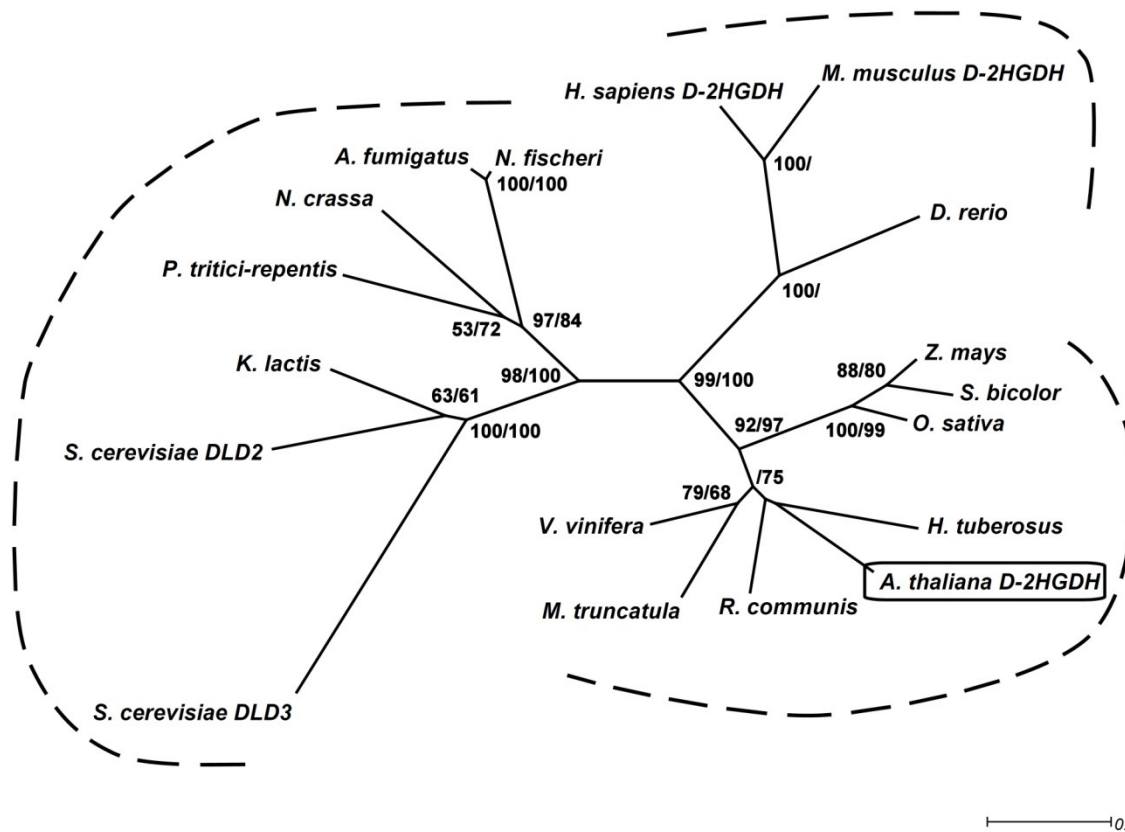


Figure 20. Phylogenetic relationships of AtD-2HGDH. Protein sequences were aligned using ClustalW2. The phylogenetic tree was constructed by the neighbor-joining method using BioNJ and visualized using Dendroscope (59). Bootstrap values at the nodes represent the percentage support from 500 replicates with neighbor-joining and maximum likelihood, respectively. Only bootstrap values over 50% are shown. The following sequences are included: *Arabidopsis thaliana* D-2HGDH (O23240); *Helianthus tuberosus* (EL452354); *Zea mays* (B4FWJ7); *Sorghum bicolor* (e_gw1.2.1014.1); *Oryza sativa* (Q7X114); *Ricinus communis* (B9S687); *Vitis vinifera* (A7QE54); *Medicago truncatula* (MtAC136451_19.4); *Homo sapiens* (Q8N465); *Danio rerio* (A1L258); *Mus musculus* (Q8CIM3); *Saccharomyces cerevisiae* DLD2 (P46681); *Saccharomyces cerevisiae* DLD3 (P39976); *Kluyveromyces lactis* (Q6CL48); *Neurospora crassa* (Q7RYX6); *Pyrenophytra tritici-repentis* (B2WHR3); *Aspergillus fulmigatus* (Q4WE96); and *Neosartorya fischeri* (A1D092).

To further visualize the conserved parts of the protein sequences, a multiple alignment was performed using the ClustalW2 algorithm with protein sequences from *A. thaliana*, *S. cerevisiae* and *H. sapiens*. While the three enzymes are not similar in their N-terminal part they show extensive similarity throughout the rest of the sequence (Fig. 21). An FAD binding domain, indicated in yellow, and a C-terminal FAD-linked oxidase domain, indicated in red, is conserved in all tree enzymes.

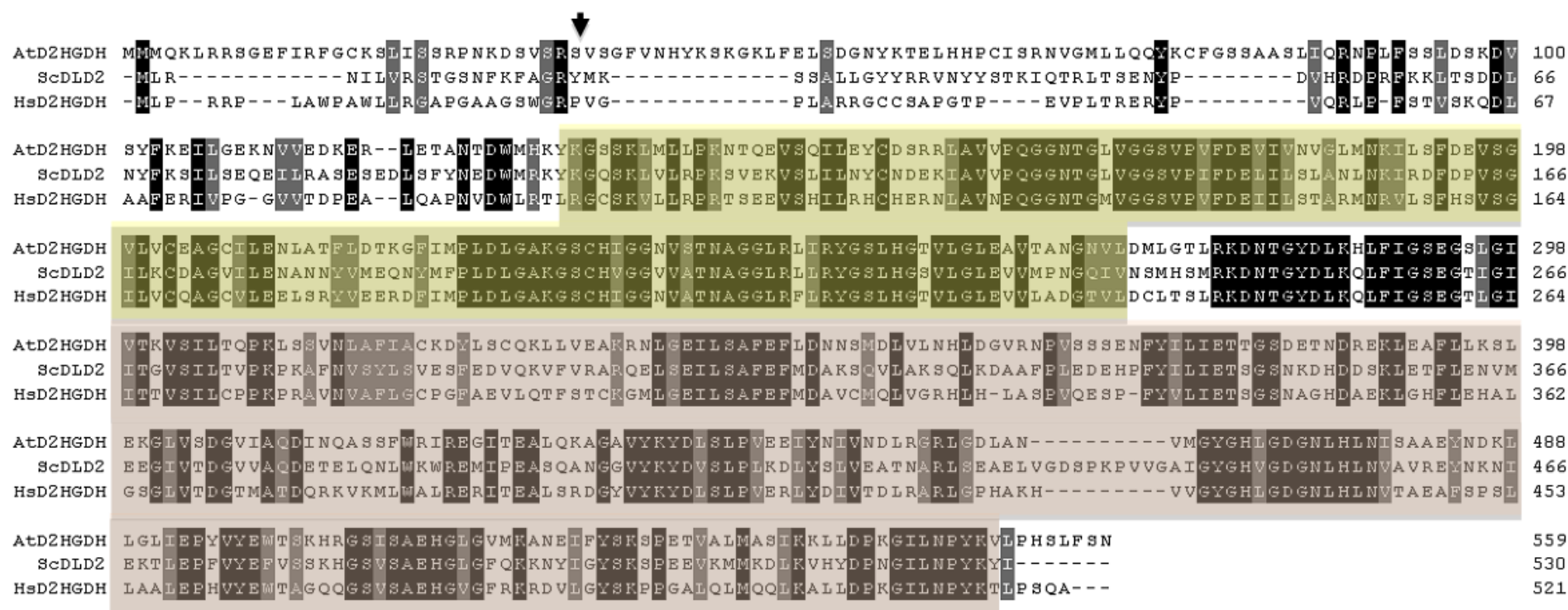


Figure 21. Multiple sequence alignment. Protein sequences from *A. thaliana* D-2HGDH (O23240), *S. cerevisiae* DLD2 (P46681) and *H. sapiens* D-2HGDH (Q8N465) were aligned using the ClustalW2 algorithm (<http://www.ebi.ac.uk/Tools/clustalw2/index.html>). Identical amino acids are indicated in black while similar amino acids are indicated in grey. The FAD binding domain and FAD-linked oxidase domain predicted by Pfam (<http://pfam.sanger.ac.uk/>) are indicated in yellow and red, respectively.

3.2.3 Cloning, heterologous expression and purification of AtD-2HGDH

AtD-2HGDH was predicted to have a mitochondrial targeting sequence by using the MitoProt II v1.101 software (Claros and Vincens, 1996). To characterize AtD-2HGDH, the part of the DNA sequence coding for the mature protein, indicated by an arrow in Fig. 21, was amplified by PCR from leaf cDNA, cloned in frame with the N-terminal His-tag of the pET16b vector and expressed in the *E. coli* BLR strain through induction with IPTG. Induced cells showed a band at 63 kDa (Fig. 22, lane 2) that was missing in uninduced cells (Fig. 22, lane 1). The protein corresponding to this band was purified by affinity chromatography to apparent homogeneity (Fig. 22, lane 4). For some measurements, this protein was further digested with factor Xa to remove the His-tag (Fig. 22, lane 5).

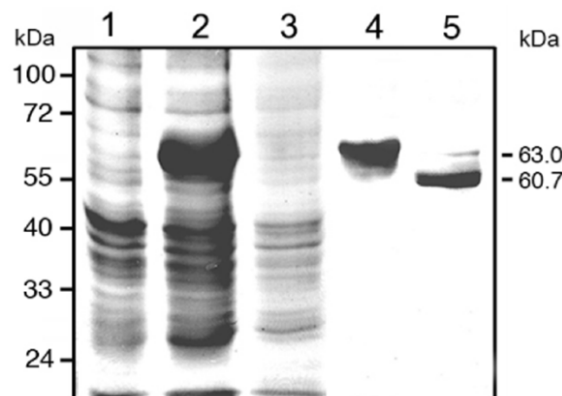


Figure 22. Purification and analysis by gel electrophoresis of the recombinant enzyme. Lane 1, 20 µg of noninduced cell culture lysate. Lane 2, 20 µg of cell culture lysate after 2 h of induction with isopropyl β-D-thiogalactopyranoside. Lane 3, 20 µg of Ni²⁺-NTA column flow through. Lane 4, 5 µg of purified recombinant D-2HGDH. Lane 5, AtD-2HGDH after factor Xa digestion. The molecular mass of the purified protein is indicated on the right. Molecular weight markers run in parallel are indicated on the left.

3.2.4 Quaternary structure of AtD-2HGDH

The purified recombinant enzyme was subjected to a native-PAGE. Part of the gel was stained with Coomassie to visualize the protein and molecular weight markers, while other parts of the gel was assayed for activity with D-2HG as substrate (Fig. 23). The enzyme showed a slightly lower mobility than the 132 kDa marker protein, indicating that it may form dimers. This was further supported by performing size-exclusion chromatography, which yielded a native molecular weight of 140 kDa. The in-gel activity-staining assay further confirmed that the enzyme has activity with D-2HG (Fig. 23), as indicated by the homology to other D-2HGDH enzymes (Fig. 21).

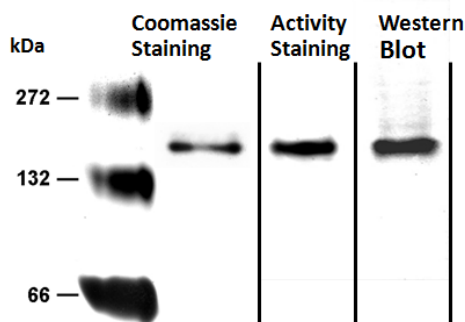


Figure 23. Native-PAGE using isolated AtD-2HGDH. Approximately 10 μg of the purified enzyme was loaded and stained with Coomassie together with molecular weight markers, whereas 1 μg protein was loaded for the D-2HG activity staining and Western blot analysis.

3.2.5 Analysis of the prosthetic group

During the purification of AtD-2HGDH it was noted that the enzyme was brightly yellow. Since this is indicative for a flavin prosthetic group, the enzyme was boiled to release the group and its visible absorption spectrum was recorded. This spectrum perfectly matches that of the FAD and FMN standards with absorption maxima at 375 and 450 nm (Fig. 24).

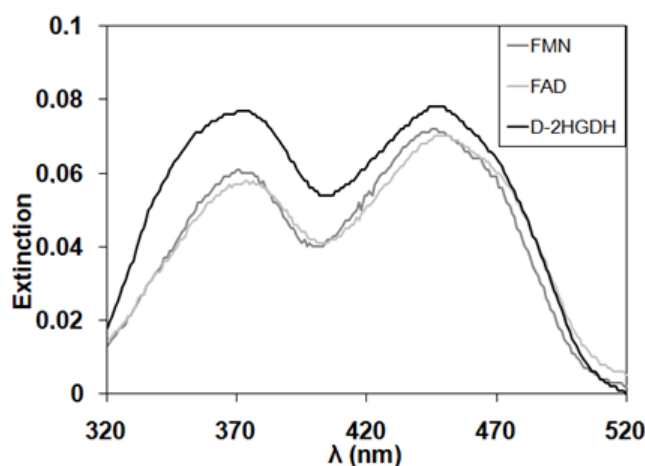


Figure 24. Absorption spectra of prosthetic group and standards. The visible spectrum of FMN, FAD and the enzyme was recorded in 2 nm steps between 320 and 520 nm.

To determine the identity of the prosthetic group bound to AtD-2HGDH, thin-layer chromatography of the isolated molecule, together with FMN, riboflavin and FAD standards was performed in two different buffer systems as well as in the native-PAGE assay. In all three experiments, the prosthetic group isolated from AtD-2HGDH has R_f values similar to those of FAD and not of the other standards (Table 6).

Table 6. Chromatographic separation of the prosthetic group. The At-D2HGDH prosthetic group was released by boiling and was spotted together with standards on a cellulose thin layer chromatography plate. The plates were run in the dark with the buffer systems (A) 5% Na₂HPO₄ in aqueous solution and (B) 1-butanol:HAc:water in a 4:1:5 relationship. Sample positions were subsequently detected under UV. Samples were also analyzed on an 18% native polyacrylamide run in the dark with subsequent determination of sample position under UV light. The values presented represent the determined R_f-values.

	Flavin standard		AtD-2HGDH	
	FMN	Riboflavin	FAD	Group
TLC A	0.72	0.38	0.61	0.59
TLC B	0.22	0.45	0.07	0.09
PAGE	0.94	0.09	0.82	0.83

Additionally, using FAD isolated from 120 µg of boiled enzyme in a final volume of 500 µl the absorption at 450 nm was 0.05. Taking into account that the extinction coefficient of FAD is 11.3 mM⁻¹ cm⁻¹ and the calculated molecular mass of the recombinant enzyme is 60.7 kDa it was calculated that each mole of enzyme binds one mole of FAD.

3.2.6 Co-factor analysis and pH optimum

To determine which co-factor the enzyme uses, the oxidation of D-2HG was tested with either cytochrome c, DCIP, NAD⁺ or NADP⁺ as acceptors. The reduction of 2-oxoglutarate (2-OG) was tested with either NADH or NADPH as electron donors (Table 7). No activity could be detected with neither NAD(P)⁺ nor NAD(P)H. While some activity was observed with cytochrome c, by far the best co-factor for AtD-2HGDH was the synthetic acceptor DCIP. This acceptor was used for all further enzymatic measurements with the enzyme.

Table 7. Co-factor analysis of AtD-2HGDH. The preferred co-factor of AtD-2HGDH was tested with the purified enzyme, 10 mM substrate and either of 200 µM cytochrome c, 200 µM DCIP and 3 mM PMS, 1 mM NAD(P)⁺ or 1 mM NAD(P)H. The activity given is the activity relative to the best acceptor. The values presented are the average of two independent experiments.

Substrate + Acceptor	Activity (%)
D-2HG + Cytochrome c	2
D-2HG + DCIP	100
D-2HG + NAD(P) ⁺	-
2-OG + NAD(P)H	-

The AtD-2HGDH pH optimum was determined using a 50 mM potassium phosphate adjusted to pH values ranging from 6 to 9.5. The AtD-2HGDH activity increases in a linear fashion with increasing pH, reaching a plateau between pH 8.5 and 9.5 (Fig. 25). However, the enzyme remains functional over the whole pH range, retaining around 15% activity at pH 6.0. pH 8.75 was used for all further enzymatic measurements with AtD-2HGDH.

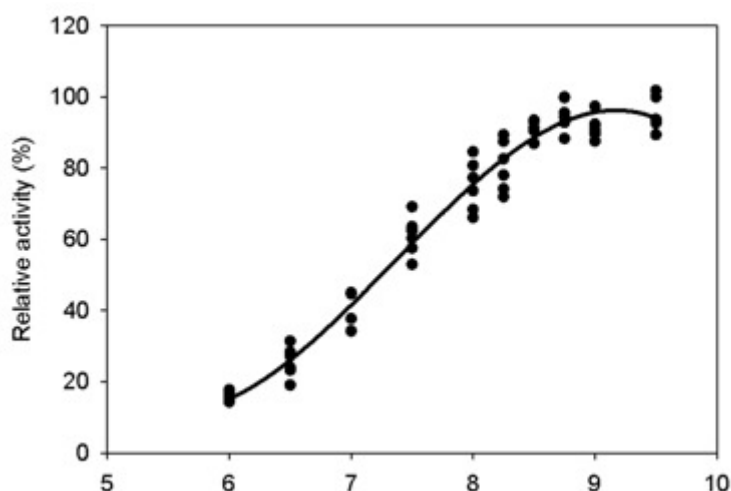


Figure 25. pH optimum of AtD-2HGDH. The pH optimum was determined using D-2HG with DCIP and PMS in 50 mM potassium phosphate buffer adjusted at different pH values.

3.2.7 Substrate screening

To determine which other substrates the enzyme might use in addition to D-2HG, a substrate screening was performed. The AtD-2HGDH activity with a range of 2-hydroxy-acids and other related molecules was tested with DCIP as an electron acceptor. However, despite intense efforts, no other substrate than D-2HG could be identified for AtD-2HGDH (Fig. 26). When repeating the substrate screening using up to 7 μg enzyme in each 200 μl reaction and cytochrome c as an electron acceptor, weak activity with meso-tartrate, D-lactate and D-2HB was recorded, but this activity was too close to the detection limit of the assay to be accurately quantified. Moreover, purified enzyme digested with factor Xa to remove the His-tag showed the same activity with the different substrates (data not shown). These results indicate that the only reaction catalyzed by AtD-2HGDH is the oxidation of D-2HG to 2-oxoglutarate.

3.2.8 Determination of kinetic constants

As D-2HG is the only substrate used by AtD-2HGDH, it was used to determine the catalytic constants of the enzyme at pH 8.75 using the acceptor DCIP (Table 8). The enzyme affinity for D-2HG was high with a K_m of 584 μM , and the catalytic rate was 48 min^{-1} .

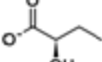
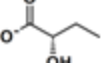
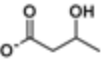
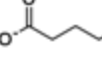
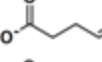
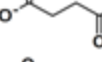
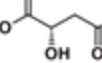
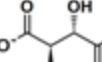
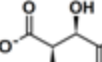
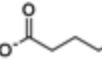
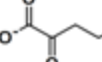
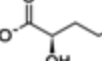
Structure	Name	Activity (%)	Structure	Name	Activity (%)
	Acetate	0.0		D-2-Hydroxybutyrate	0.0
	Ethanol	0.0		L-2-Hydroxybutyrate	0.0
	Glycolate	0.0		DL-3-Hydroxybutyrate	0.0
	Propionate	0.0		4-Hydroxybutyrate	0.0
	D-Lactate	0.0		Succinate Semialdehyde	0.0
	L-Lactate	0.0		Succinate	0.0
	D-Glycerate	0.0		L-Malate	0.0
	DL-Glycerate	0.0		Meso-Tartrate	0.0
				L-Tartrate	0.0
				Glutarate	0.0
				2-Oxoglutarate	0.0
				D-2-Hydroxyglutarate	100.0

Figure 26. Substrate screening with AtD-2HGDH. Purified AtD-2HGDH was used to assay a range of substrates (10 mM) using DCIP as an electron acceptor at pH 8.75. The change in absorption was monitored at 600 nm. The values presented are activity relative to the best substrate and are the averages of two separate experiments.

Table 8. Catalytic constants of AtD-2HGDH. Assays were performed with 5 μ g purified enzyme, in 50 mM potassium phosphate buffer pH 8.75 with 3 mM PMS and 200 μ M DCIP as electron acceptors in a reaction volume of 200 μ L. Substrate concentrations between 50 mM and 5 μ M were assayed and the catalytic constants were determined using non-linear regression. The values presented are the averages of three separate experiments and the standard error is indicated.

AtD-2HGDH	with DCIP		
	K_m (μ M)	k_{cat} (min^{-1})	k_{cat}/K_m ($\text{min}^{-1} \text{mM}^{-1}$)
D-2HG	584 ± 45	48 ± 0.9	82

3.2.9 The catalytic site of AtD-2HGDH

To identify the catalytically active amino acid residues in AtD-2HGDH, the approach described in section 3.1.9 was employed. In brief, the sequences used to create the AtD-2HGDH phylogenetic tree (Fig. 20) and the AtD-LDH sequence were aligned using a multiple sequence alignment software. The residues that were conserved in all these sequences were then identified in homology model of AtD-2HGDH built based on the crystal structure of D-lactate dehydrogenase from *E. coli* (PDB ID: 1f0x), retrieved from the SWISS-MODEL repository (<http://swissmodel.expasy.org/repository/>). Again, this homology model was based on a rather distant sequence. As a consequence, the exact structure of the catalytic site of AtD-2HGDH could not be inferred. Residues conserved in all sequences, but not close to the catalytic site, are indicated in grey in Fig. 27, whereas conserved residues that are close to the active site are indicated in black.

```

MMMQLRRSGEFIRFGCKSLISSRPNKDSVSRVSGFVNHYKSKGKLFELSDGNYKTELHHPCISRNVGM
LLQQYKCFGSSAASLIQRNPLFSSLDKDVSYFKEILGEKNVVEDKERLETANTDWMHKYKGSSKLMLLPK
NTQEVSQILEYCDRRLAVVPQGGNTGLVGGVSPVFDEVIVNVGLMNKILSFDEVSGVLVCEAGCILENLA
TFLDTKGFIMPLDLGAKGSCHIGGNVSTNAGGLRLIRYGSLSHGTVLGLEAVTANGNVLDMLGLTRKDNTG
YDLKHLFIGSEGLGIVTKVSILTQPKLSSVNLAFIACKDYLSQCQLLVEAKRNLGEILSAFEFLDNNMMDLVL
NHLDGVRNPVSSSENFYILIEITGSDETNDREKLEAFLLKSLEKGLVSDGVIAQDINQASSFWRIREGITEAL
QKAGAVYKYDLSLPVEEIYNIVNDLRGRLGDLANVMGYGHLGDGNLHLNISAAYNDKLLGLIEPYVYEW
TSKHRGSISAHEHGLGVMKANEIFYSKSPETVALMASIKKLLDPKGILNPYKVLPHSLFSN

```

Figure 27. Conserved residues in AtD-2HGDH. An alignment was made with a total of 18 homologous sequences, including that of AtD-LDH. Based on a homology model of AtD-2HGDH, residues close to the catalytic site were identified. Conserved residues that are not close to the active site are indicated in grey. Conserved residues that are close to the active site are indicated in black.

3.2.10 Isolation of knock-out mutants

While AtD-2HGDH only catalyzes the oxidation of D-2HG, the participation of this particular metabolite in plant metabolism has not been described so far. To investigate the physiological role of AtD-2HGDH three independent T-DNA insertion lines for At4g36400, the gene encoding AtD-2HGDH, were ordered from NASC. The insertion lines were SALK_061383, SAIL_844_G06 and GABI_127F12, here referred to as *d2hgdh 1-1*, *d2hgdh 1-2*, and *d2hgdh 1-3*, respectively (Fig. 28 A). These plants were grown on soil and tested by PCR for homozygosity for the insertions. Lack of native At4g36400 transcript in the mutants was confirmed by PCR on cDNA using primers spanning the T-DNA insertion sites. None of the insertion mutants showed any native transcript (Fig. 28 B).

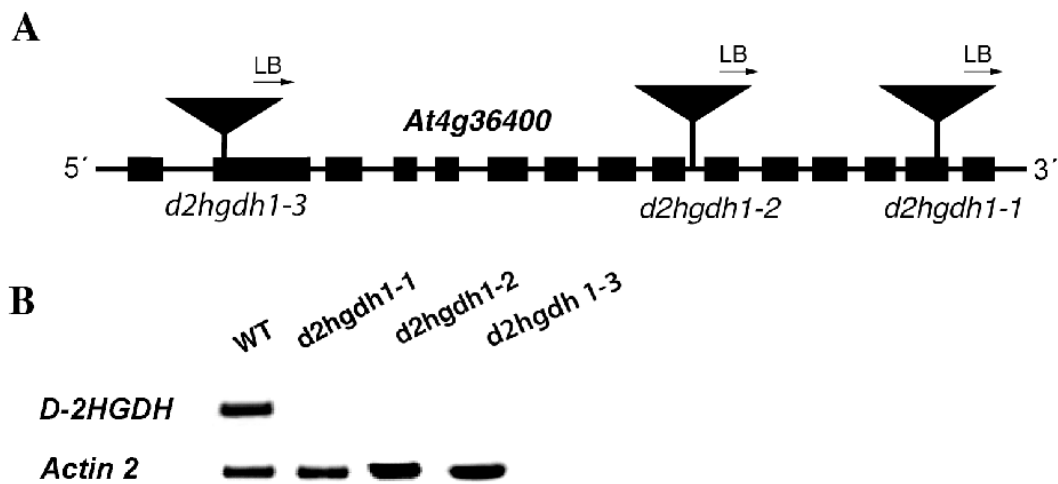


Figure 28. Confirmation of *At4g36400* T-DNA insertion lines. (A) A schematic representation of *At4g36400*, exons are represented by blocks and introns by lines. Sites of T-DNA insertions are indicated. T-DNA insertions are not drawn to scale. (B) To confirm gene disruption RNA was extracted from KO- and wild-type plants and first-strand cDNA synthesis was performed. Primers spanning the T-DNA insertion sites were used for PCR amplification and were separated by agarose gel electrophoresis.

3.2.11 In-gel assays of knock-out plants

To test whether AtD-2HGDH activity could be detected in plants, total root protein from wild-type, *d2hgdh 1-1* and *dldh 1-1* plants was run on a native-PAGE and stained for activity using D-2HG as substrate. Already after 2 h of incubation a band indicating D-2HGDH activity could be observed in the wild-type and *dldh 1-1* mutant samples whereas it was missing in the *d2hgdh 1-1* mutant (Fig. 29, A). The T-DNA mutants *d2hgdh 1-2* and *d2hgdh 1-3* were also tested for AtD-2HGDH activity with in-gel assays and it was absent also in these lines (data not shown). This confirmed that *At4g36400* encodes a D-2HG dehydrogenase *in planta* and that this is the only enzyme with such an activity in *A. thaliana*. Moreover, as this band had a similar mobility as the band obtained with D-lactate (Fig. 16), extracts from wild-type and knock-out plants were further assayed for activity with D-lactate as substrate (Fig. 29 B). After prolonged incubation for 20 h the same banding pattern as in gels assayed for activity using D-2HG could be observed. These results show that the band observed on the gels assayed for activity with D-lactate in Fig. 16 and Fig. 29 results from the activity of AtD-2HGDH.

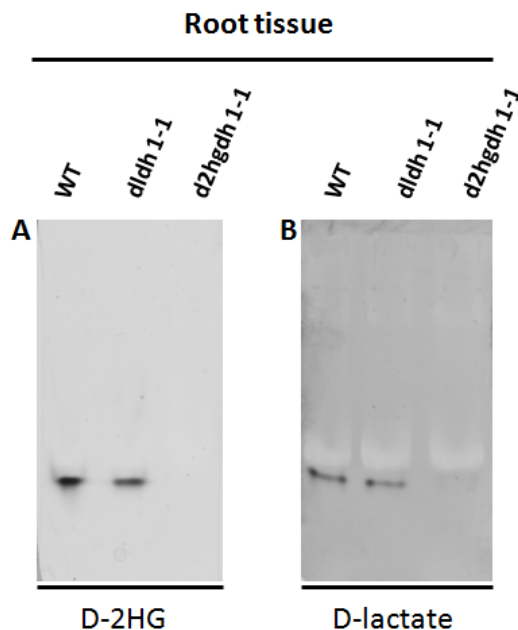


Figure 29. In-gel activity assays of plant protein extracts. Total root protein was extracted from wild-type and knock-out mutants and was run on native-PAGE (50 μ g protein in each lane). The gels were subsequently stained for activity using substrates as indicated and PMS as an acceptor. Gels were assayed with D-lactate for 20 h and D-2HG for 2 h in the dark at 30°C.

To test in which subcellular compartment AtD-2HGDH is localized, total protein was extracted from wild-type, *dlah 1-1* and *d2hgdh 1-1* plants using fresh plant tissue and an extraction method not involving freezing so that the organelles remained intact. Some of the raw extract from leaves and roots was loaded on a native gel and assayed for AtD-2HGDH activity with D-2HG (Fig. 30). Both root and leaf extracts from wild-type and *dlah 1-1* had the same level of AtD-2HGDH activity, whereas it was missing in the *d2hgdh 1-1* mutant extracts. The remainder of the root extracts was subjected to differential centrifugation to separate plastids, mitochondria and cytosol. When assaying these fractions for AtD-2HGDH activity on a native gel, a very strong band could be seen in the fraction containing enriched mitochondria (Fig. 30). These data strongly indicate a mitochondrial localization of AtD-2HGDH.



Figure 30. In-gel activity assays of plant tissues and mitochondria. Fresh plant tissue (leaves and roots) was disrupted, the root sample was then subjected to differential centrifugation. 50 μ g leaf protein, root protein and enriched mitochondrial protein was subjected to native-PAGE and stained for 2 h with D-2HG and PMS in the dark at 30°C. WT= wild-type plants.

3.2.12 *In silico* co-expression analysis

Little is known about D-2HG metabolism in plants and in which pathway the metabolite might participate. To get clues about the *in vivo* function of AtD-2HGDH the ATTED database (<http://atted.jp/>) (Obayashi et al., 2009) was searched for genes co-expressed with *AtD-2HGDH*. In the top 300 co-regulated genes there were many participating in β -oxidation, chlorophyll breakdown and branched chain amino-acid degradation. The co-regulated genes participating in these pathways are listed in Table 9.

Table 9 List of genes coordinately expressed with *AtD-2HGDH*. A subset of the data retrieved from ATTED (<http://atted.jp/>) is displayed. Only co-regulated genes involved in β -oxidation, branched-chain amino acid degradation and chlorophyll breakdown are shown. The abbreviations used in Fig. 31 are also listed. MR: Mutual Rank.

Locus	Function	Abbrev. as used in Fig. 31	MR
β-oxidation			
At4g29010	fatty acid multifunctional protein (AIM1; 2-trans-enoylCoA hydratase, L-3-hydroxyacylCoA dehydrogenase)	ECH/HCD	2.8
At4g05160	acyl-coenzyme A synthetase	ACS	5.1
At4g13360	enoyl-CoA hydratase/isomerase	ECH/ECI	15.0
At2g33150	3-ketoacyl-CoA thiolase (KAT2/PED1)	KAT	31.1
At3g06810	acyl-CoA dehydrogenase-related (IBR3)	HCD	39.2
At1g76150	enoyl-CoA hydratase 2	ECH	40.9
At2g42790	citrate synthase 3 (CYS3)	CYS	48.2
At4g13250	acyl-CoA oxidase 4 (ACX4)	ACX	62.5
At5g65110	acyl-CoA oxidase 2 (ACX2)	ACX	85.9
At3g06690	acyl-CoA oxidase	ACX	101.5
At3g12800	2,4-dienoyl-CoA reductase	dECR	114.2
At3g58750	citrate synthase 2 (CYS2)	CYS	124.1
At4g39850	peroxisomal ABC transporter (PXA1)	PXA	125.2
At3g06860	fatty acid multifunctional protein (MFP2; 2-trans-enoylCoA hydratase, L-3-hydroxyacylCoA dehydrogenase)	ECH/HCD	147.8
At1g20630	catalase 1	CAT	209.2
Branched-chain amino acid degradation			
At3g45300	isovaleryl-CoA-dehydrogenase branched-chain alpha-keto acid decarboxylase E1 β	IVD	48.9
At1g55510	nit branched-chain alpha keto acid decarboxylase E1 α	BCKDC	72.6
At1g21400	subunit	BCKDC	106.1
At4g20930	3-hydroxyisobutyrate dehydrogenase	3-HIBD	117.5
At2g43400	electron transfer flavoprotein:ubiquinone oxidoreductase	ETFQO	148.0
At5g43430	electron transfer flavoprotein β subunit	ETF	150.4
At1g10070	branched-chain aminotransferase (ATBCAT-2)	BCAT	201.2
Chlorophyll breakdown			
At5g13800	pheophytinase (AtPPH)	PPH	17.6
At3g44880	pheophorbide a oxygenase	PaO	20.8
At2g01490	phytanoyl-CoA dioxygenase	PhCd	34.0

To make this data more accessible, the pathways in question are schematically shown in Fig. 31. Proteins corresponding to the co-expressed genes in the pathways are written in red. It is notable that almost all genes in three separate pathways are co-expressed with *AtD-2HGDH*. All three pathways have in common that they ultimately produce propionyl-CoA.

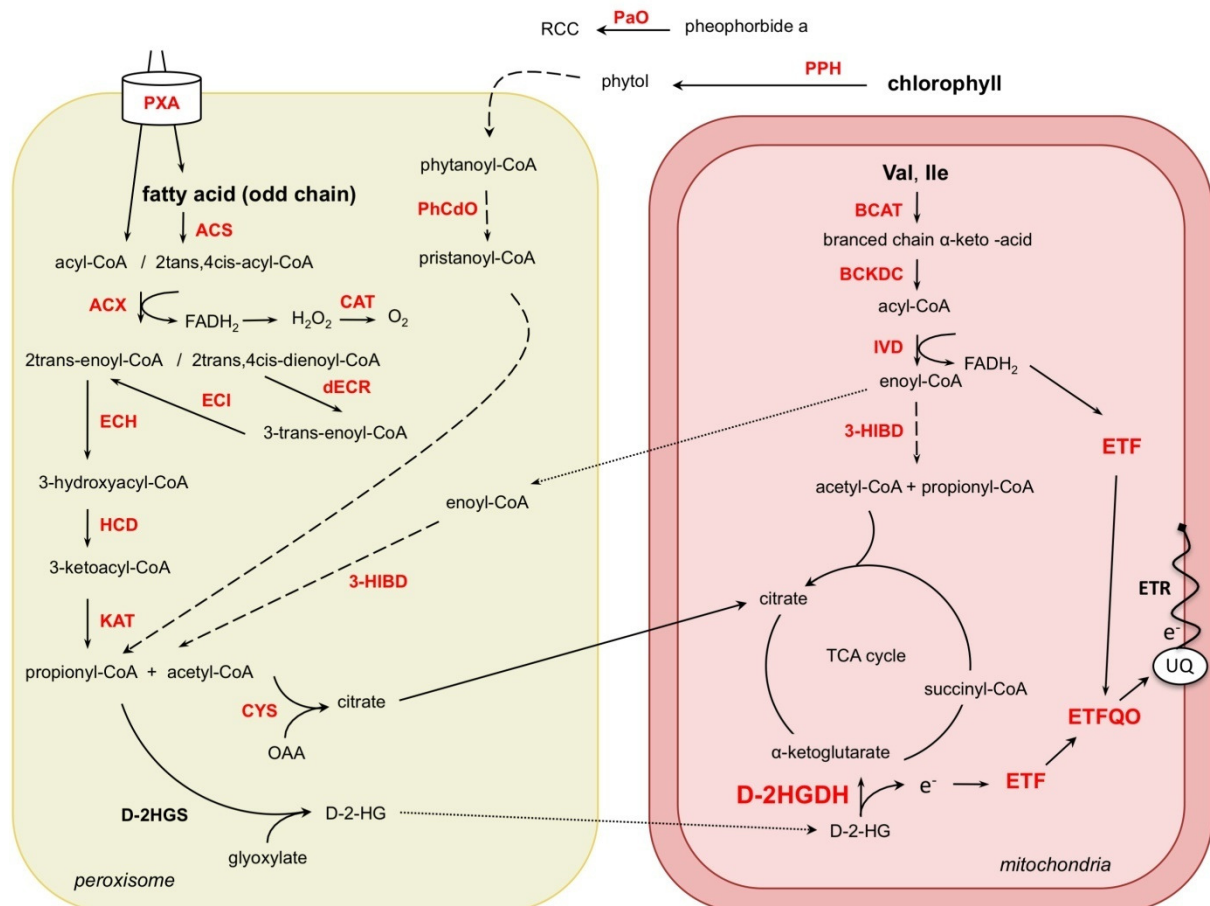


Figure 31. *In silico* co-expression analysis of *AtD-2HGDH*. Genes co-expressed with *AtD-2HGDH* (from Table 9) are indicated in red. Only genes participating in valine (Val) and isoleucine (Ile) catabolism, phytol breakdown and β -oxidation are shown.

3.2.13 Dark-induced senescence and metabolite profiling

Based on the indications that *AtD-2HGDH* is co-regulated with genes from fatty acid β -oxidation, phytol breakdown and catabolism of valine and isoleucine, plant dark-induced-senescence experiments were performed. Control samples were taken in the middle of the light period of 5-week-old short-day grown wild-type and *d2hgdh* plants. At the end of the light period the plants were transferred to complete darkness for 4 days. During this dark incubation further samples were taken after 16 h of darkness, which is the normal length of the night, and subsequently after 24, 48, 72 and 96 h of extended darkness. As a measurement of plant fitness during this experiment the Fv/Fm ratio of live plants was recorded at each time point using an imaging-PAM (Fig. 32). From the tissue samples taken, total metabolites were extracted, and a metabolic fingerprinting was conducted by GC-MS

(Fig. 33). Both metabolite measurements and PAM imaging were done for the two knock-out lines *d2hgdh 1-1* and *d2hgdh 1-3*, but since they showed the same profile, only the metabolite data of *d2hgdh 1-1* is displayed for simplicity.

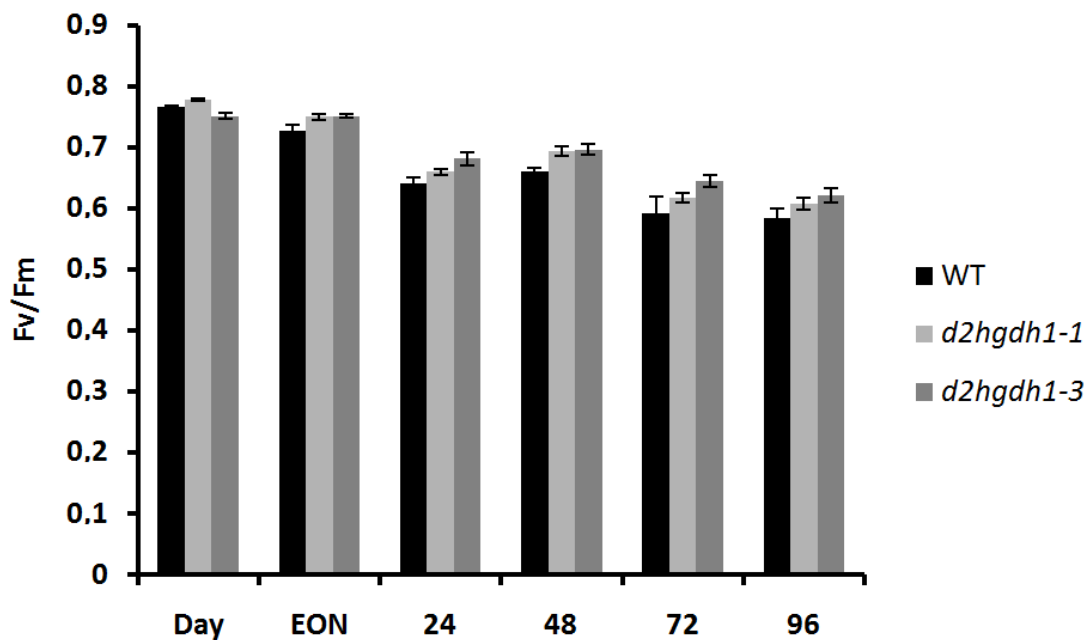


Figure 32. Fv/Fm ratio of dark-treated plants. An IMAGING-PAM Maxi system was used for the measurements. For the first time-point plants were incubated 20 min in the dark before measurement, the other time-points were measured directly. Fv/Fm ratio was recorded in the middle of the light period (Day), at end of the night (EON) and after 24, 48, 72 and 96 h of extended darkness and was calculated for at least 4 leaves of each plant and the averages are displayed. Bars indicate standard error.

Several differences were observed between the metabolite profiles of wild-type and knock-out plants. There was a slight elevation of the organic acids citrate, isocitrate, succinate and fumarate at 48, 72 and 96 hours of extended darkness (Fig. 33). 2-oxoglutarate, the product of the D-2HDGH reaction, was also constitutively higher in knock-out plants. In contrast, malate levels remained identical between the two genotypes. Moreover, no accumulation of lactate or glycolate could be observed in the mutant plants, showing once more that AtD-2HDGH does not participate in the metabolism of these substrates. There was also no difference in sugar metabolism as indicated by the mannose, sucrose, fructose and glucose levels. However, in the knock-out mutants there was a substantial accumulation of most amino acids (Fig. 33), including those known as markers of senescence like valine, isoleucine, phenylalanine, tyrosine and tryptophan (Fahnenstich et al., 2007). By far the most striking difference between wild-type and knock-out plants is the continuous accumulation of 2HG in dark-treated knock-out plants (Fig. 33, top right).

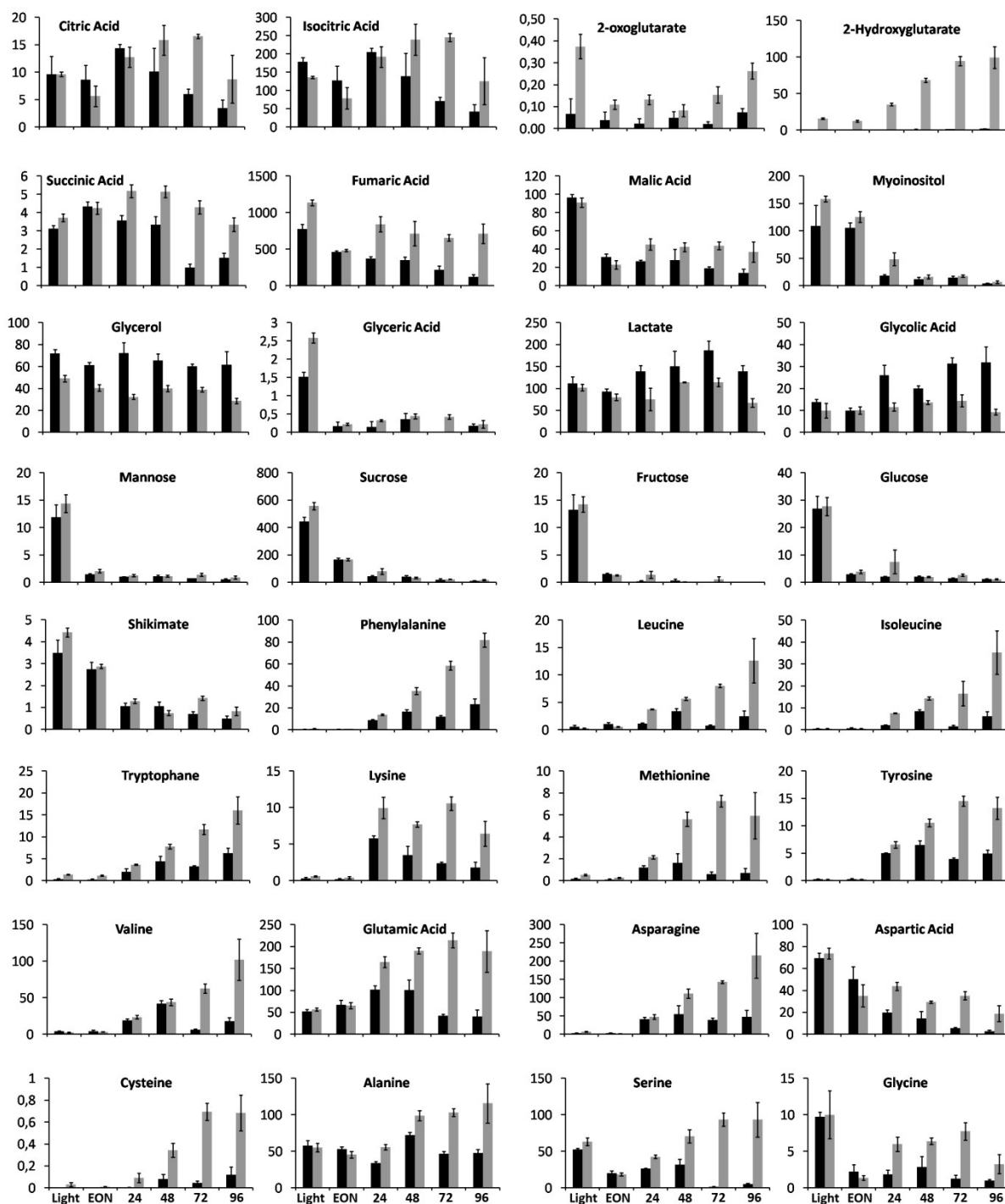


Figure 33. GC-MS metabolite profile of wild-type and *d2hgdh* plants. Leaf tissue from 5-week old short-day grown plants was analyzed by GC-MS. The samples were taken at the following timepoints: Light: in the middle of the light period (4h of light), EON: at the end of a night (16h dark), 24: 24 h of extended darkness, 48: 48 h of extended darkness, 72: 72 h of extended darkness, 96: 96 h of extended darkness. The y-axis denotes the peak area. Black bars represent wild-type and grey bars *d2hgdh1-1* plants.

To better visualize this drastic accumulation of 2HG the same data is reproduced in Fig. 34, but in this case with both knock-out lines. While the relative accumulation of 2-HG in wild-type and knock-out plants is similar after 96 hours of extended darkness, the levels of this metabolite was close to the detection limit in wild-type plants and 50-100 times higher in the knock-out plants.

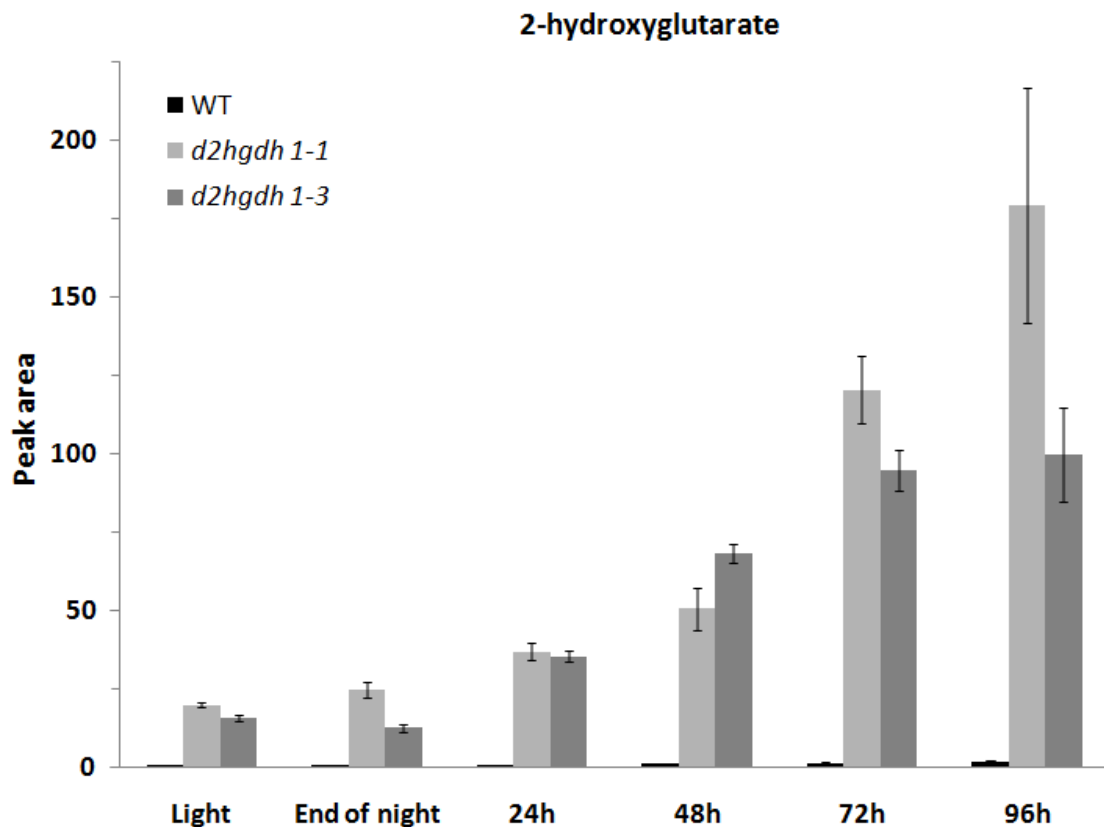


Figure 34. Accumulation of 2HG in knock-out plants during extended night. Leaf tissue from 5-week-old short-day grown plants was analyzed by GC-MS. The samples were taken at the following time points: Light: in the middle of the light period (4h of light), at the end of a night (16 h dark), 24: 24 h of extended darkness, 48: 48 h of extended darkness, 72: 72 h of extended darkness, 96: 96 h of extended darkness.

3.3 Characterization of the enzyme encoded by At4g18360

All the data collected for AtD-LDH and AtD-2HGDH indicate that they do not efficiently metabolize glycolate *in vitro* or *in vivo*. Another approach thus needs to be pursued to find a GDH suitable for the chloroplastic GMK pathway (Fig. 5). To determine whether a suitable enzyme is already present in *A. thaliana*, total protein was extracted from leaves and roots. The proteins were subsequently separated by native-PAGE and assayed for activity using either D-lactate, L-lactate or glycolate as substrates and using one of the two electron carriers PMS or NAD⁺ (Fig. 35). This method enables separation of enzymes and specific visualization of their respective activities. By separately employing PMS and NAD⁺ one can visualize proteins with different co-factor preference.

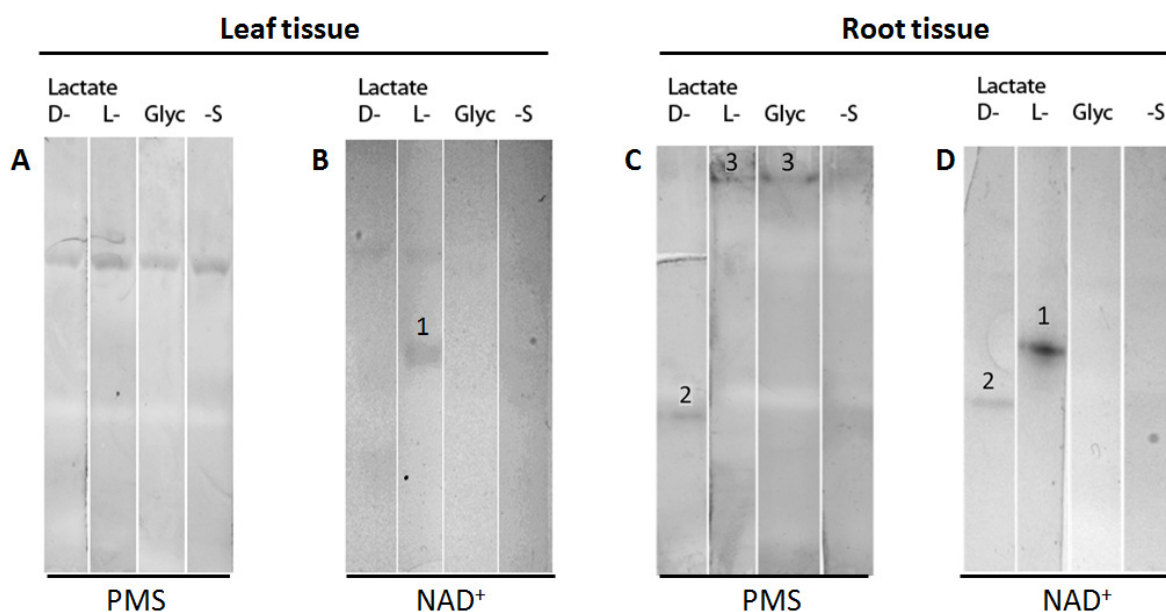


Figure 35. In-gel staining of plant total protein. Total root and leaf protein was extracted from *A. thaliana* and were run on native-PAGE with 30 µg protein in each lane. The gels were subsequently cut in pieces and stained with different substrates and acceptors for 16 h in the dark at 30°C.

Assaying leaf protein extracts with PMS as an electron carrier yielded a band of low mobility (Fig. 35 A). This is the same unspecific band that was observed previously (Fig. 19 A), and can therefore be disregarded. When leaf extracts were further assayed with NAD⁺ one single band was observed with L-lactate (Fig. 35, B 1). Root extracts assayed with PMS yielded bands for each of the three substrates (Fig 35 C). It is likely that the band observed with L-lactate and glycolate on this gel resulted from the same enzyme as they had the same mobility (Fig. 35, C 3). When assaying root extracts with NAD⁺, two bands of different mobility could be observed with D-lactate and L-lactate (Fig. 35, D 1 and 2). The band observed with D-lactate using both PMS and NAD⁺ as electron carriers had the same mobility (Fig. 35, C 2 and D 2). When loading more leaf protein on the gels and extending the incubation time a band with the same mobility as that found in root tissue (Fig. 35, C and D) could be detected when staining with D-lactate (data not shown)

It thus appears that three distinct activities have been detected using this approach; one activity that is present in leaves and roots, capable of oxidizing L-lactate with NAD^+ as a co-factor (Fig. 35, B 1 and D 1), one activity present in roots, and to a lesser extent in leaves (not shown), which oxidizes D-lactate with either NAD^+ or PMS as a co-factor (Fig. 35, C 2 and D 2), and finally, one activity present only in roots that oxidizes L-lactate and glycolate using PMS as a co-factor (Fig. 35, C 3).

This latter enzymatic activity seemed a fitting new candidate for a GDH as it evidently consumes glycolate. However, the identity of the enzyme responsible for this activity was not known and must therefore be determined before the enzyme could be used in further experiments.

3.3.1 Identification of the candidate

From the in-gel assays performed previously, a few properties about the enzyme could be determined. It could oxidize glycolate, L-lactate and L-2HB using PMS as an electron acceptor, but not with NAD^+ or NADP^+ as electron acceptors. Moreover, the enzyme did not show any activity with the D-enantiomer of either lactate or 2HB. Using this information, the existing literature, as well as enzyme databases, were searched for enzymes with similar characteristics. Such an enzyme was found among the L-lactate cytochrome c oxidoreductases (L-LDHc, EC 1.1.2.3) as well as among the (S)-2-hydroxy-acid oxidases (HAOX, EC 1.1.3.15). From the L-LDHc enzyme properties deposited in the BRENDA database (Chang et al., 2009) only the *S. cerevisiae* CYB2 had a low level of activity with glycolate, but could use DCIP as an electron acceptor in enzyme assays. In contrast, several of the HAOX enzymes in the database had activity with glycolate, L-lactate and L-2HB using either oxygen or DCIP as an electron acceptor. When performing a BLAST search on *A. thaliana* protein, using the amino acid sequence of either the *S. cerevisiae* CYB2 or the *H. sapiens* HAOX1, the same top five hits were retrieved both times. These were AtGOX1, AtGOX2, AtGOX3, AtHAOX1 and AtHAOX2, all five *A. thaliana* GOs (Fig. 2). Furthermore, from these five candidates only At4g18360, coding for AtGOX3, was expressed in roots and not in leaves (<http://bar.utoronto.ca/efp/cgi-bin/efpWeb.cgi>), a pattern also observed on the activity gels in Fig. 35. AtGOX3 therefore became the main candidate gene suspected to encode the glycolate dehydrogenase seen on the native gel. A multiple sequence alignment of the five GOs together with the *H. sapiens* HAOX1 is shown in Fig. 36.

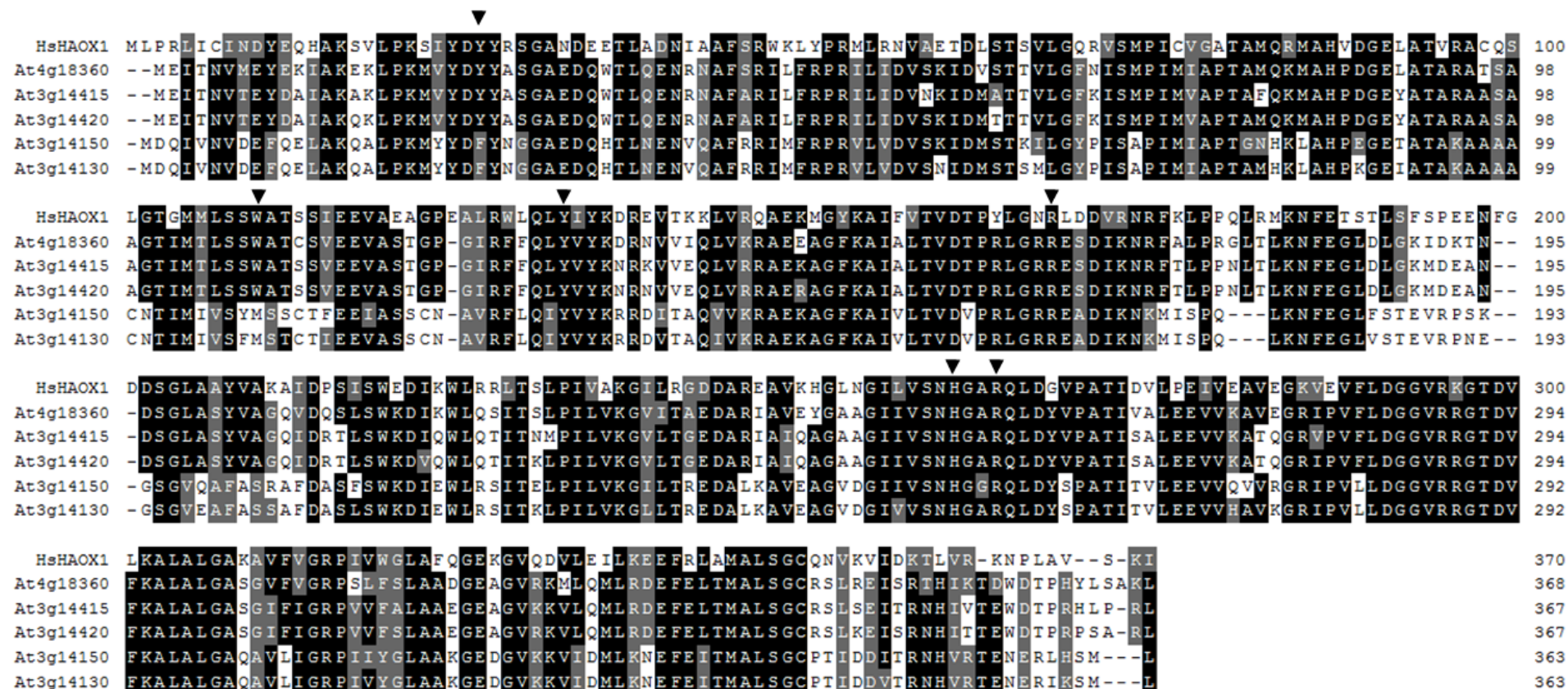


Figure 36. Sequence alignment of HAOX1 from *H. sapiens* and the five glycolate oxidases from *A. thaliana*. At3g14420 (GOX1), At3g14415 (AtGOX2), At4g18360 (AtGOX3), At3g14130 (AtHAOX1), At3g14150 (AtHAOX2) and *H. sapiens* HAOX1 protein sequences were aligned using the multiple alignment software MUSCLE. Conserved amino acids are shown with a black background, amino acids with similar properties are shown in grey. The residues are only colored if more than 4 of the sequences show the same property. A conserved FMN dependent dehydrogenase domain stretches over the whole protein. Residues in the catalytic site are indicated by arrowheads.

3.3.2 Isolation of knock-out mutants

To test whether the enzyme detected in the in-gel assays using glycolate, L-lactate and L-2HB is encoded by At4g18360 the T-DNA insertion line GK_523D09, here referred to as *gox 3-1*, was ordered from NASC (Fig. 37 A). The lines were grown on soil, and checked for homozygous T-DNA insertions by PCR. RNA was further isolated from the homozygous plants and first strand cDNA synthesis performed. Using primers spanning the T-DNA insertions the knock-out plants were checked for native transcript for the disrupted gene. The *gox 3-1* line lacks native transcript (Fig. 37 B).

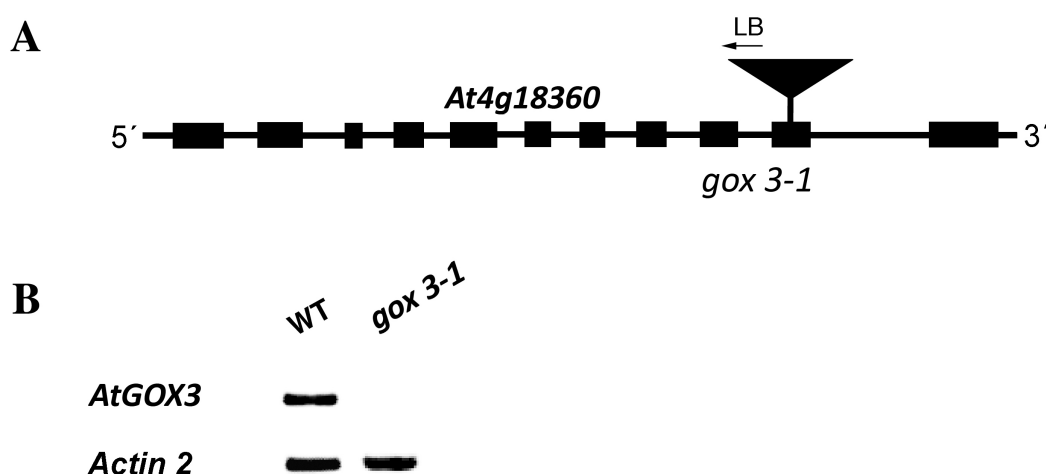


Figure 37. Confirmation of At4g18360 T-DNA insertion mutants. (A) A schematic representation of At4g18360, exons are represented by blocks and introns by lines. The sites of the T-DNA insertion is indicated. T-DNA insertion is not drawn to scale. (B) To confirm gene disruption RNA was extracted from knock-out and wild-type roots and first-strand cDNA synthesis was performed. Primers spanning the T-DNA insertion sites were used for PCR-amplification and were separated by agarose gel electrophoresis.

3.3.3 In-gel assays of knock-out mutants

Total root protein was isolated from wild-type and *gox 3-1*, run on a native-PAGE and assayed for activity using L-lactate, glycolate or D-2HG as substrates and PMS as an electron carrier (Fig. 38). In the two gels assayed with L-lactate and glycolate, a clear band can be seen in the wild-type sample whereas it is missing in the knock-out extract (Fig. 38, A and B). Also the band observed when assaying with L-2HB was absent in the knock-out extracts (data not shown). These results identify At4g18360 to encode the glycolate, L-lactate and L-2HB oxidizing enzyme seen on the native-PAGE gels. The D-2HG-stained gel serves as a positive control for equal loading and activity (Fig. 38, C).

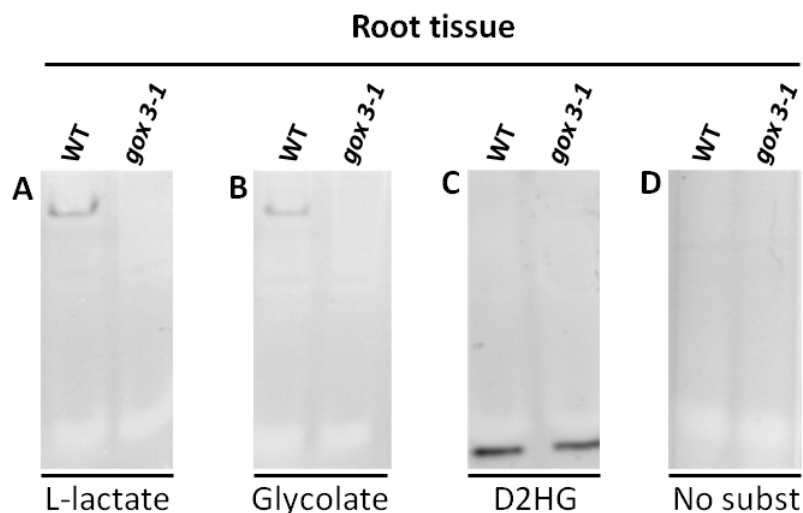


Figure 38. In-gel activity assays of plant protein extracts. Total root protein was extracted from *A. thaliana* and run on native-PAGE with 50 μg protein in each lane. The gels were subsequently stained with substrates as indicated using PMS as an acceptor. Gels were stained with D-2HG for 2 h and with L-lactate and glycolate for 16 h in the dark at 30°C.

3.3.3 Cloning, heterologous expression and purification of AtGOX3

The entire *GOX3* coding sequence was amplified from root cDNA and cloned in-frame with the N-terminal His-tag present in the pET16b expression vector and transformed in BLR cells. Cultures were grown and samples were taken before and after expression induction through IPTG addition (Fig. 39, 1 and 2). Western blot experiments using anti His antibodies confirmed the expression in induced cells. AtGOX3 was further purified to over 95% purity from the induced cells using Ni^{2+} -NTA affinity chromatography (Fig. 39, 3).

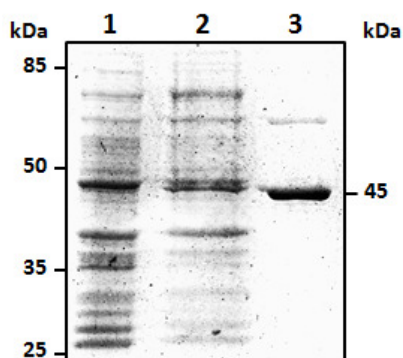


Figure 39. SDS gel of AtGOX3 purification. Lane 1, 20 μg of noninduced cell culture lysate. Lane 2, 20 μg of cell culture lysate after 4 h of induction with isopropyl β -D-thiogalactopyranoside. Lane 3, 5 μg of purified recombinant AtGOX3.

3.3.4 Co-factor analysis and pH optimum

To biochemically characterize AtGOX3, the enzyme activity with glycolate was tested using a number of different electron acceptors (Table 10). Glycolate was used due to the high sequence similarity of AtGOX3 with glycolate oxidases (Fig. 36) and since in-gel assays showed the enzyme to be active with this substrate (Fig. 38). No activity could be detected

when assaying the enzyme with either NAD^+ , NADP^+ or cytochrome c, or with glyoxylate and either NADH or NADPH. In contrast, when assaying for activity using no acceptor, by measuring product accumulation, or when assaying with DCIP high activity could be detected.

Table 10. Co-factor analysis of AtGOX3. The preferred co-factor of AtGOX3 was tested with the purified enzyme, 10 mM substrate and either of 200 μM cytochrome c, 200 μM DCIP and 3 mM PMS, 1 mM NAD(P)^+ or 1 mM NAD(P)H . Reduction of the acceptors was monitored photometrically. When measuring the activity with O_2 as an acceptor the product accumulation was monitored using phenylhydrazine. The activity given is the activity relative to the best acceptor. The values presented are the average of two independent experiments.

Substrate + Acceptor	Activity (%)
Glycolate + O_2	100
Glycolate + Cytochrome c	-
Glycolate + DCIP	99
Glycolate + NAD(P)^+	-
Glyoxylate + NAD(P)H	-

The pH optimum for AtGOX3 was further determined in 100 mM TRIS-HCl buffer, using glycolate as substrate and with the two best acceptors, O_2 and DCIP (Fig. 40). With both acceptors, the enzyme pH dependent activity has a bell-shaped curve with a pH optimum at about 7.5, while retaining about 20% of the activity at pH 6.0 and pH 9.5.

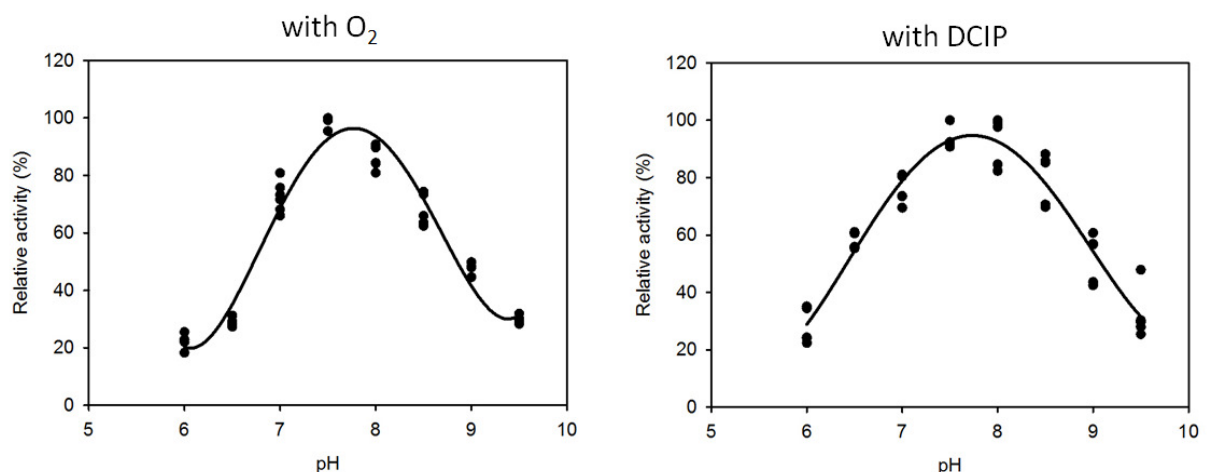


Figure 40. pH optimum of AtGOX3. The pH optima of AtGOX3 was determined in standard assay conditions with 100 mM TRIS-HCl using either no added acceptor (left panel), in which case O_2 served as the ultimate electron acceptor, or PMS and DCIP (right panel). The values presented in each separate figure are the relative activity compared to the highest activity obtained.

3.3.5 Substrate screening

In-gel assays of AtGOX3 from plant extracts showed that the enzyme oxidizes both glycolate and L-lactate, but not D-lactate (Fig. 35, C and D, Fig. 38). These substrates were tested in a substrate screening with the purified enzyme. The activity with glycolate and both enantiomers of lactate and 2HB were assayed using oxygen or DCIP as acceptors (Fig. 41). Recombinant, purified AtGOX3 has activity with glycolate, L-lactate and L-2HB, but not with D-lactate or D-2HB. These results, perfectly parallel those from the in-gel assays performed with native plant protein. Interestingly, the enzyme shows different preferences for the substrates depending on which acceptor is used. While the activity with glycolate is around 43% with both acceptors, the activity decreases with larger substrates when O₂ is used as an acceptor, whereas the activity increases with larger substrates when DCIP is used as an acceptor. This effect was reproduced with different batches of purified enzyme.

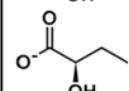
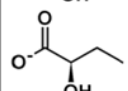
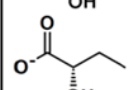
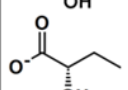
with O ₂			with DCIP		
Structure	Name	Activity (%)	Structure	Name	Activity (%)
	Glycolate	42		Glycolate	43
	D-Lactate	0		D-Lactate	0
	L-Lactate	32		L-Lactate	100
	D-2-Hydroxybutyrate	0		D-2-Hydroxybutyrate	0
	L-2-Hydroxybutyrate	16		L-2-Hydroxybutyrate	96

Figure 41. Substrate screening with AtGOX3. Purified AtGOX3 was assayed at pH 7.5 with a range of substrates present at a concentration of 10 mM. Either oxygen or PMS and DCIP served as electron acceptors. The values presented are the averages of two separate experiments and indicate the activity relative to the best substrate, with the best acceptor.

3.3.6 Determination of kinetic constants

The AtGOX3 kinetic constants with glycolate, L-lactate and L-2HB were determined using oxygen and DCIP as acceptors in a 100 mM TRIS-HCl buffer pH 7.5. When using oxygen as an acceptor the enzyme showed high affinity for all substrates with K_m values of a few hundred μM (Table 11). In contrast, when using DCIP as an acceptor the enzyme had a K_m in the μM range with glycolate, whereas it was in the mM range with the two other substrates. However, the catalytic rates were higher when using DCIP as an acceptor. Thus, the catalytic efficiency (k_{cat}/K_m) indicates that the best substrate with both acceptors is glycolate although the difference to the other substrates is small.

Table 11. AtGOX3 kinetic constants. Assays were performed with 1-2 μg purified enzyme, in 100 mM TRIS-HCl buffer pH 7.5 with either no acceptor or 3 mM PMS and 200 μM DCIP as acceptors in a reaction volume of 200 μl . Substrate concentrations between 50 mM and 5 μM were assayed and the catalytic constants were determined using non-linear regression. The values presented are the averages of three separate experiments and the standard error is indicated.

AtGOX3	with O ₂		
	K _m (μM)	k _{cat} (min ⁻¹)	k _{cat} /K _m (min ⁻¹ mM ⁻¹)
L-2HB	355 \pm 2	39 \pm 1	110
L-lactate	420 \pm 4	80 \pm 2	190
Glycolate	144 \pm 10	104 \pm 1	725
AtGOX3	with DCIP		
	K _m (μM)	K _{cat} (min ⁻¹)	K _{cat} /K _m (min ⁻¹ mM ⁻¹)
L-2HB	1065 \pm 43	238 \pm 2	223
L-lactate	1479 \pm 117	247 \pm 5	167
Glycolate	344 \pm 29	105 \pm 2	304

3.3.7 Structural considerations

AtGOX3 shares high sequence homology with the *S. oleaceae* glycolate oxidase (not shown) and the *H. sapiens* HAOX1 (Fig. 36), both enzymes for which high-resolution crystal structures exist (PDB ID: 1gox and 2nzi, respectively). The HAOX1 crystal structure was determined in a complex with glyoxylate at 1.35Å resolution. To gain further insight into the catalytic site of AtGOX3, with particular focus on which amino acids coordinate the substrate, the crystal structure of HAOX1 was analyzed. In the analysis, six amino acids playing an important role in the catalytic site could be identified (Fig. 42). All six of these amino acids are conserved in AtGOX3. Moreover, a homology model of AtGOX3, based on the crystal structure of *S. oleaceae* glycolate oxidase (PDB ID: 1gox), was retrieved from the SWISS-MODEL repository. In this model the six amino acids were positioned in the active site.

3.3.8 Plant feeding experiments

The *in vitro* activity assays with purified recombinant AtGOX3 revealed high enzyme activity with both glycolate and L-lactate. To elucidate which of these substrates is the physiological one wild-type and knock-out plants were grown on sterile medium supplemented with either L-lactate or glycolate. On control plates and on plates supplemented with glycolate root growth was similar for both genotypes (Fig. 43, left and right panel), even though a dose-dependent toxicity of glycolate could be observed (not shown). In contrast, root growth on medium supplemented with L-lactate was impaired in *gox3-1* as compared to wild-type plants (Fig. 43, center panel). This difference in root growth was consistently seen in a dose-dependent manner over the concentration range of 0.5 mM to 10 mM L-lactate.

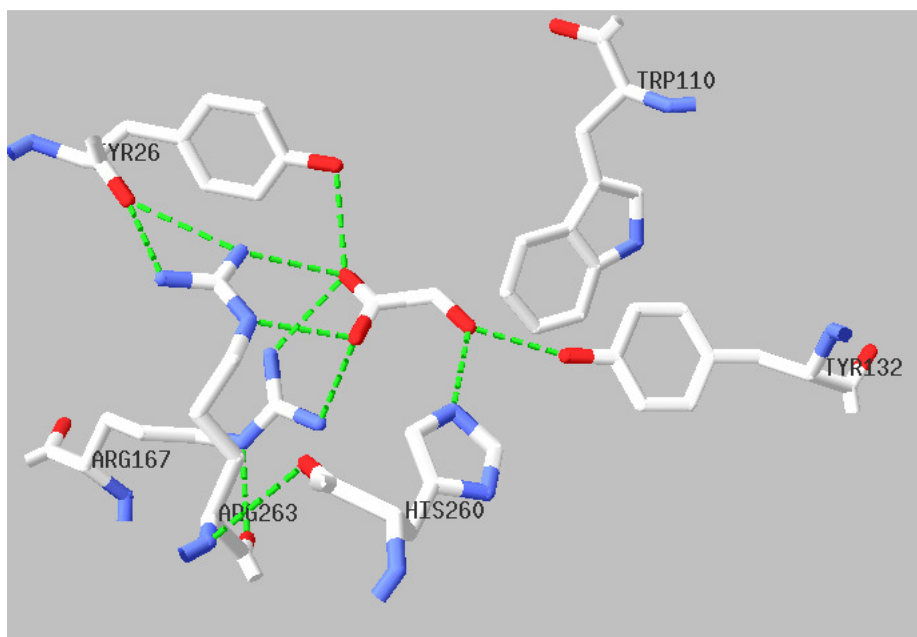


Figure 42. Active site of *H. sapiens* HAOX1 complexed with glyoxylate. The crystal structure for *H. sapiens* HAOX1 (PDB ID: 2nzi) was analyzed to identify catalytically important amino acid residues. Glyoxylate is shown in the middle, kept in place through hydrogen bonds (green dotted lines). Red indicates oxygen atoms and blue nitrogen atoms.

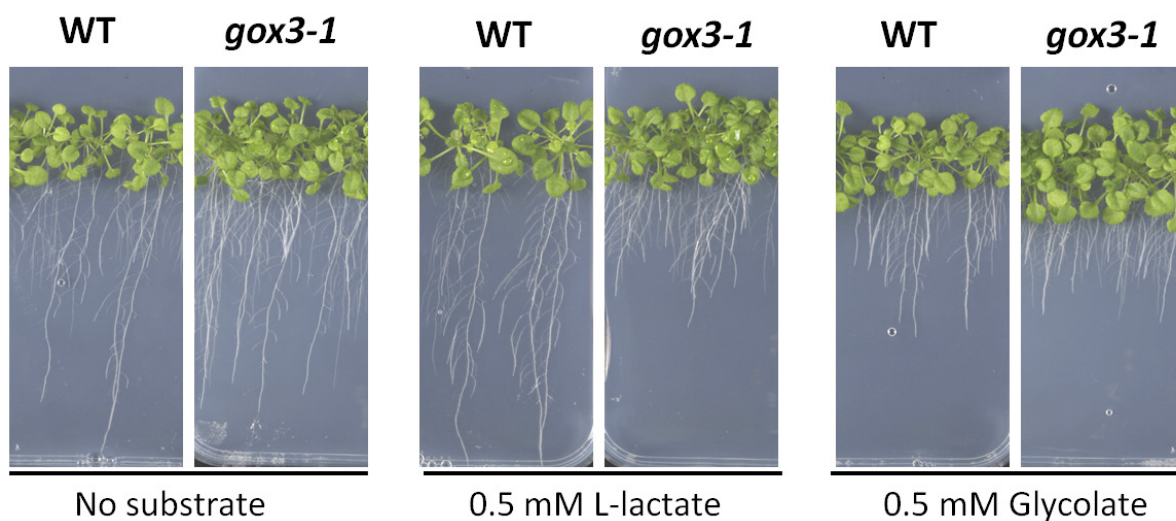


Figure 43. Plant feeding experiments of wild-type and *gox3-1* plants. $\frac{1}{2}$ MS plates without sugar were supplemented with substrates as indicated. Plants were grown at $100 \mu\text{mol m}^{-2} \text{s}^{-1}$ photons in LD conditions for three weeks.

4. Discussion

The main goal of this work was to identify and characterize a glycolate dehydrogenase capable of replacing the H₂O₂-producing glycolate oxidase in the chloroplastic GMK pathway (Fig. 5). The expectations were that the novel pathway should at least parallel, and most likely exceed, the old one in efficiency in decreasing photorespiration. With this purpose in mind, three putative glycolate dehydrogenases from *A. thaliana* were biochemically characterized. Moreover, *in silico* and *in planta* analysis allowed for roles of these enzymes in novel metabolic pathways to be proposed.

4.1 At5g06580 encodes a D-LDH

4.1.1 AtD-LDH is conserved in evolution and localizes to mitochondria

The enzyme encoded by At5g06580 was identified as a good candidate for the chloroplastic GMK pathway since it had previously been described as a glycolate dehydrogenase (Bari et al., 2004; Niessen et al., 2007). To ensure that the enzyme would be suited for the pathway its complete characterization was undertaken. A phylogenetic analysis performed with the amino acid sequence of At5g06580 showed that the enzyme shares strong homology with enzymes from plants, animals, fungi and yeasts (Figs. 7 and 8). The conservation of this enzyme in such a wide range of organisms is an indication that it may play an important role in metabolism, as it may otherwise easily have been lost. The orthologs in mammals, (Flick and Konieczny, 2002) and unicellular fungi (Gregolin and Singer, 1963; Lodi and Ferrero, 1993; Lodi et al., 1994) are cytochrome c- dependent D-lactate dehydrogenases (EC 1.1.2.4).

The purified mature AtD-LDH protein, lacking the transit peptide, was shown to be a homodimeric FAD-containing flavoprotein (Fig. 11 and Table 3). Consistent with this, the protein was predicted to have a conserved FAD binding domain, and a C-terminal FAD-linked oxidase domain (Fig. 8). The enzyme was found to have high activity with both cytochrome c and DCIP as acceptors (Table 4). Activity with both these acceptors is a common feature of many D-lactate dehydrogenases (Table 2). Since DCIP is a synthetic electron acceptor it must therefore be concluded that cytochrome c is the likely *in vivo* acceptor of AtD-LDH. Cytochrome c is present in the mitochondrial intermembrane space where it shuttles electrons between complex III and complex IV in the respiratory chain. This is consistent with the mitochondrial localization of AtD-LDH which is predicted by targeting sequence prediction software (<http://aramemnon.botanik.uni-koeln.de/index.ep>) and additionally confirmed by subcellular localization studies performed using a GFP fusion protein (Bari et al., 2004). Moreover, there is a predicted hydrophobic α -helix between amino acid 48-68 of AtD-LDH (<http://aramemnon.botanik.uni-koeln.de/index.ep>) that may serve to anchor the protein in the mitochondrial inner membrane. This would bring AtD-LDH closer to cytochrome c, which is associated with the mitochondrial inner membrane (Kostrzewa et al., 2000).

4.1.2 AtD-LDH is specific for D-lactate and D-2HB

AtD-LDH was highly specific for D-2-hydroxy-acids (Fig. 13 and Table 5). Even though the enzyme had moderate catalytic rates with L-lactate and D-glycerate, the enzyme had very low affinity for these substrates (Table 5). Through a combination of low K_m - values and a high k_{cat} of AtD-LDH with D-lactate and D-2HB, the catalytic efficiency (k_{cat}/K_m) with these two substrates exceeds by far that of the other substrates and one of them are likely to be the *in vivo* substrate (Table 5). Moreover, while AtD-LDH displayed high affinity for glycolate, it had an extremely low catalytic rate towards this substrate. It is therefore highly unlikely that the enzyme participates in glycolate metabolism *in planta*. High cytochrome c-dependent activity with D-lactate and D-2HB and low or no activity with L-lactate and glycolate, are characteristics similar to those of characterized D-LDHs from *P. elsdonii* (Brockman and Wood, 1975), *S. cerevisiae* (Gregolin and Singer, 1963), *R. palustris* (Horikiri et al., 2004), and *D. vulgaris* (Ogata et al., 1981) (Table 2). The obtained results therefore indicate that At5g06580 should be re-classified from the EC 1.1.99.14 group into the EC 1.1.2.4 group (cytochrome c-dependent D-LDH).

No crystal structure exists of any cytochrome c- dependent D-LDH and the catalytically important residues are therefore not known. However, in this work, nine amino acid residues with putative catalytic roles in AtD-LDH were identified through a combination of multiple sequence alignment and evaluation of a homology model (Fig. 14, indicated in black). All these residues share the feature that they are highly conserved and are also positioned in the catalytic site of the homology model. The use of homology models for identifying catalytic residues is frequently performed with much success (Ito et al., 2009; Rahier et al., 2009). The purpose of this analysis was to identify targets for directed mutagenesis of AtD-LDH and the function of these residues must be confirmed using such an approach.

4.1.3 AtD-LDH metabolizes D-lactate *in vivo*

Two independent T-DNA insertion lines for At5g06580 were isolated and these were shown to be completely devoid of native AtD-LDH transcript (Fig. 15), but still showed no phenotype deviating from that of wild-type plants. Expression of AtD-LDH in *E. coli* mutants lacking any of the three subunits of glycolate oxidase restores growth on glycolate (Bari et al., 2004), indicating the enzyme would be able to metabolize glycolate, at least when high concentrations of this substrate are present. However, when growing *lddh* plants on high concentrations of glycolate, no difference between wild-type and knock-out plants could be observed, even though toxic levels of the substrates were reached as seen by the stunted growth of plants in these experiments (Fig. 17). The lack of difference between wild-type and knock-out plants growing on this substrate strongly indicates that AtD-LDH does not metabolize it *in planta* as the knock-out plants should otherwise be more sensitive than wild-type plants. The low catalytic activity determined for AtD-LDH using glycolate (Table 5) is a further indication that glycolate may not be the substrate *in vivo*.

In contrast, when plants were grown on plates containing D-lactate or D-2HB, the knock-out mutants were much more sensitive than wild-type plants, indicating that AtD-LDH can detoxify these substrates *in vivo*. While 2-ketobutyrate, the product of D-2HB oxidation, is an intermediate in isoleucine biosynthesis, there are no reports about possible production of D-2HB in plant tissues. In mammals, D-2HB is produced principally in hepatic tissues as a by-product during L-threonine catabolism (Hammer et al., 1996) and glutathione biosynthesis (Fernández-Checa et al., 1992) but this has not been shown in plants. It is therefore likely that the high activity of AtD-LDH toward D-2HB represents a side reaction of no physiological importance.

There is, however, evidence of D-lactate production through the consecutive action of glyoxalase I and glyoxalase II in the methylglyoxal detoxification pathway (Fig. 6) (Atlante et al., 2005; Thornalley, 1990). In *A. thaliana*, glyoxalase I (At1g67280) and glyoxalase II (At1g06130) have been identified and are ubiquitously expressed. Glyoxalase I is found exclusively in the cytosol (Thornalley, 1990), and glyoxalase II is localized to the cytosol and mitochondria (Atlante et al., 2005; Maiti et al., 1997). The import of D-lactate into plant mitochondria by a D-lactate/H⁺ symporter or a D-lactate/malate carrier and its subsequent metabolism by a flavoprotein has been reported in *H. tuberosus*, but no genes encoding the responsible enzymes were identified (Atlante et al., 2005; de Bari et al., 2005). The ubiquitous expression of AtD-LDH (Winter et al., 2007), its mitochondrial localization (Bari et al., 2004; Schwacke et al., 2003), and its preference for D-lactate indicate that this enzyme may perform the oxidation of D-lactate produced in mitochondria or cytosol through the glyoxalase system in *A. thaliana* (Fig. 6). A role of AtD-LDH in the MG detoxification pathway was further substantiated by growing plants on different concentrations of D-lactate and MG (Fig. 18). AtD-LDH knock-out plants are more sensitive than wild-type towards both D-lactate as well as its precursor MG. This shows that AtD-LDH is needed by *A. thaliana* plants to cope with high levels of MG and is a very strong indication for the participation of AtD-LDH in the MG detoxification pathway.

4.1.4 Plants may have a second MG detoxification pathway

Given the importance of MG detoxification, the fact that AtD-LDH knock-out mutants show no phenotype in standard growth conditions is surprising. Even on high salt or mannitol medium, conditions where MG detoxification is of increased importance (Xu and Chen, 2006; Yadav et al., 2005), there is no visible phenotype. Moreover, MG would rapidly accumulate in cells if it was not metabolized (Phillips and Thornalley, 1993). These facts all point towards the existence of a second, alternative MG detoxification pathway in plants. One such pathway is known in mammals, where an α -ketoaldehyde dehydrogenase (EC 1.2.1.23), also known as methylglyoxal dehydrogenase, directly converts MG into pyruvate. This enzyme has been purified from sheep (Monder, 1967) and goat liver extracts (Ray and Ray, 1982a; Ray and Ray, 1982b). The same enzyme has also been assayed in rat extracts by separating protein on a starch gel with subsequent activity staining (Bender et al., 1994). This approach was adapted here and used to show the presence of methylglyoxal

dehydrogenase activity in *A. thaliana* root extracts (Fig. 19). The existence of a second MG detoxification pathway in plants is therefore plausible, and may explain the lack of a phenotype in the AtD-LDH knock-out mutants. The gene coding for the rat methylglyoxal dehydrogenase has been mapped to the top of chromosome 13 using inbred lines (Bender et al., 1994; Pravenec et al., 1996) but unfortunately its identity is not known.

4.1.5 Model

The results presented here indicate that At5g06580 encodes a D-LDH with a role in D-lactate metabolism (Fig. 44). D-lactate is produced from the MG detoxification pathway with the final step being catalyzed in the cytosol and mitochondria. The produced D-lactate is then oxidized by AtD-LDH to pyruvate inside the mitochondrial intermembrane space. The resulting electrons are donated to cytochrome c and used in the electron transport chain.

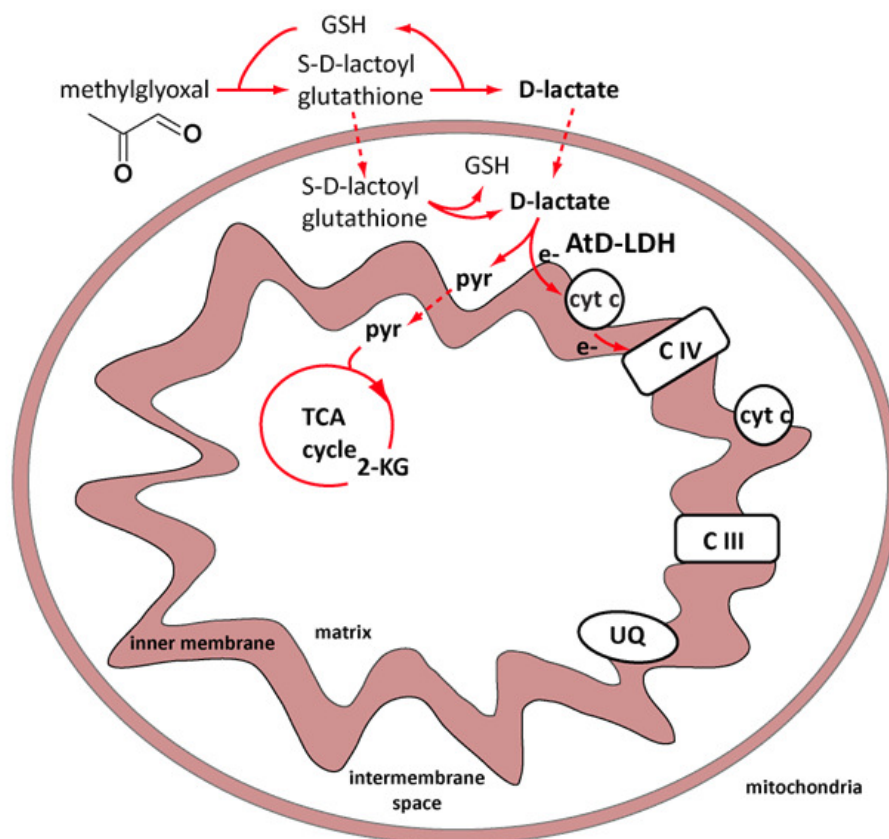


Figure 44. Schematic model of AtD-LDH function in plants. D-Lactate resulting from the glyoxalase system is converted to pyruvate by AtD-LDH. The electrons may be transferred to the respiratory chain through cytochrome c in the intermembrane space. Dotted arrows represent possible transport processes. 2-KG, 2-oxoglutarate. CIII, complex III. CIV, complex IV. e⁻, electron. GSH, glutathione. Pyr, pyruvate. TCA cycle, tricarboxylic acid cycle; UQ, ubiquinone.

4.1.6 Outlook

To verify the proposed model (Fig. 44), a metabolic fingerprinting analysis by GC-MS of *dl dh* knock-out plants in comparison with wild-type plants should be undertaken to better understand the physiological role of AtD-LDH. Moreover, as GC-MS analysis cannot discriminate between L- and D- enantiomers, the measurements need to be combined with enzymatic determination of D- and L-lactate levels in plant extracts. Additionally, mitochondria could be purified from wild-type and knock-out plants and respiration with D-lactate in comparison with glycolate should be measured. The *in vivo* use of cytochrome c as a co-factor could also be confirmed or disproved using purified mitochondria. Poisoning of complex III can be achieved using KCN and the electrons originating from the TCA cycle would then not lead to oxygen consumption. In contrast, giving D-lactate to poisoned mitochondria should lead to oxygen consumption as AtD-LDH would be able to donate electrons directly to cytochrome c, which then transports them to complex IV.

4.2 At4g36400 encodes a D-2HGDH

4.2.1 AtD-2HGDH is conserved in evolution and localizes to mitochondria

The amino acid sequence of At4g36400 shows strong similarity to enzymes from plants, animals and fungi (Fig. 20). Moreover, out of the homologous sequences, those from *R. norvegicus* (Achouri et al., 2004) and *H. sapiens* have been identified as D-2-hydroxyglutarate dehydrogenases (D-2HGDH) (Achouri et al., 2004; Struys et al., 2005b) whereas the two *S. cerevisiae* sequences have been identified as D-lactate dehydrogenases (Chelstowska et al., 1999). Based on the high sequence similarity of the two yeast sequences with the human D-2HGDH (Fig. 21), it is highly likely that these enzymes are also D-2HGDH enzymes, but this has never been tested. This conclusion is not only supported by the phylogenetic tree and alignments presented here, but also by a recent study that extensively investigated the phylogenetic relationship of D-LDH and D-2HGDH enzymes (Cristescu and Egbosimba, 2009).

The purified recombinant AtD-2HGDH was shown to be a dimeric FAD-containing flavoenzyme (Fig. 24 and Table 6). Consistent with this, the protein was predicted to have a conserved FAD binding domain and a C-terminal FAD-linked oxidase domain (Fig. 21). The purified AtD-2HGDH almost exclusively uses the synthetic molecule DCIP as an electron acceptor (Table 7). Since the enzyme uses none of the other natural acceptors tested the question is which acceptor is used *in vivo*. The mammalian D-2HGDH is localized to mitochondria (Achouri et al., 2004), where it donates electrons to an electron transfer protein (ETF) which further donates them to ETF-ubiquinone oxidoreductase (ETFQO). ETF and ETFQO are present in the mitochondrial matrix where they serve to transfer electrons collected from soluble mitochondrial dehydrogenases, to the respiratory chain (Frerman and Goodman, 2001; Parker and Engel, 2000). ETF and ETFQO have also been characterized in

plants where they were shown to participate in metabolism of leucine and chlorophyll, especially when plants were subjected to prolonged darkness (Ishizaki et al., 2005; Ishizaki et al., 2006). Since AtD-2HGDH is also localized to mitochondria, as indicated by the predicted mitochondrial targeting sequence (<http://aramemnon.botanik.uni-koeln.de/index.ep>) and further substantiated through activity measurements in enriched mitochondria (Fig. 30), it is highly likely that AtD-2HGDH uses ETF as an electron acceptor *in vivo*. Moreover, the co-expression of ETFQO (At2g43400) and ETFbeta (At5g43430) with AtD-2HGDH further supports this notion (Table 9 and Fig. 31).

The only substrate with which AtD-2HGDH has activity is D-2HG (Fig. 26). This is in contrast to D-2HGDH from rat that has activity with D-lactate, D-2HB and meso-tartrate (Achouri et al., 2004). AtD-2HGDH affinity for D-2HG was 584 μM (Table 8), which is in stark contrast the rat D-2HGDH which has a K_m of $<10 \mu\text{M}$ (Achouri et al., 2004). This may indicate that plants can tolerate higher levels of D-2HG than animals. AtD-2HGDH has no activity with lactate or glycolate and thus belongs to the 2-hydroxyglutarate group (EC 1.1.99.2).

Very little is known about the catalytically important residues in D-2HGDH enzymes and no crystal structures exist. A few mutations have been identified in human D-2HGDH that lead to decreased enzyme activity and therefore result in accumulation of D-2HG in the body (Struys et al., 2005a; Struys et al., 2005b). To extend this knowledge, an approach combining multiple sequence alignment with analysis of homology models was performed and resulted in the identification of eight amino acids located in the catalytic site (Fig. 27). Strikingly, the same kinds of residues, with approximately the same relative position were identified in AtD-2HGDH as in AtD-LDH. Testing the importance of these amino acids through directed mutagenesis should yield a wealth of information about their catalytic function.

4.2.2 D-2HG accumulates in *d2hgdh* mutants

Even though the enzymatic properties of AtD-2HGDH clearly point towards a role in D-2HG catabolism, the participation of this metabolite in plant metabolism was not known. It was, however, detected by GC-MS analysis when *d2hgdh* knock-out and wild-type plants were subjected to conditions of extended darkness. In these conditions there was a strong accumulation of 2HG in the knock-out mutants, but not in wild-type plants (Fig. 34). The levels of this metabolite was already much higher in the mutants than in wild-type under normal light/dark cycles, but after 96 h of extended darkness the levels of 2HG had increased 7-fold. Also the wild-type plants accumulated 2HG in extended darkness, but at a level that was approximately 50-100 times lower than in the *d2hgdh* lines. Despite this high accumulation of D-2HG in the knock-out plants they showed neither visible phenotype nor any change in the Fv/Fm ratio (Fig. 32). These results indicate that D-2HG is not very toxic to plants. Consistent with this, the K_m of AtD-2HGDH was rather high (Table 8). At later time points (48-96 h) there was an elevated level of most amino acids in the knock-out plants (Fig. 33). Amino acid breakdown is usually initiated by a transamination with 2-oxoglutarate, the product of D-2HG oxidation. In the experiments conducted here the accumulation of amino

acids coincided with increasing levels of 2HG and it is thus possible that this metabolite competitively binds and inhibits the catalytic site of transaminases (Dang et al., 2009), resulting in the observed accumulation of amino acids.

4.2.3 D-2HG is most likely produced in a condensation reaction

In mammals, D-2HG is formed as a degradation product of aminolevulinate (Lindahl et al., 1967) and also forms within the mitochondria from 2-oxoglutarate through a hydroxyacid-oxoacid-transhydrogenase in a reaction in which 4-hydroxybutyrate is converted to succinic semialdehyde (Struys et al., 2004). However, no ortholog of this enzyme has been found in plants. In propionate-grown *E. coli* and the slime mold *Aspergillus glaucus* glyoxylate and propionate are condensed into D-2HG by a D-2HG synthase (EC 2.3.3.11) in a reaction analogous to that of malate synthase (Bleiweis et al., 1967; Reeves and Aji, 1962). Normally one would expect a condensation between glyoxylate and propionyl-CoA to proceed on the α -carbon of propionyl-CoA, producing β -methylmalate. The *E. coli* D-2HG synthase, however, catalyzes the addition of glyoxylate on the β -carbon of propionyl-CoA, producing D-2HG directly (Reeves et al., 1963). Unfortunately the gene coding for this enzyme is not known and it is therefore not clear whether it is present in plants.

However, AtD-2HGDH is co-expressed with many of the genes involved in odd-chain fatty acid β -oxidation, chlorophyll breakdown and branched-chain amino acid degradation (Table 9 and Fig. 31), pathways where propionyl-CoA is produced (Lucas et al., 2007). Moreover, it is still unclear how propionyl-CoA is metabolized in plants. In animals, propionyl-CoA is converted, in a series of enzymatic steps, to succinyl-CoA which can enter the TCA cycle. The committing step is catalyzed by propionyl-CoA carboxylase. However, no ortholog corresponding to this enzyme has been found in plants (Lucas et al., 2007). The metabolism of propionyl-CoA must therefore proceed along a different route in plants, and this route may be through the condensation with glyoxylate to produce D-2HG, catalyzed by a D-2HG synthase.

4.2.4 Model

In the current working-model D-2HG is produced, most likely by a D-2HG synthase, outside of the mitochondria. This metabolite is subsequently imported to the mitochondrial matrix where AtD-2HGDH oxidizes it to 2-oxoglutarate, using ETF as an electron acceptor (Fig. 45). The produced 2-oxoglutarate then enters the TCA cycle and the electrons are donated to ETFQO and finally to the electron transport chain.

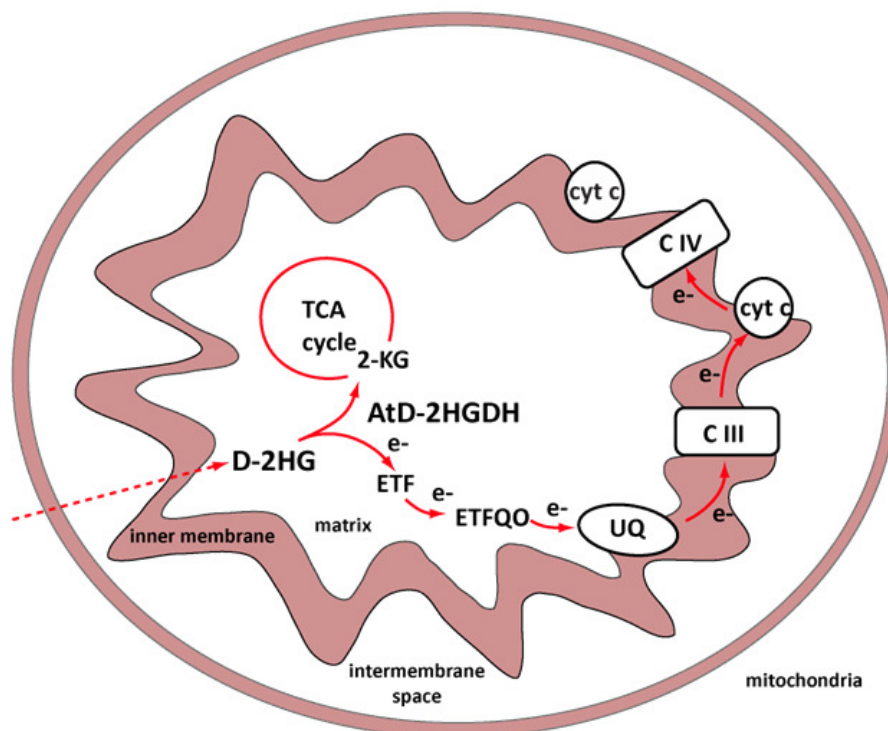


Figure 45. Schematic model of AtD-2HGDH function in plants. D-2HG produced in the peroxisomes is transported to the mitochondria and converted to 2-oxoglutarate by AtD-2HGDH. Electrons are donated to the electron transport chain through the ETF/ETFQO system. 2-KG, 2-oxoglutarate. CIII, complex III. CIV, complex IV. ETF, electron transfer protein. ETFQO, ETF-ubiquinone oxidoreductase. e^- , electron. Pyr, pyruvate. TCA cycle, tricarboxylic acid cycle; UQ, ubiquinone.

4.2.5 Outlook

The accumulation of D-2HG in humans can result either from a mutation in the D-2HGDH enzyme, or in the ETF electron acceptor. In this work it was confirmed that D-2HG also accumulates in plants when the activity of AtD-2HGDH is lacking. It would be of great interest to confirm ETF as the *in vivo* electron acceptor of AtD-2HGDH by measuring D-2HG levels in an ETF or ETFQO mutant. ETF as an acceptor for AtD-2HGDH could further be confirmed by purifying mitochondria from wild-type, AtD-2HGDH mutants and ETF mutants and measure respiration with D-2HG as a substrate. Furthermore, identifying the source of D-2HG in plants would be highly interesting. A first step in this direction should be to try measuring D-2HG synthase activity in plant protein extracts, analogous to the experiments performed in *E. coli*. Moreover, the L- form of 2HG is formed in mammals due to a side reaction catalyzed by the mitochondrial L-malate dehydrogenase and a L-2HGDH exists to remove it (Van Schaftingen et al., 2009). If this production of L-2HG also occurs in plants is unclear, but should be investigated.

4.3 At4g18360 encodes an (S)-2-hydroxy-acid oxidase

Glycolate dehydrogenase activity was observed when assaying wild-type root extract in a native gel (Fig. 35, C 3). The enzyme responsible for this activity appeared highly suitable for use in the GMK pathway. To identify which gene codes for this enzyme a combined approach employing bioinformatics and a literature search was followed. At4g18360 (AtGOX3) was confirmed to encode the enzyme in question as T-DNA insertion mutants in this gene resulted in a loss of enzyme activity (Fig. 38).

4.3.1 AtGOX3 oxidizes glycolate and L-lactate with high efficiency

The complete AtGOX3 coding sequence was cloned and the protein expressed and purified. In enzyme assays AtGOX3 only used the L-enantiomer of substrates such as L-lactate and L-2HB (Fig. 41) and could readily use both the synthetic acceptor DCIP as well as molecular oxygen at equal rates for the oxidation of glycolate (Table 10). Ability to use both these acceptors as well as the total stereospecificity for L- enantiomers are common features of glycolate oxidases (Nelson and Tolbert, 1970). One curiosity seen in the substrate screening is that the best substrate with O₂ as an acceptor is glycolate, whereas the best substrates using DCIP as an acceptor are L-lactate and L-2HB (Fig. 41). However, when analyzing the K_m values for the different substrates it is clear that the high activity with L-2HB and L-lactate using DCIP as an acceptor is accompanied with a K_m in the mM range (Table 11), indicating that these reactions may not be physiological. The lowest K_m values were invariably measured using O₂ as an acceptor. From these measurements it can be concluded that AtGOX3 belongs to the (S)-2-hydroxy-acid oxidase group of enzymes (EC 1.1.3.15), but the *in vivo* substrate could not be inferred.

4.3.2 Identifying important amino acids in the catalytic site

When analyzing the active site of *H. sapiens* HAOX1, six important amino acid residues in the active site could be identified. The residues Arg167, Arg263, Tyr26, Tyr132 appear important for coordinating the substrate through hydrogen bonds while Trp110 is important for filling out the substrate binding pocket and His260 is the catalytic residue (Fig. 42). The importance of some of these residues has been determined in related enzymes from other organisms. For example, the importance of Tyr26 and Trp110 for catalysis have been shown in the *S. oleaceae* glycolate oxidase (Stenberg et al., 1995), and the importance of the residues corresponding to Arg167 and Arg263 have been shown in (S)-mandelate dehydrogenase from *Pseudomonas putida* (Xu et al., 2002). All six identified residues are conserved in AtGOX3 and the two glycolate oxidases expressed in leaves, AtGOX1 and AtGOX2 (Fig. 36). Interestingly, in AtHAOX1 and AtHAOX2 Tyr26 is substituted for phenylalanine and Trp110 is substituted for methionine. The change of these two amino acid residues should lead to a dramatically different substrate binding pocket, especially considering that their importance for catalysis has been shown (Stenberg et al., 1995). It is therefore likely that AtHAOX1 and AtHAOX2 catalyze the conversion of some other substrate than glycolate (Jones et al., 2000; Reumann et al., 2004).

4.3.3 *In vivo* role of AtGOX3

AtGOX3 is unique among the *A. thaliana* GOs in that it is the only isoform almost exclusively expressed in roots (Fig. 35, and <http://bar.utoronto.ca/efp/cgi-bin/efpWeb.cgi>). Moreover, AtGOX3 protein contains a C-terminal peroxisomal targeting sequence and has been identified in plant peroxisomes in a proteomic approach (Reumann et al., 2007). The catalytic constants of the enzyme indicate a role in glycolate or L-lactate metabolism. L-lactate is known to accumulate to high levels in roots during hypoxic stress. A NAD⁺-dependent L-LDH expressed in leaves and roots has been characterized in *A. thaliana* and is involved in L-lactate production (Dolferus et al., 2008). Surprisingly, root uptake experiments show that L-LDH loss-of-function mutants take up and metabolize L-lactate at the same rate as wild-type plants (Dolferus et al., 2008). This indicates that another enzyme is responsible for L-lactate breakdown in plant roots and AtGOX3 is a good candidate to fulfill this role. In contrast, not much is known about glycolate metabolism in roots. A recent report suggests glycolate accumulation in hypoxic roots (Kumari and Pandey, 2007), but little is known about the physiological reason for this. Glycolate production in roots might result from the conversion of glycolaldehyde by an aldehyde dehydrogenase. In an attempt to determine which is the physiologically important substrate, plants were grown on medium supplemented with either glycolate or L-lactate (Fig. 43). In these experiments *gox3-1* root growth was severely inhibited on L-lactate, but not on glycolate or control plates. Together, the data support a role for AtGOX3 in root L-lactate oxidation inside peroxisomes.

4.3.4 Outlook

To further elucidate the *in vivo* role of AtGOX3, a metabolic profile analysis by GC-MS of wild-type and knock-out plant root extracts need to be undertaken. Hopefully, this will yield insights into which pathway AtGOX3 may participate. Moreover, root stress conditions such as hypoxia, salt and drought stress could be tested.

5 Conclusions and future directions

In the work presented here three putative glycolate dehydrogenases from *A. thaliana* have been biochemically characterized with the hope to use them in the GMK pathway. Three new activities as well as novel metabolic pathways have been identified. For the first time a cytochrome c- dependent D-lactate dehydrogenase, with a likely function in MG detoxification, has been characterized in plants. Furthermore, a D-2HGDH has been characterized, and the accumulation of D-2HG in knock-out plants has been determined, showing the participation of this metabolite in plant metabolism for the first time. Finally, a new (S)-2-hydroxy-acid dehydrogenase, that may participate in glycolate and/or L-lactate metabolism in roots, has been biochemically characterized.

The kinetic characteristics of AtD-LDH, AtD-2HGDH and AtGOX3 indicate that they are not suitable for pathways aimed to reduce photorespiration. The activity of AtD-LDH and AtD-2HGDH with glycolate is too low and AtGOX3 cannot be used since it uses molecular oxygen as an electron acceptor, producing H₂O₂. There is therefore a need to explore alternatives and to identify new candidate enzymes. At least three distinct approaches can be pursued, each with both benefits and drawbacks: using the *C. reinhardtii* GDH, performing a large-scale screen of algae, or performing directed evolution of lactate dehydrogenases.

The *C. reinhardtii* GDH is a 119 kDa protein with one FAD-binding domain and one Fe-S cluster-containing domain. While the enzyme has a high activity with glycolate it also oxidizes D-lactate with similar catalytic rates (Nakamura et al., 2005). Since the enzyme is not specific for glycolate the enzyme might adversely affect chloroplast metabolism. Moreover, the protein is very large and it is not sure that it will correctly re-fold inside plant chloroplasts after import. The first step towards resolving these questions would be to clone and heterologously express this enzyme in *E. coli* and further biochemically characterize it. It is also crucial that the co-factor used by the enzyme is identified. If the enzyme properties are suitable for use in the GMK pathway it can be fused with an *A. thaliana* plastid targeting sequence. Correct targeting and folding could be tested by isolating chloroplasts of transgenic plants and test for GDH activity.

Alternatively, an extensive screen for glycolate dehydrogenase activity could be performed with extracts from a large range of different algae. Algae are well suited for such an approach since they are known to employ glycolate dehydrogenases in the place of glycolate oxidases in metabolism. While the chance of discovering a completely new enzyme activity is possible using screening approaches, the risk is always that one invests a considerable amount of work screening for an enzyme that does not exist in the chosen organisms. This risk is further underscored by the fact that as of yet, no pure glycolate dehydrogenase activity has been identified in nature. Moreover, if a suitable glycolate dehydrogenase activity is measured, the responsible enzyme must be identified, something that requires a considerable effort. In a variation of this approach, a range of lactate dehydrogenases – which frequently use glycolate – could be cloned and screened for high glycolate activity.

An alternative to a screening approach is directed evolution. This approach uses cycles of mutation and selection to improve the catalytic activity of a target enzyme. One of the benefits with this approach is that the template enzyme can be freely chosen as long as there is a small amount of activity with the target substrate. The NAD^+ and NADP^+ -dependent lactate dehydrogenases make for good targets in such an approach since NAD^+ and NADP^+ are both available in chloroplasts.

6. References

- Achouri, Y., Noël, G., Vertommen, D., Rider, M.H., Veiga-Da-Cunha, M. and Van Schaftingen, E. (2004) Identification of a dehydrogenase acting on D-2-hydroxyglutarate. *Biochem. J.*, **381**, 35-42.
- Amichay, D., Levitz, R. and Gurevitz, M. (1993) Construction of a *Synechocystis PCC6803* mutant suitable for the study of variant hexadecameric ribulose biphosphate carboxylase/oxygenase enzymes. *Plant Molecular Biology*, **23**, 465-476.
- Arp, W.J., Van Mierlo, J.E.M., Berendse, F. and Snijders, W. (1998) Interactions between elevated CO₂ concentration, nitrogen and water: effects on growth and water use of six perennial plant species. *Plant Cell and Environment*, **21**, 1-11.
- Atlante, A., de Bari, L., Valenti, D., Pizzuto, R., Paventi, G. and Passarella, S. (2005) Transport and metabolism of d-lactate in Jerusalem artichoke mitochondria. *Biochimica et Biophysica Acta (BBA) - Bioenergetics*, **1708**, 13-22.
- Bari, R., Kebeish, R., Kalamajka, R., Rademacher, T. and Peterhänsel, C. (2004) A glycolate dehydrogenase in the mitochondria of *Arabidopsis thaliana*. *J. Exp. Bot.*, **55**, 623-630.
- Bauwe, H. (2010) Recent developments in photorespiration research. *Biochem Soc Trans*, **38**, 677-682.
- Bauwe, H. and Kolukisaoglu, U. (2003) Genetic manipulation of glycine decarboxylation. *Journal of Experimental Botany*, **54**, 1523-1535.
- Bender, K., Seibert, R.T., Wienker, T.F., Kren, V., Pravenec, M. and Bissbort, S. (1994) Biochemical Genetics of Methylglyoxal Dehydrogenases in the Laboratory Rat (*Rattus-Norvegicus*). *Biochemical Genetics*, **32**, 147-154.
- Betsche, T. (1981) L-Lactate Dehydrogenase from Leaves of Higher-Plants - Kinetics and Regulation of the Enzyme from Lettuce (*Lactuca sativa*). *Biochemical Journal*, **195**, 615-622.
- Bleiweis, A.S., Reeves, H.C. and Ajl, S.J. (1967) Formation of Alpha-Hydroxyglutaric Acid by *Aspergillus glaucus*. *Journal of Bacteriology*, **94**, 1560-8.
- Boldt, R., Edner, C., Kolukisaoglu, U., Hagemann, M., Weckwerth, W., Wienkoop, S., Morgenthal, K. and Bauwe, H. (2005) D-GLYCERATE 3-KINASE, the last unknown enzyme in the photorespiratory cycle in Arabidopsis, belongs to a novel kinase family. *Plant Cell*, **17**, 2413-2420.
- Bradford, M.M. (1976) A rapid and sensitive method for the quantitation of microgram quantities of protein utilizing the principle of protein-dye binding. *Analytical Biochemistry*, **72**, 248-254.
- Brockman, H.L. and Wood, W.A. (1975) D-Lactate dehydrogenase of *Peptostreptococcus elsdenii*. *J. Bacteriol.*, **124**, 1454-1461.
- Castresana, J. (2000) Selection of Conserved Blocks from Multiple Alignments for Their Use in Phylogenetic Analysis. *Mol Biol Evol*, **17**, 540-552.
- Chang, A., Scheer, M., Grote, A., Schomburg, I. and Schomburg, D. (2009) BRENDA, AMENDA and FRENDA the enzyme information system: new content and tools in 2009. *Nucleic Acids Research*, **37**, D588-D592.
- Chelstowska, A., Liu, Z., Jia, Y., Amberg, D. and Butow, R.A. (1999) Signalling between mitochondria and the nucleus regulates the expression of a new d-lactate dehydrogenase activity in yeast. *Yeast*, **15**, 1377-1391.
- Chung, C.T., Niemela, S.L. and Miller, R.H. (1989) One-Step Preparation of Competent *Escherichia coli*: Transformation and Storage of Bacterial Cells in the Same Solution.

- Proceedings of the National Academy of Sciences of the United States of America*, **86**, 2172-2175.
- Claros, M.G. and Vincens, P. (1996) Computational Method to Predict Mitochondrially Imported Proteins and their Targeting Sequences. *European Journal of Biochemistry*, **241**, 779-786.
- Cristescu, M. and Egbosimba, E. (2009) Evolutionary History of d-Lactate Dehydrogenases: A Phylogenomic Perspective on Functional Diversity in the FAD Binding Oxidoreductase/Transferase Type 4 Family. *Journal of Molecular Evolution*, **69**, 276-287.
- Cristescu, M., Innes, D., Stillman, J. and Crease, T. (2008) D- and L-lactate dehydrogenases during invertebrate evolution. *BMC Evolutionary Biology*, **8**, 268.
- Dang, L., White, D.W., Gross, S., Bennett, B.D., Bittinger, M.A., Driggers, E.M., Fantin, V.R., Jang, H.G., Jin, S., Keenan, M.C., Marks, K.M., Prins, R.M., Ward, P.S., Yen, K.E., Liau, L.M., Rabinowitz, J.D., Cantley, L.C., Thompson, C.B., Vander Heiden, M.G. and Su, S.M. (2009) Cancer-associated IDH1 mutations produce 2-hydroxyglutarate. *Nature*, **462**, 739-744.
- Davies, D.D. and Davies, S. (1972) Purification and Properties of L(+)-Lactate Dehydrogenase from Potato-Tubers. *Biochemical Journal*, **129**, 831-8.
- de Bari, L., Valenti, D., Pizzuto, R., Paventi, G., Atlante, A. and Passarella, S. (2005) Jerusalem artichoke mitochondria can export reducing equivalents in the form of malate as a result of d-lactate uptake and metabolism. *Biochemical and Biophysical Research Communications*, **335**, 1224-1230.
- Dolferus, R., Wolansky, M., Carroll, R., Miyashita, Y., Ismond, K. and Good, A. (2008) Functional analysis of lactate dehydrogenase during hypoxic stress in Arabidopsis. *Functional Plant Biology*, **35**, 131-140.
- Du, Y.-C., Hong, S. and Spreitzer, R.J. (2000) RbcS suppressor mutations improve the thermal stability and CO₂/O₂ specificity of rbcL- mutant ribulose-1,5-bisphosphate carboxylase/oxygenase. *Proceedings of the National Academy of Sciences of the United States of America*, **97**, 14206-14211.
- Edwards, G.E., Franceschi, V.R. and Voznesenskaya, E.V. (2004) Single-cell C-4 photosynthesis versus the dual-cell (Kranz) paradigm. *Annual Review of Plant Biology*, **55**, 173-196.
- Eisenhut, M., Kahlon, S., Hasse, D., Ewald, R., Lieman-Hurwitz, J., Ogawa, T., Ruth, W., Bauwe, H., Kaplan, A. and Hagemann, M. (2006) The Plant-Like C₂ Glycolate Cycle and the Bacterial-Like Glycerate Pathway Cooperate in Phosphoglycolate Metabolism in Cyanobacteria. *Plant Physiol.*, **142**, 333-342.
- Eisenhut, M., Ruth, W., Haimovich, M., Bauwe, H., Kaplan, A. and Hagemann, M. (2008) The photorespiratory glycolate metabolism is essential for cyanobacteria and might have been conveyed endosymbiotically to plants. *Proceedings of the National Academy of Sciences*, **105**, 17199-17204.
- Engel, N., van den Daele, K., Kolukisaoglu, U., Morgenthal, K., Weckwerth, W., Parnik, T., Keerberg, O. and Bauwe, H. (2007) Deletion of glycine decarboxylase in arabidopsis is lethal under nonphotorespiratory conditions. *Plant Physiology*, **144**, 1328-1335.
- Fahnenstich, H. (2008) Biotechnologische Ansätze zur Reduktion photorespiratorischer Verluste in *A. thaliana*. *PhD thesis, University of Cologne*.
- Fahnenstich, H., Saigo, M., Niessen, M., Zanol, M.I., Andreo, C.S., Fernie, A.R., Drincovich, M.F., Flugge, U.I. and Maurino, V.G. (2007) Alteration of organic acid metabolism in

- Arabidopsis overexpressing the maize C(4)NADP-malic enzyme causes accelerated senescence during extended darkness. *Plant Physiology*, **145**, 640-652.
- Fernández-Checa, J., Lu, S., Ookhtens, M., DeLeve, L., Runnegar, M., Yoshida, H., Saiki, H., Kannan, R., Garcia-Ruiz, C., Kuhlenkamp, J. and Kaplowitz, N. (1992) The regulation of hepatic glutathione. In *Hepatic Anion Transport and Bile Secretion: Physiology and Pathophysiology*. Edited by: Tavoloni N, Berk PD. New York: Marcel Dekker, 363-395.
- Fiehn, O. (2007) Validated high quality automated metabolome analysis of *Arabidopsis thaliana* leaf disks. In Nikolau, B. and Wurtele, E. (eds.), *Concepts in Plant Metabolomics*, New York, pp. 1-18.
- Flick, M.J. and Konieczny, S.F. (2002) Identification of putative mammalian D-lactate dehydrogenase enzymes. *Biochemical and Biophysical Research Communications*, **295**, 910-916.
- Flügge, U.-I. (1999) PHOSPHATE TRANSLOCATORS IN PLASTIDS. *Annual Review of Plant Physiology and Plant Molecular Biology*, **50**, 27-45.
- Forrester, M.L., Krotkov, G. and Nelson, C.D. (1966) Effect of Oxygen on Photosynthesis, Photorespiration and Respiration in Detached Leaves. I. Soybean. *Plant Physiol.*, **41**, 422-427.
- Frerman, F.E. and Goodman, S.I. (2001) Defects of electron transfer flavoprotein and electron transfer flavoprotein:ubiquinone oxidoreductase: glutaric aciduria type II. In Childs, B., Kinzler, K. and Vogelstein, B. (eds.), *The Metabolic and Molecular Bases of Inherited Disease*. McGraw-Hill, New York, pp. 2357–2365.
- Fukayama, H., Hatch, M., Tamai, T., Tsuchida, H., Sudoh, S., Furbank, R. and Miyao, M. (2003) Activity regulation and physiological impacts of maize C4-specific phospho enol pyruvate carboxylase overproduced in transgenic rice plants. *Photosynthesis Research*, **77**, 227-239.
- Gascuel, O. (1997) BIONJ: an improved version of the NJ algorithm based on a simple model of sequence data. *Mol Biol Evol*, **14**, 685-695.
- Gatenby, A.A., Castleton, J.A. and Saul, M.W. (1981) Expression in *E. coli* of maize and wheat chloroplast genes for large subunit of ribulose biphosphate carboxylase. *Nature*, **291**, 117-121.
- Greene, D.N., Whitney, S.M. and Matsumura, I. (2007) Artificially evolved *Synechococcus PCC6301* Rubisco variants exhibit improvements in folding and catalytic efficiency. *Biochemical Journal*, **404**, 517-524.
- Gregolin, C. and Singer, T.P. (1963) The lactic dehydrogenase of yeast: III. d(-)lactic cytochrome c reductase, a zinc-flavoprotein from aerobic yeast. *Biochimica et Biophysica Acta*, **67**, 201-218.
- Guex, N. and Peitsch, M.C. (1997) SWISS-MODEL and the Swiss-PdbViewer: An environment for comparative protein modeling. *Electrophoresis*, **18**, 2714-2723.
- Gutteridge, S. and Gatenby, A.A. (1995) Rubisco Synthesis, Assembly, Mechanism, and Regulation. *Plant Cell*, **7**, 809-819.
- Hammer, V.A., Rogers, Q.R. and Freedland, R.A. (1996) Threonine Is Catabolized by L-Threonine 3-Dehydrogenase and Threonine Dehydratase in Hepatocytes from Domestic Cats (*Felis domestica*). *J. Nutr.*, **126**, 2218-2226.
- Hartman, F.C. and Harpel, M.R. (1994) Structure, Function, Regulation, and Assembly of D-Ribulose-1,5-Bisphosphatecarboxylase Oxygenase. *Annual Review of Biochemistry*, **63**, 197-234.
- Hasse, D., Hagemann, M., Andersson, I. and Bauwe, H. (2010) Crystallization and preliminary X-ray diffraction analyses of the homodimeric glycine decarboxylase (P-protein) from

- the cyanobacterium *Synechocystis* sp PCC 6803. *Acta Crystallographica Section F-Structural Biology and Crystallization Communications*, **66**, 187-191.
- Häusler, R.E., Hirsch, H.J., Kreuzaler, F. and Peterhänsel, C. (2002) Overexpression of C-4-cycle enzymes in transgenic C-3 plants: a biotechnological approach to improve C-3-photosynthesis. *Journal of Experimental Botany*, **53**, 591-607.
- Hong, S. and Spreitzer, R.J. (1997) Complementing Substitutions at the Bottom of the Barrel Influence Catalysis and Stability of Ribulose-bisphosphate Carboxylase/Oxygenase. *Journal of Biological Chemistry*, **272**, 11114-11117.
- Horikiri, S., Aizawa, Y., Kai, T., Amachi, S., Shinoyama, H. and Fujii, T. (2004) Electron Acquisition System Constructed from an NAD-Independent D-Lactate Dehydrogenase and Cytochrome c2 in *Rhodospseudomonas palustris* No. 7. *Bioscience, Biotechnology, and Biochemistry*, **68**, 516-522.
- Huson, D., Richter, D., Rausch, C., DeZulian, T., Franz, M. and Rupp, R. (2007) Dendroscope: An interactive viewer for large phylogenetic trees. *BMC Bioinformatics*, **8**, 460.
- Igarashi, D., Miwa, T., Seki, M., Kobayashi, M., Kato, T., Tabata, S., Shinozaki, K. and Ohsumi, C. (2003) Identification of photorespiratory glutamate : glyoxylate aminotransferase (GGAT) gene in Arabidopsis. *Plant Journal*, **33**, 975-987.
- Igarashi, D., Tsuchida, H., Miyao, M. and Ohsumi, C. (2006) Glutamate: Glyoxylate aminotransferase modulates amino acid content during photorespiration. *Plant Physiology*, **142**, 901-910.
- Ishizaki, K., Larson, T.R., Schauer, N., Fernie, A.R., Graham, I.A. and Leaver, C.J. (2005) The Critical Role of Arabidopsis Electron-Transfer Flavoprotein:Ubiquinone Oxidoreductase during Dark-Induced Starvation. *Plant Cell*, **17**, 2587-2600.
- Ishizaki, K., Schauer, N., Larson, T.R., Graham, I.A., Fernie, A.R. and Leaver, C.J. (2006) The mitochondrial electron transfer flavoprotein complex is essential for survival of Arabidopsis in extended darkness. *The Plant Journal*, **47**, 751-760.
- Ito, S., Hamada, S., Ito, H., Matsui, H., Ozawa, T., Taguchi, H. and Ito, S. (2009) Site-directed mutagenesis of possible catalytic residues of cellobiose 2-epimerase from *Ruminococcus albus*. *Biotechnology Letters*, **31**, 1065-1071.
- Jamai, A., Salome, P.A., Schilling, S.H., Weber, A.P.M. and McClung, R. (2009) Arabidopsis Photorespiratory Serine Hydroxymethyltransferase Activity Requires the Mitochondrial Accumulation of Ferredoxin-Dependent Glutamate Synthase. *Plant Cell*, **21**, 595-606.
- Jiao, D.M., Huang, X.Q., Li, X., Chi, W., Kuang, T.Y., Zhang, Q.D., Ku, M.S.B. and Cho, D.H. (2002) Photosynthetic characteristics and tolerance to photo-oxidation of transgenic rice expressing C-4 photosynthesis enzymes. *Photosynthesis Research*, **72**, 85-93.
- Jones, J.M., Morrell, J.C. and Gould, S.J. (2000) Identification and Characterization of HAOX1, HAOX2, and HAOX3, Three Human Peroxisomal 2-Hydroxy Acid Oxidases. *Journal of Biological Chemistry*, **275**, 12590-12597.
- Jordan, D.B. and Ogren, W.L. (1984) The CO₂/O₂ Specificity of Ribulose 1,5-Bisphosphate Carboxylase Oxygenase - Dependence on Ribulosebisphosphate Concentration, Ph and Temperature. *Planta*, **161**, 308-313.
- Kalapos, M.P. (1999) Methylglyoxal in living organisms: Chemistry, biochemistry, toxicology and biological implications. *Toxicology Letters*, **110**, 145-175.
- Kamada, T., Nito, K., Hayashi, H., Mano, S., Hayashi, M. and Nishimura, M. (2003) Functional Differentiation of Peroxisomes Revealed by Expression Profiles of Peroxisomal Genes in *Arabidopsis thaliana*. *Plant Cell Physiol.*, **44**, 1275-1289.

- Kanevski, I., Maliga, P., Rhoades, D.F. and Gutteridge, S. (1999) Plastome engineering of ribulose-1,5-bisphosphate carboxylase/oxygenase in tobacco to form a sunflower large subunit and tobacco small subunit hybrid. *Plant Physiology*, **119**, 133-141.
- Kebeish, R., Niessen, M., Thiruveedhi, K., Bari, R., Hirsch, H.J., Rosenkranz, R., Stäbler, N., Schönfeld, B., Kreuzaler, F. and Peterhänsel, C. (2007) Chloroplastic photorespiratory bypass increases photosynthesis and biomass production in *Arabidopsis thaliana*. *Nature Biotechnology*, **25**, 593-599.
- Keech, O., Dizengremel, P. and Gardeström, P. (2005) Preparation of leaf mitochondria from *Arabidopsis thaliana*. *Physiologia Plantarum*, **124**, 403-409.
- Kendall, A.C., Keys, A.J., Turner, J.C., Lea, P.J. and Mifflin, B.J. (1983) The Isolation and Characterization of a Catalase-Deficient Mutant of Barley (*Hordeum vulgare*). *Planta*, **159**, 505-511.
- Kiefer, F., Arnold, K., Kunzli, M., Bordoli, L. and Schwede, T. (2009) The SWISS-MODEL Repository and associated resources. *Nucl. Acids Res.*, **37**, D387-392.
- Kochhar, S., Chuard, N. and Hottinger, H. (1992) Glutamate 264 modulates the pH dependence of the NAD(+)-dependent D-lactate dehydrogenase. *Journal of Biological Chemistry*, **267**, 20298-20301.
- Kostrzewa, A., Pali, T., Froncisz, W. and Marsh, D. (2000) Membrane location of spin-labeled cytochrome c determined by paramagnetic relaxation agents. *Biochemistry*, **39**, 6066-6074.
- Kozaki, A. and Takeba, G. (1996) Photorespiration protects C3 plants from photooxidation. *Nature*, **384**, 557-560.
- Ku, M.S.B., Agarie, S., Nomura, M., Fukayama, H., Tsuchida, H., Ono, K., Hirose, S., Toki, S., Miyao, M. and Matsuoka, M. (1999) High-level expression of maize phosphoenolpyruvate carboxylase in transgenic rice plants. *Nature Biotechnology*, **17**, 76-80.
- Ku, S.-B. and Edwards, G.E. (1977) Oxygen Inhibition of Photosynthesis: I. Temperature Dependence and Relation to O₂/CO₂ Solubility Ratio. *Plant Physiol.*, **59**, 986-990.
- Kumari, A. and Pandey, O.P. (2007) Effect of waterlogging on metabolic constituents in maize. *Indian Journal of Plant Physiology*, **12**.
- Laemmli, U.K. (1970) Cleavage of Structural Proteins during the Assembly of the Head of Bacteriophage T4. *Nature*, **227**, 680-685.
- Lara, M.V., Casati, P. and Andreo, C.S. (2002) CO₂-concentrating mechanisms in *Egeria densa*, a submersed aquatic plant. *Physiologia Plantarum*, **115**, 487-495.
- Leegood, R.C. (2002) C-4 photosynthesis: principles of CO₂ concentration and prospects for its introduction into C-3 plants. *Journal of Experimental Botany*, **53**, 581-590.
- Liepmann, A.H. and Olsen, L.J. (2001) Peroxisomal alanine: glyoxylate aminotransferase (AGT1) is a photorespiratory enzyme with multiple substrates in *Arabidopsis thaliana*. *Plant Journal*, **25**, 487-498.
- Lindahl, G., Lindstedt, G. and Lindstedt, S. (1967) Metabolism of 2-amino-5-hydroxyadipic acid in the rat. *Archives of Biochemistry and Biophysics*, **119**, 347-352.
- Lodi, T. and Ferrero, I. (1993) Isolation of the DLD gene of *Saccharomyces cerevisiae* encoding the mitochondrial enzyme D-lactate ferricytochrome c oxidoreductase. *Molecular and General Genetics MGG*, **238**, 315-324.
- Lodi, T. and Guiard, B. (1991) Complex transcriptional regulation of the *Saccharomyces cerevisiae* CYB2 gene encoding cytochrome b₂: CYP1(HAP1) activator binds to the CYB2 upstream activation site UAS1-B2. *Mol. Cell. Biol.*, **11**, 3762-3772.

- Lodi, T., O'Connor, D., Goffrini, P. and Ferrero, I. (1994) Carbon catabolite repression in *Kluyveromyces lactis*: isolation and characterization of the KINLD gene encoding the mitochondrial enzyme D-lactate ferricytochrome c oxidoreductase. *Molecular and General Genetics MGG*, **244**, 622-629.
- Long, S.P., Zhu, X.-G., Naidu, S.L. and Ort, D.R. (2006) Can improvement in photosynthesis increase crop yields? *Plant, Cell & Environment*, **29**, 315-330.
- Lord, J.M. (1972) Glycolate oxidoreductase in *Escherichia coli*. *Biochimica et Biophysica Acta (BBA) - Bioenergetics*, **267**, 227-237.
- Lorimer, G.H. (1981) The Carboxylation and Oxygenation of Ribulose 1,5-Bisphosphate - the Primary Events in Photosynthesis and Photo-Respiration. *Annual Review of Plant Physiology and Plant Molecular Biology*, **32**, 349-383.
- Lucas, K.A., Filley, J.R., Erb, J.M., Graybill, E.R. and Hawes, J.W. (2007) Peroxisomal Metabolism of Propionic Acid and Isobutyric Acid in Plants. *J. Biol. Chem.*, **282**, 24980-24989.
- Lyles, G.A. and Chalmers, J. (1992) The metabolism of aminoacetone to methylglyoxal by semicarbazide-sensitive amine oxidase in human umbilical artery. *Biochemical Pharmacology*, **43**, 1409-1414.
- Madgwick, P.J., Colliver, S.P., Banks, F.M., Habash, D.Z., Dulieu, H., Parry, M.A.J. and Paul, M.J. (2002) Genetic Manipulation of Rubisco: *Chromatium vinosum* *rbcl* is expressed in *Nicotiana tabacum* but does not form a functional protein. *Annals of Applied Biology*, **140**, 13-19.
- Maiti, M.K., Krishnasamy, S., Owen, H.A. and Makaroff, C.A. (1997) Molecular characterization of glyoxalase II from *Arabidopsis thaliana*. *Plant Molecular Biology*, **35**, 471-481.
- Mann, C.C. (1999) FUTURE FOOD: BIOENGINEERING: Genetic Engineers Aim to Soup Up Crop Photosynthesis. *Science*, **283**, 314-316.
- Matsuoka, M., Furbank, R.T., Fukayama, H. and Miyao, M. (2001) Molecular engineering of C-4 photosynthesis. *Annual Review of Plant Physiology and Plant Molecular Biology*, **52**, 297-314.
- Maurino, V.G. and Flügge, U.-I. (2009) Means for improving agrobiological traits in a plant by providing a plant cell comprising in its chloroplasts enzymatic activities for converting glycolate into malate. *Patent*, EP2093283A2093281.
- Maurino, V.G. and Peterhänsel, C. (2010) Photorespiration: current status and approaches for metabolic engineering. *Current Opinion in Plant Biology*, **In Press, Corrected Proof**.
- Miyao, M. (2003) Molecular evolution and genetic engineering of C-4 photosynthetic enzymes. *Journal of Experimental Botany*, **54**, 179-189.
- Miziorko, H.M. and Lorimer, G.H. (1983) Ribulose-1,5-Bisphosphate Carboxylase-Oxygenase. *Annual Review of Biochemistry*, **52**, 507-535.
- Monder, C. (1967) alfa-Keto Aldehyde Dehydrogenase, An Enzyme That Catalyzes the Enzymic Oxidation of Methylglyoxal to Pyruvate. *Journal of Biological Chemistry*, **242**, 4603-4609.
- Mueller-Cajar, O., Morell, M. and Whitney, S.M. (2007) Directed Evolution of Rubisco in *Escherichia coli* Reveals a Specificity-Determining Hydrogen Bond in the Form II Enzyme *Biochemistry*, **46**, 14067-14074.
- Mulcahy, P. and Ocarra, P. (1997) Purification and substrate kinetics of plant lactate dehydrogenase. *Phytochemistry*, **45**, 889-896.

- Nakamura, Y., Kanakagiri, S., Van, K., He, W. and Spalding, M.H. (2005) Disruption of the glycolate dehydrogenase gene in the high-CO₂-requiring mutant HCR89 of *Chlamydomonas reinhardtii*. *Canadian Journal of Botany-Revue Canadienne De Botanique*, **83**, 820-833.
- Nelson, E.B. and Tolbert, N.E. (1970) Glycolate dehydrogenase in green algae. *Archives of Biochemistry and Biophysics*, **141**, 102-110.
- Niessen, M., Thiruveedhi, K., Rosenkranz, R., Kebeish, R., Hirsch, H.-J., Kreuzaler, F. and Peterhänsel, C. (2007) Mitochondrial glycolate oxidation contributes to photorespiration in higher plants. *J. Exp. Bot.*, **58**, 2709-2715.
- Noctor, G., Veljovic-Jovanovic, S., Driscoll, S., Novitskaya, L. and Foyer, C.H. (2002) Drought and Oxidative Load in the Leaves of C3 Plants: a Predominant Role for Photorespiration? *Ann Bot*, **89**, 841-850.
- Norton, S., Principato, G., Talesa, V., Lupattelli, M. and Rosi, G. (1989) Glyoxalase II from *Zea mays*: properties and inhibition study of the enzyme purified by use of a new affinity ligand. *Enzyme*, **42**, 189-196.
- Obayashi, T., Hayashi, S., Saeki, M., Ohta, H. and Kinoshita, K. (2009) ATTED-II provides coexpressed gene networks for Arabidopsis. *Nucl. Acids Res.*, **37**, D987-991.
- Ogata, M., Arihara, K. and Yagi, T. (1981) D-Lactate Dehydrogenase of *Desulfovibrio vulgaris*. *J Biochem*, **89**, 1423-1431.
- Ogren, W.L. (2003) Affixing the O to Rubisco: discovering the source of photorespiratory glycolate and its regulation. *Photosynthesis Research*, **76**, 53-63.
- Parikh, M.R., Greene, D.N., Woods, K.K. and Matsumura, I. (2006) Directed evolution of RuBisCO hypermorphs through genetic selection in engineered *E. coli*. *Protein Engineering Design & Selection*, **19**, 113-119.
- Parker, A. and Engel, P.C. (2000) Preliminary evidence for the existence of specific functional assemblies between enzymes of the beta-oxidation pathway and the respiratory chain. *Biochem. J.*, **345**, 429-435.
- Parry, M.A.J., Andralojc, P.J., Mitchell, R.A.C., Madgwick, P.J. and Keys, A.J. (2003) Manipulation of Rubisco: the amount, activity, function and regulation. *Journal of Experimental Botany*, **54**, 1321-1333.
- Passarella, S., de Bari, L., Valenti, D., Pizzuto, R., Paventi, G. and Atlante, A. (2008) Mitochondria and l-lactate metabolism. *FEBS letters*, **582**, 3569-3576.
- Paul, J.S. and Volcani, B.E. (1976) A mitochondrial glycolate: Cytochrome C reductase in *Chlamydomonas reinhardtii*. *Planta*, **129**, 59-61.
- Paventi, G., Pizzuto, R., Chieppa, G. and Passarella, S. (2007) L-lactate metabolism in potato tuber mitochondria. *FEBS Journal*, **274**, 1459-1469.
- Phillips, S.A. and Thornalley, P.J. (1993) The formation of methylglyoxal from triose phosphates. *European Journal of Biochemistry*, **212**, 101-105.
- Pierce, J., Carlson, T.J. and Williams, J.G. (1989) A cyanobacterial mutant requiring the expression of ribulose biphosphate carboxylase from a photosynthetic anaerobe. *Proceedings of the National Academy of Sciences of the United States of America*, **86**, 5753-5757.
- Pompliano, D.L., Peyman, A. and Knowles, J.R. (1990) Stabilization of a reaction intermediate as a catalytic device: definition of the functional role of the flexible loop in triosephosphate isomerase. *Biochemistry*, **29**, 3186-3194.
- Pravenec, M., Gauguier, D., Schott, J., Buard, J., Křen, V., Bílá, V., Szpirer, C., Szpirer, J., Wang, J., Huang, H., St. Lezin, E., Spence, M., Flodman, P., Printz, M., Lathrop, G.,

- Vergnaud, G. and Kurtz, T. (1996) A genetic linkage map of the rat derived from recombinant inbred strains. *Mammalian Genome*, **7**, 117-127.
- Queval, G., Issakidis-Bourguet, E., Hoerberichts, F.A., Vandorpe, M., Gakiere, B., Vanacker, H., Miginiac-Maslow, M., Van Breusegem, F. and Noctor, G. (2007) Conditional oxidative stress responses in the Arabidopsis photorespiratory mutant *cat2* demonstrate that redox state is a key modulator of daylength-dependent gene expression, and define photoperiod as a crucial factor in the regulation of H₂O₂-induced cell death. *Plant Journal*, **52**, 640-657.
- Rahier, A., Bergdoll, M., Genot, G., Bouvier, F. and Camara, B. (2009) Homology Modeling and Site-Directed Mutagenesis Reveal Catalytic Key Amino Acids of 3 beta-Hydroxysteroid-Dehydrogenase/C4-Decarboxylase from Arabidopsis. *Plant Physiology*, **149**, 1872-1886.
- Ray, M. and Ray, S. (1982a) On the interaction of nucleotides and glycolytic intermediates with NAD-linked alpha-ketoaldehyde dehydrogenase. *Journal of Biological Chemistry*, **257**, 10571-10574.
- Ray, S. and Ray, M. (1981) Isolation of methylglyoxal synthase from goat liver. *J. Biol. Chem.*, **256**, 6230-6233.
- Ray, S. and Ray, M. (1982b) Purification and characterization of NAD and NADP-linked alpha-ketoaldehyde dehydrogenases involved in catalyzing the oxidation of methylglyoxal to pyruvate. *Journal of Biological Chemistry*, **257**, 10566-10570.
- Read, B.A. and Tabita, F.R. (1994) High Substrate Specificity Factor Ribulose Biphosphate Carboxylase/Oxygenase from Eukaryotic Marine Algae and Properties of Recombinant Cyanobacterial Rubisco Containing "Algal" Residue Modifications. *Archives of Biochemistry and Biophysics*, **312**, 210-218.
- Reed, D.W. and Hartzell, P.L. (1999) The Archaeoglobus fulgidus D-Lactate Dehydrogenase Is a Zn²⁺ Flavoprotein. *J. Bacteriol.*, **181**, 7580-7587.
- Reeves, H.C. and Ajl, S.J. (1962) ALPHA-HYDROXYGLUTARIC ACID SYNTHETASE. *J. Bacteriol.*, **84**, 186-187.
- Reeves, H.C., Stahl, W.J. and Ajl, S.J. (1963) Alpha-Hydroxyglutarate - Product of an Enzymatic Beta-Condensation between Glyoxylate and Propionyl-Coenzyme A. *Journal of Bacteriology*, **86**, 1352-&.
- Renne, P., Dressen, U., Hebbeker, U., Hille, D., Flugge, U.I., Westhoff, P. and Weber, A.P.M. (2003) The Arabidopsis mutant *dct* is deficient in the plastidic glutamate/malate translocator DiT2. *Plant Journal*, **35**, 316-331.
- Reumann, S., Babujee, L., Ma, C.L., Wienkoop, S., Siemsen, T., Antonicelli, G.E., Rasche, N., Luder, F., Weckwerth, W. and Jahn, O. (2007) Proteome analysis of Arabidopsis leaf peroxisomes reveals novel targeting peptides, metabolic pathways, and defense mechanisms. *Plant Cell*, **19**, 3170-3193.
- Reumann, S., Ma, C., Lemke, S. and Babujee, L. (2004) AraPeroX. A Database of Putative Arabidopsis Proteins from Plant Peroxisomes. *Plant Physiol.*, **136**, 2587-2608.
- Reumann, S. and Weber, A.P.M. (2006) Plant peroxisomes respire in the light: Some gaps of the photorespiratory C₂ cycle have become filled--Others remain. *Biochimica et Biophysica Acta (BBA) - Molecular Cell Research*, **1763**, 1496-1510.
- Ridderström, M. and Mannervik, B. (1997) Molecular cloning and characterization of the thiolesterase glyoxalase II from *Arabidopsis thaliana*. *Biochem J.*, **322**, 449-454.
- Sambrook, J. and Russel, D.W. (2002) *Molecular Cloning - A Laboratory Manual*. Cold Spring Harbour Laboratory Press., New York.

- Schreiber, U., Schliwa, U. and Bilger, W. (1986) Continuous recording of photochemical and non-photochemical chlorophyll fluorescence quenching with a new type of modulation fluorometer. *Photosynthesis Research*, **10**, 51-62.
- Schwacke, R., Schneider, A., van der Graaff, E., Fischer, K., Catoni, E., Desimone, M., Frommer, W.B., Flugge, U.-I. and Kunze, R. (2003) ARAMEMNON, a Novel Database for Arabidopsis Integral Membrane Proteins. *Plant Physiol.*, **131**, 16-26.
- Schwarte, S. and Bauwe, H. (2007) Identification of the photorespiratory 2-phosphoglycolate phosphatase, PGLP1, in Arabidopsis. *Plant Physiology*, **144**, 1580-1586.
- Shinoda, T., Arai, K., Shigematsu-Iida, M., Ishikura, Y., Tanaka, S., Yamada, T., Kimber, M.S., Pai, E.F., Fushinobu, S. and Taguchi, H. (2005) Distinct Conformation-mediated Functions of an Active Site Loop in the Catalytic Reactions of NAD-dependent D-Lactate Dehydrogenase and Formate Dehydrogenase. *Journal of Biological Chemistry*, **280**, 17068-17075.
- Smith, S.A. and Tabita, F.R. (2003) Positive and negative selection of mutant forms of prokaryotic (cyanobacterial) ribulose-1,5-bisphosphate carboxylase/oxygenase. *Journal of Molecular Biology*, **331**, 557-569.
- Somerville, C.R. and Ogren, W.L. (1979) Phosphoglycolate Phosphatase-Deficient Mutant of Arabidopsis. *Nature*, **280**, 833-836.
- Somerville, C.R. and Ogren, W.L. (1980a) Inhibition of Photosynthesis in Arabidopsis Mutants Lacking Leaf Glutamate Synthase Activity. *Nature*, **286**, 257-259.
- Somerville, C.R. and Ogren, W.L. (1980b) Photorespiration mutants of *Arabidopsis thaliana* deficient in serine-glyoxylate aminotransferase activity. *Proceedings of the National Academy of Sciences of the United States of America*, **77**, 2684-2687.
- Somerville, C.R. and Ogren, W.L. (1981) Photorespiration-Deficient Mutants of *Arabidopsis thaliana* Lacking Mitochondrial Serine Transhydroxymethylase Activity. *Plant Physiology*, **67**, 666-671.
- Somerville, C.R. and Ogren, W.L. (1982) Mutants of the Cruciferous Plant *Arabidopsis thaliana* Lacking Glycine Decarboxylase Activity. *Biochemical Journal*, **202**, 373-380.
- Somerville, S.C. and Ogren, W.L. (1983) An *Arabidopsis thaliana* mutant defective in chloroplast dicarboxylate transport. *Proceedings of the National Academy of Sciences of the United States of America*, **80**, 1290-1294.
- Spreitzer, R.J., Esquivel, M.G., Du, Y.-C. and McLaughlin, P.D. (2001) Alanine-Scanning Mutagenesis of the Small-Subunit β A- β B Loop of Chloroplast Ribulose-1,5-Bisphosphate Carboxylase/Oxygenase: Substitution at Arg-71 Affects Thermal Stability and CO₂/O₂ Specificity *Biochemistry*, **40**, 5615-5621.
- Spreitzer, R.J. and Salvucci, M.E. (2002) Rubisco: Structure, regulatory interactions, and possibilities for a better enzyme. *Annual Review of Plant Biology*, **53**, 449-475.
- Stenberg, K., Clausen, T., Lindqvist, Y. and Macheroux, P. (1995) Involvement of Tyr24 and Trp108 in Substrate Binding and Substrate Specificity of Glycolate Oxidase. *European Journal of Biochemistry*, **228**, 408-416.
- Struys, E.A., Korman, S.H., Salomons, G.S., Darmin, P.S., Achouri, Y., Schaftingen, E.V., Verhoeven, N.M. and Jakobs, C. (2005a) Mutations in phenotypically mild D-2-hydroxyglutaric aciduria. *Annals of Neurology*, **58**, 626-630.
- Struys, E.A., Salomons, G.S., Achouri, Y., Van Schaftingen, E., Grosso, S., Craigen, W.J., Verhoeven, N.M. and Jakobs, C. (2005b) Mutations in the d-2-Hydroxyglutarate Dehydrogenase Gene Cause d-2-Hydroxyglutaric Aciduria. *The American Journal of Human Genetics*, **76**, 358-360.

- Struys, E.A., Verhoeven, N.M., Brunengraber, H. and Jakobs, C. (2004) Investigations by mass isotopomer analysis of the formation of D-2-hydroxyglutarate by cultured lymphoblasts from two patients with D-2-hydroxyglutaric aciduria. *FEBS letters*, **557**, 115-120.
- Suzuki, K., Marek, L.F. and Spalding, M.H. (1990) A Photorespiratory Mutant of *Chlamydomonas reinhardtii*. *Plant Physiology*, **93**, 231-237.
- Taiz, L. and Zeiger, E. (2006) *Plant Physiology*. Sinauer Associates, Inc.
- Takeuchi, K., Akagi, H., Kamasawa, N., Osumi, M. and Honda, H. (2000) Aberrant chloroplasts in transgenic rice plants expressing a high level of maize NADP-dependent malic enzyme. *Planta*, **211**, 265-274.
- Taniguchi, M., Taniguchi, Y., Kawasaki, M., Takeda, S., Kato, T., Sato, S., Tahata, S., Miyake, H. and Sugiyama, T. (2002) Identifying and characterizing plastidic 2-oxoglutarate/malate and dicarboxylate transporters in *Arabidopsis thaliana*. *Plant and Cell Physiology*, **43**, 706-717.
- Tcherkez, G.G.B., Farquhar, G.D. and Andrews, T.J. (2006) Despite slow catalysis and confused substrate specificity, all ribulose biphosphate carboxylases may be nearly perfectly optimized. *Proceedings of the National Academy of Sciences of the United States of America*, **103**, 7246-7251.
- Thompson, J.D., Higgins, D.G. and Gibson, T.J. (1994) CLUSTAL W: improving the sensitivity of progressive multiple sequence alignment through sequence weighting, position-specific gap penalties and weight matrix choice. *Nucl. Acids Res.*, **22**, 4673-4680.
- Thornalley, P.J. (1990) The glyoxalase system: new developments towards functional characterization of a metabolic pathway fundamental to biological life. *Biochem. J.*, **269**, 1-11.
- Tian, B.J., Wang, Y., Zhu, Y.R., Lu, X.Y., Huang, K.Y., Shao, N. and Beck, C.F. (2006) Synthesis of the photo respiratory key enzyme serine: glyoxylate aminotransferase in *C. reinhardtii* is modulated by the light regime and cytokinin. *Physiologia Plantarum*, **127**, 571-582.
- Timm, S., Nunes-Nesi, A., Pamik, T., Morgenthal, K., Wienkoop, S., Keerberg, O., Weckwerth, W., Kleczkowski, L.A., Fernie, A.R. and Bauwe, H. (2008) A Cytosolic Pathway for the Conversion of Hydroxypyruvate to Glycerate during Photorespiration in *Arabidopsis*. *Plant Cell*, **20**, 2848-2859.
- Tolbert, N.E. (1997) THE C₂ OXIDATIVE PHOTOSYNTHETIC CARBON CYCLE. *Annual Review of Plant Physiology and Plant Molecular Biology*, **48**, 1-25.
- Uemura, K., Anwaruzzaman, Miyachi, S. and Yokota, A. (1997) Ribulose-1,5-bisphosphate carboxylase/oxygenase from thermophilic red algae with a strong specificity for CO₂ fixation. *Biochemical and Biophysical Research Communications*, **233**, 568-571.
- Uemura, K., Suzuki, Y., Shikanai, T., Wadano, A., Jensen, R.G., Chmara, W. and Yokota, A. (1996) A rapid and sensitive method for determination of relative specificity of RuBisCO from various species by anion-exchange chromatography. *Plant and Cell Physiology*, **37**, 325-331.
- Van Schaftingen, E., Rzem, R. and Veiga-da-Cunha, M. (2009) I -2-Hydroxyglutaric aciduria, a disorder of metabolite repair. *Journal of Inherited Metabolic Disease*, **32**, 135-142.
- Vandenabeele, S., Vanderauwera, S., Vuylsteke, M., Rombauts, S., Langebartels, C., Seidlitz, H.K., Zabeau, M., Van Montagu, M., Inze, D. and Van Breusegem, F. (2004) Catalase deficiency drastically affects gene expression induced by high light in *Arabidopsis thaliana*. *Plant Journal*, **39**, 45-58.

- Voll, L.M., Jamai, A., Renne, P., Voll, H., McClung, C.R. and Weber, A.P.M. (2006) The Photorespiratory Arabidopsis shm1 Mutant Is Deficient in SHM1. *Plant Physiol.*, **140**, 59-66.
- Watson, G.M.F. and Tabita, F.R. (1997) Microbial ribulose 1,5-bisphosphate carboxylase/oxygenase: A molecule for phylogenetic and enzymological investigation. *Fems Microbiology Letters*, **146**, 13-22.
- Weber, A., Menzlaff, E., Arbinger, B., Gutensohn, M., Eckerskorn, C. and Flugge, U.I. (1995) The 2-Oxoglutarate Malate Translocator of Chloroplast Envelope Membranes - Molecular-Cloning of a Transporter Containing a 12-Helix Motif and Expression of the Functional Protein in Yeast-Cells. *Biochemistry*, **34**, 2621-2627.
- Weber, A.P.M. and von Caemmerer, S. (2010) Plastid transport and metabolism of C3 and C4 plants -- comparative analysis and possible biotechnological exploitation. *Current Opinion in Plant Biology*, **In Press, Corrected Proof**.
- Whitney, S.M. and Andrews, T.J. (2001) Plastome-encoded bacterial ribulose-1,5-bisphosphate carboxylase/oxygenase (RubisCO) supports photosynthesis and growth in tobacco. *Proceedings of the National Academy of Sciences of the United States of America*, **98**, 14738-14743.
- Whitney, S.M., Baldet, P., Hudson, G.S. and Andrews, T.J. (2001) Form I Rubiscos from non-green algae are expressed abundantly but not assembled in tobacco chloroplasts. *The Plant Journal*, **26**, 535-547.
- Wingler, A., Lea, P.J., Quick, W.P. and Leegood, R.C. (2000) Photorespiration: metabolic pathways and their role in stress protection. *Philosophical Transactions of the Royal Society B-Biological Sciences*, **355**, 1517-1529.
- Winter, D., Vinegar, B., Nahal, H., Ammar, R., Wilson, G.V. and Provart, N.J. (2007) An "Electronic Fluorescent Pictograph" Browser for Exploring and Analyzing Large-Scale Biological Data Sets. *PLoS ONE*, **2**, e718.
- Xu, H.W., Zhang, J.J., Zeng, J.W., Jiang, L.R., Liu, E., Peng, C.L., He, Z.H. and Peng, X.X. (2009) Inducible antisense suppression of glycolate oxidase reveals its strong regulation over photosynthesis in rice. *Journal of Experimental Botany*, **60**, 1799-1809.
- Xu, Y. and Chen, X. (2006) Glyoxalase II, a Detoxifying Enzyme of Glycolysis Byproduct Methylglyoxal and a Target of p63 and p73, Is a Pro-survival Factor of the p53 Family. *J. Biol. Chem.*, **281**, 26702-26713.
- Xu, Y., Dewanti, A.R. and Mitra, B. (2002) Arginine 165/arginine 277 pair in (S)-mandelate dehydrogenase from *Pseudomonas putida*: Role in catalysis and substrate binding. *Biochemistry*, **41**, 12313-12319.
- Yadav, S.K., Singla-Pareek, S.L., Kumar, M., Pareek, A., Saxena, M., Sarin, N.B. and Sopory, S.K. (2007) Characterization and functional validation of glyoxalase II from rice. *Protein Expression and Purification*, **51**, 126-132.
- Yadav, S.K., Singla-Pareek, S.L., Ray, M., Reddy, M.K. and Sopory, S.K. (2005) Methylglyoxal levels in plants under salinity stress are dependent on glyoxalase I and glutathione. *Biochemical and Biophysical Research Communications*, **337**, 61-67.
- Zelitch, I., Schultes, N.P., Peterson, R.B., Brown, P. and Brutnell, T.P. (2009) High Glycolate Oxidase Activity Is Required for Survival of Maize in Normal Air. *Plant Physiology*, **149**, 195-204.

7. Abstract

Photorespiration results from the incorporation of oxygen into ribulose-1,5-bisphosphate due to the failure of RuBisCO to properly discriminate between oxygen and carbon dioxide. This process lowers photosynthetic efficiency in that CO₂ and ammonia should be re-assimilated with the concomitant consumption of both ATP and reducing power. Two recent approaches, aimed at decreasing the detrimental effects of photorespiration by introducing novel metabolic pathways into plant chloroplasts, show great promise. The goal of this work was to identify and biochemically characterize a single-gene glycolate dehydrogenase for use in further improving the synthetic pathways. Forward and reverse genetics were used to identify three candidate genes in *Arabidopsis thaliana*; At5g06580, At4g36400 and At4g18360. The proteins encoded by these genes were expressed in *Escherichia coli*, purified and characterized. Moreover, *in silico* analysis and the analysis of loss-of-function mutants yielded insights into the significance of these novel enzymatic activities in plant metabolism.

AtD-LDH, encoded by At5g06580, is a homodimeric FAD-binding flavoprotein that catalyzes the cytochrome c- dependent oxidation of substrates. The enzyme has high activity with D- and L-lactate, D-2-hydroxybutyrate and D-glycerate, but of these only D-lactate and D-2-hydroxybutyrate are bound with high affinity. Knock-out mutants show impaired growth on medium containing methylglyoxal and D-lactate. Together, the data indicates a role for AtD-LDH in the mitochondrial intermembrane space where it oxidizes D-lactate to pyruvate in the final step of methylglyoxal detoxification. AtD-2HGDH, encoded by At4g36400, is a homodimeric FAD-binding flavoprotein. The enzyme only has activity with D-2-hydroxyglutarate and uses a synthetic electron acceptor *in vitro*. Metabolic analysis of knock-out mutants reveals high accumulation of D-2-hydroxyglutarate in plants exposed to long periods of extended darkness, confirming that this is the *in vivo* substrate for the enzyme. Co-expression analysis reveals that AtD-2HGDH is co-expressed with enzymes and transporters participating in the breakdown of lipids, branched-chain amino acids and chlorophyll, all pathways that converge in the production of propionyl-CoA. Together, the data suggest a role for AtD-2HGDH in the mitochondrial matrix where it oxidizes D-2-hydroxyglutarate, most probably originating from propionyl-CoA metabolism, to 2-oxoglutarate, using an electron transfer flavoprotein as an electron acceptor. Finally, AtGOX3, encoded by At4g18360, is a peroxisomal (S)-2-hydroxy-acid oxidase with specificity towards glycolate, L-lactate and L-2-hydroxybutyrate. *AtGOX3* is almost exclusively expressed in roots where it might participate in either the metabolism of L-lactate produced during hypoxia, or glycolate produced from glycolaldehyde.

In this work, the identification and thorough characterization of three novel enzymatic activities in the model plant *A. thaliana* are described. Moreover, novel plant metabolic pathways in which these enzymes participate were discovered. The biochemical characterization of these enzymes indicated that they are not suited for use in pathways aimed at decreasing photorespiration and thus, the search for a single-gene glycolate dehydrogenase should continue.

8. Kurzzusammenfassung

Die Kohlenstofffixierung der Photosynthese wird durch das Enzym Ribulose-1,5-bisphosphat-Carboxylase/Oxygenase katalysiert. Sauerstoff und Kohlenstoffdioxid konkurrieren um die katalytische Stelle des Enzyms. Da die Oxygenaseaktivität, eine Verlustreaktion darstellt, gibt es technische Ansätze zur Reduzierung der mit der Photorespiration verbundenen Verluste. Zwei Strategien, mit dem Ziel die energetisch ineffizienten Effekte der Photorespiration durch das Einbringen neuer Stoffwechselwege in den Chloroplasten zu vermindern sind vielversprechend. Das Ziel dieser Arbeit war die Identifizierung und biochemische Charakterisierung einer Glykolat Dehydrogenase für weitere Untersuchungen und Verbesserungen dieser Stoffwechselwege. „Forward“ und „reverse“ Genetik wurde verwendet, um drei Gene in *Arabidopsis thaliana* zu identifizieren; At5g06580, At4g36400 und At4g18360. Diese Gene wurden in *Escherichia coli* kloniert und das rekombinante Protein exprimiert, aufgereinigt und charakterisiert. Weiterhin gaben *in silico* Analysen und die Untersuchung von Mutanten Einblicke in die physiologische Relevanz dieser Gene.

AtD-LDH, welches durch At5g06580 kodiert wird, ist ein homodimeres FAD-bindendes Flavoprotein, welches die Cytochrom C-abhängige Oxidation von Substraten katalysiert. Dieses Enzym zeigt eine hohe Aktivität mit D- und L-Lactat, D-2-Hydroxybutyrat und D-Glycerat, von denen jedoch nur D-Lactat und D-2-Hydroxybutyrat mit hoher Affinität gebunden werden. Deletionsmutanten zeigen sowohl auf Medium mit Methylglyoxal und D-Lactat, als auch auf Medium mit D-2-Hydroxybutyrat ein beeinträchtiges Wachstum. Die Daten deuten eine Rolle der AtD-LDH im mitochondrialen Intermembranraum an, wo es im finalen Schritt der Methylglyoxal Entgiftung D-Lactat zu Pyruvat oxidiert. AtD-2HGDH, welches durch At4g36400 kodiert wird, ist ebenfalls ein homodimeres FAD-bindendes Flavoprotein. Dieses Enzym zeigt nur mit D-2-Hydroxyglutarat Aktivität und nutzt *in vitro* einen künstlichen Elektronenakzeptor. Metabolische Analysen der Deletionsmutanten dieses Gens zeigen eine hohe Akkumulation von D-2-Hydroxyglutarat in Pflanzen, welche einer längeren Dunkelphase ausgesetzt waren. Dies deutet darauf hin, dass es sich *in vivo* bei diesem Molekül um das Substrat der AtD-2HGDH handelt. Co-Expressionsanalysen zeigen wichtige Enzyme und Transporter, welche am Abbau von Fetten, verzweigte Aminosäuren und Chlorophyll beteiligt sind. Zusammengefasst zeigen die Daten eine Rolle der AtD-2HGDH in der mitochondrialen Matrix, wo sie D-2-Hydroxyglutarat, welches vermutlich aus dem Propionyl-CoA Metabolismus stammt, zu 2-Oxoglutarat oxidiert. Als letztes Gen wurde At4g18360, welches für AtGOX3 kodiert, untersucht. Hierbei handelt es sich um eine peroxisomale (S)-2-Hydroxysäure Oxidase mit einer Spezifität für Glykolat, L-Lactat und L-2-Hydroxybutyrat. AtGOX3 wird nahezu ausschließlich in Wurzeln exprimiert, wo es entweder an dem Abbau von L-Lactat während einer Hypoxie oder an dem Abbau von Glykolat stammend aus Glykolaldehyd beteiligt sein könnte.

Die vollständige biochemische Charakterisierung dieser Enzyme, zeigt dass sie nicht für den Gebrauch in Stoffwechselwegen zur Verminderung der Photorespiration geeignet sind. Die Suche nach einer funktionellen Glykolat Dehydrogenase wird weiter fortgesetzt.

9. Acknowledgements

First and foremost I am grateful to Prof. Dr. Ulf- Ingo Flügge and PD Dr. Verónica Maurino for their scientific guidance, their ceaseless support and for granting me the opportunity to work on the project presented in this thesis.

I thank Prof. Dr. Sabine Waffenschmidt and Prof. Dr. Hermann Bauwe for agreeing to read and grade this thesis.

I thank Prof. Dr. Reinhard Krämer for agreeing to be the head the thesis committee.

I thank all of AG-Flügge and especially Dr. Henning Kunz, Dr. Markus Gierth and Dr. Frank Ludewig for many exciting scientific discussions in the past years.

I thank the members of the Maurino workgroup: Dr. Holger Fahnenstich, Martina Zell, Alexandra Maier, Nils Jaspert, Anke Kuhn, Judith Wienstroer, Claudia Nothelle and Ulrike Hebbeker.

I thank “Stiftelsen Markussens Studiefond” for honoring me with a personal stipend. Especially I would like to thank Björn Hedin for his patience when my application got lost in the mail.

I thank my wife Anna Engqvist and my parents Stig and Isa Engqvist for always supporting me in all my endeavors.

10. Erklärung

Ich versichere, dass ich die von mir vorgelegte Dissertation selbständig angefertigt habe, die benutzten Quellen und Hilfsmittel vollständig angegeben und die Stellen der Arbeit – einschließlich Tabellen, Karten und Abbildungen –, die anderen Werken im Wortlaut oder dem Sinn nach entnommen sind, in jedem Einzelfall als Entlehnung kenntlich gemacht habe; dass diese Dissertation noch keiner anderen Fakultät oder Universität zur Prüfung vorgelegen hat; dass sie abgesehen von unten angegebenen Teilpublikationen noch nicht veröffentlicht worden ist sowie, dass ich eine solche Veröffentlichung vor Abschluss des Promotionsverfahrens nicht vornehmen werde. Die Bestimmungen dieser Promotionsordnung sind mir bekannt. Die von mir vorgelegte Dissertation ist von Prof. Dr. U.-I. Flügge betreut worden.

Martin Engqvist